Physics Reports 540 (2014) 167–218

Contents lists available at ScienceDirect

Physics Reports

journal homepage: www.elsevier.com/locate/physrep

Control of multistability

Alexander N. Pisarchik [a,b,*], Ulrike Feudel [c]

[a] Centro de Investigaciones en Optica, Loma del Bosque 115, Lomas del Campestre, 37150 Leon, Guanajuato, Mexico

[b] Centre for Biomedical Technology, Technical University of Madrid, Campus Montegancedo, 28223 Pozuelo de Alarcon, Madrid, Spain

[c] Theoretical Physics/Complex Systems, Institute for Chemistry and Biology of the Marine Environment, Carl von Ossietzky University Oldenburg, PF 2503, 26111 Oldenburg, Germany

ARTICLE INFO

Article history:
Accepted 5 February 2014
Available online 2 March 2014
editor: D.K. Campbell

Keywords:
Nonlinear dynamics
Dissipative systems
Coexisting attractors
Multistability
Nonlinear control

ABSTRACT

Multistability or coexistence of different attractors for a given set of parameters is one of the most exciting phenomena in dynamical systems. It can be found in different areas of science, such as physics, chemistry, biology, economy, and in nature. The final state of a multistable system depends crucially on the initial conditions. From the viewpoint of applications, there are two major issues related to the emergence of multistability. On one hand, this phenomenon often can create inconvenience, as for instance, in the design of a commercial device with specific characteristics, where multistability needs to be avoided or the desired state has to be stabilized against a noisy environment, and on the other hand, the coexistence of different stable states offers a great flexibility in the system performance without major parameter changes, that can be used with the right control strategies to induce a definite switching between different coexisting states. These two examples alone illustrate the importance of multistability control in applied nonlinear science. For the last decade a lot of research has been devoted to the development of control techniques of multistable systems. These methods cover several strategies, going from feedback control methods to nonfeedback, such as periodic or stochastic perturbations capable of changing the coexisting states stability and driving the system from multistability to monostability. We review the most representative control strategies, discuss their theoretical background and experimental realization.

Contents

* Corresponding author at: Centre for Biomedical Technology, Technical University of Madrid, Campus Montegancedo, 28223 Pozuelo de Alarcon, Madrid, Spain. Tel.: +34 913364647.
E-mail addresses: apisarch@cio.mx, apisarch@hotmail.com (A.N. Pisarchik).

http://dx.doi.org/10.1016/j.physrep.2014.02.007
0370-1573/

1. Introduction

In dissipative systems, multistability means the coexistence of several possible final stable states (attractors) for a given set of parameters. The final state to which the system will converge depends crucially on the initial conditions, i.e., the long-term dynamics corresponding to one of the attractors is defined by the initial conditions. The set of initial conditions that give rise to a set of trajectories converging towards to the same attractor, called basin of attraction, can have a rather complicated, fractal structure. There exists a nontrivial relationship between the coexisting asymptotic states and their complexly interwoven basins of attraction that makes multistable systems extremely sensitive to any perturbation. The region of coexistence of many stable states is a critical one, because small noise or any other external perturbation may switch the system from one attractor to any other, adding a new feature to the dynamical behavior.

The phenomenon of multistability has been found in almost all areas of science and nature. The first study, which also coined the term multistability, was devoted to visual perception [1]. A qualitative hint on the role of multiple basins of attraction of coexisting states is contained in some experimental observations of hydrodynamic instabilities [2,3]. However, clear evidence of the coexistence of attractors was manifested by Arecchi and his coworkers, first in electronic circuits [4,5]

and then in a gas laser [6]. In both cases, multistability was revealed as appearance of a low-frequency spectral component in the power spectrum due to noise-induced switches between coexisting states.

The phenomenon of multistability has been identified in different classes of systems, such a weakly dissipative systems, coupled systems, delayed feedback systems, parametrically excited systems, and stochastic systems (cf. [7] and references therein). Experiments as well as theoretical models have revealed different routes to multistability in the different system classes. The appearance of a multitude of attractors depends in general on the most important parameters characterizing a particular system class, such as, the strength of dissipation, the kind and strength of coupling, the value of the time delay, amplitude and frequency of the parameter perturbation and the noise intensity. However, despite all differences in mechanisms of the multistability emergence, multistable systems belonging to every system class share the property of their extreme sensitivity to noise. Additionally, multistable systems offer a great flexibility in different behaviors taking into account that each attractor represents a different system performance. The control of multistability is a major challenge for nonlinear sciences due to the high sensitivity of multistable systems to any perturbation. The control should be robust against noise when a certain system performance is desired. If the coexistence of multiple attractors is undesirable, what is required for many applications, control strategies to suppress multistability must be developed, by contrast, one may use multistability as an advantage by applying control techniques to induce switches between some of the coexisting states, i.e. different system performances.

In the last decade, various approaches to control multistability have been developed (see, e.g. [8] and references therein). Feedback control for stabilizing attractors via targeting methods to reach certain preselected attractors by applying random or periodic perturbations to a control parameter or a system variable is a valuable technique. Control strategies are not only theories that use simple dynamical models as paradigms, but have already been successfully applied in many experiments.

In this Report, we review the most important techniques for controlling multistability in diverse fields of science, such as electronics, optics, chemistry, and biology in order to give some insight into the current research. To emphasize the problem omnipresence, we start with an overview of the detection of multistability in various systems. Then, in Section 2 we formulate control goals and illustrate its necessity in different research areas. Nonfeedback control strategies mainly designed to annihilate certain attractors are discussed in Section 3 in order to turn a multistable system into a monostable one. Section 4 is devoted to feedback control to reach a preselected performance of the system. The role of noise in the control problem is examined in Section 5, followed by a discussion of the state of the art in Section 6 that includes the perspectives for future research.

The development and application of the methods for controlling multistability is far from being complete. Particularly, during the last decade the number of papers reporting the coexistence of attractors is enormously increasing so that one can expect a further rapid development of this field during the next decade.

1.1. Multistability: a widespread phenomenon in dynamical systems

Many dissipative nonlinear dynamical systems exhibit the coexistence of several stable states (attractors) for a given set of parameters. This phenomenon known as multistability has be found in almost all natural sciences, including electronics [2], optics [9], mechanics [10], and biology [11]. Each attractor possesses its own basin of attraction, i.e. a well defined set of initial conditions that in a long-term limit will all reach it. The properties of the basins of attraction are largely determined by the insets and outsets of regular saddles [12]. The knowledge of the systematic organization of coexisting basins of attraction of multiple states is important to predict the system's behavior in the long-term run. A nontrivial relationship between these coexisting asymptotic states and their complexly interwoven basins of attraction makes multistable systems both, extremely sensitive to any perturbation and crucially dependent on the initial conditions.

When a control parameter is varied and passes through a bifurcation, the system dynamics may drastically change, for instance, a limit cycle may change its period or an attractor may change its type, e.g. from stationary to periodic. Additionally, attractors can be born or die at various bifurcations. Very often, a new attractor is born in a saddle–node bifurcation where a pair of stable and unstable fixed points or periodic orbits appear. The birth of the attractor comes with the emergence of its basin of attraction whose boundaries can be either smooth or fractal. While a bistable system having only two coexisting attractors often possesses smooth boundaries of their respective basins of attraction, a multistable system habitually exhibits fractal basin boundaries.

Next, we will give a brief review of the most important research directions related to multistable systems, going from perception, following by biological, physical, and chemical systems to ecosystems, neuroscience, climate, and social dynamics.

1.1.1. Multistability in perception

The perception of visual and auditory signals in the brain was among the first issues discussed in terms of multistability that has been introduced to provide mechanisms for information processing in biological neural systems. The term "multistability" was first used with respect to visual perception in 1971 [1]. Multistability occurs when a single physical stimulus produces alternations between different subjective percepts [13]. In vision science, multistable perception characterizes the wavering percepts that can be brought about by certain visually ambiguous patterns, such as the Necker cube and Rubin vase, as shown in Fig. 1. Some authors argue, that every pattern is, in a way, an ambiguous multistable pattern, but that in everyday life we are usually able to resolve and avoid ambiguity by the introduction of additional

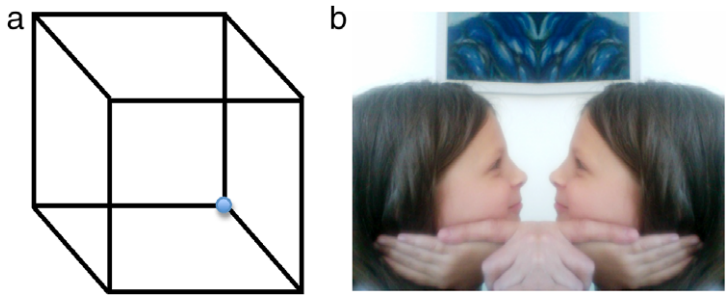

Fig. 1. Examples of bistable visual perception. These are famous optical illusion pictures, which can be seen in one of two different ways. (a) Necker cube. The isometric perspective of a wire-frame drawing makes the ball perceived plan being in front ambiguous. (b) Rubin vase. The picture can be seen as either two facing profiles or as a symmetrical vase in the center.

information [14]. When such figures are viewed for an extended time, the two percepts alternate spontaneously, changing as often as every few seconds. This alternation has been attributed to neural adaptation or satiation [15,16]. Perceptual multistability can be evoked by visual patterns that are too ambiguous for the human visual system to recognize with one unique interpretation. Since most of such images lead to an alternation between two mutually exclusive perceptual states, they are sometimes also referred to as bistable perception [17]. Magnetoencephalographic (MEG) measurements of early visual cortex activity displayed a good correlation with intermittent switches between face and vase percepts in Rubin's face–vase illusion [18].

It is supposed that the biological origin of bistable visual perception lies in noise, inherent to brain neuron cells activity, which induces switches between different perception states [19,20]. The interpretation of visible images is defined by previous knowledge and personal experience that act as initial conditions. The switches are stochastic processes according to a Markov chain [21] and are measured by recording either phase durations or percept frequencies [22]. Mamassian and Goutcher [23] developed a method to analyze instantaneous measures of dominance and transition between percepts. The analysis extracts three time-varying probabilities. First, the transient preference represents the probability of perceiving one interpretation at one instant. Second, the reversal probability is the probability that the current percept will change at the next evaluation. Finally, the survival probability is the probability that at one instant the current percept will not switch to the alternative interpretation.

Multistability is also evident in auditory perception, where discontinuous presentation is the rule. Repeated presentation of an ambiguous word can lead to verbal transformations [24,25], but these often involve multiple alternatives that follow an irregular progression. A famous example is the tritone paradox [26] which involves pairs of tones that can be perceived as either ascending or descending in pitch. Although such a pair may be perceived differently in different contexts [27], repeated presentation of the same pair generally does not lead to a change in perception. Although neural adaptation occurs in hearing, it seems to take place mainly at a more peripheral level than that of the categorical percept (see, e.g., [28]).

Multistability in metrical interpretation of a melody was studied by Repp et al. [29,30]. They have shown that although the metrical structure rarely changes spontaneously, it is both multistable and highly susceptible to effects of intention. While it is similar in some ways to reversible visual figures, it is also very different in other ways. Two striking differences between visual chimeras and melodies, however, are in the switching rate and in the extent to which the switching is under intentional control. Visual figures tend to reverse every few seconds, and the viewer's intentions have only relatively mild effects on the rate of switching. By contrast, metrical interpretations are stable for minutes before they switch, if ever they do; furthermore, when they do, it seems unlikely that they will ever switch back spontaneously to the original interpretation.

Although several attempts have been made to voluntary control multistable perception, this control seems to be limited [31,32].

1.1.2. Multistability in biological systems

The existence of multiple operating regimes is essential for biological systems since they display functional flexibility in responding to various stimuli. It was in the context of a metabolic system investigation [33] that multistability was first discussed in terms of dynamical system theory. Since then, multistability is an important recurring theme in cell signaling. We believe it will be found very relevant to any biological system that switches between discrete states, generates oscillatory responses, or "remembers" transitory stimuli [34]. The presence of multiple attractors has fundamental biological significance, notably in cell differentiation and sympatric speciation [35–39].

Biological mechanisms and topological structures leading to multistability have been extensively studied in genetic oscillators [40–45]. Very simple biochemical systems regulated at the level of gene expression or protein function are capable of displaying a complex dynamic behavior. Among the various patterns of regulation associated with nonlinear kinetics, multistability allows a graded signal to be turned into a discontinuous evolution of the system along one of several possible distinct pathways; this process can be either reversible or irreversible. Multistability plays a significant role in some of the basic processes of life. It might account for maintenance of phenotypic differences in the absence of genetic or environmental

distinctions, as has been demonstrated experimentally for the regulation of the lactose operon in *Escherichia coli*, where cell differentiation was explained by multistability [35].

Multistability has certain unique properties not shared by other mechanisms of integrative control. These features will prove to play an essential role in living cells and organisms dynamics; multistability has been invoked to explain mitogen-activated protein kinase cascades in animal cells [46–48], cell cycle regulatory circuits in *Xenopus* and *Saccharomyces cerevisiae* [49,50], the generation of switch-like biochemical responses [46,47,51], and the establishment of cell cycle oscillations and mutually exclusive cell cycle phases [50,52], among other biological phenomena. On the other hand, there are also serious doubts that the coexistence of attractors is the dynamical origin of all biological switches [53]. Nevertheless, it is generally accepted that two paradigmatic gene-regulatory networks in bacteria, the phage switch and the lac operon (at least when induced by non-metabolizable inducers), do show bistability [34,54,55]. In the former, bistability arises through a mutually inhibitory double-negative-feedback loop, while in the latter, a positive-feedback loop is responsible for the bistability.

1.1.3. Multistability in hydrodynamics

Shiau et al. [56] have found the coexistence of two or three periodic regimes in a two-dimensional flow passing to a square cylinder at low Reynolds numbers. They showed that when the system exhibits the coexistence of the period-1 and period-3 vortices behind the cylinder, the spatial symmetry is still maintained, however, when the system is tristable, the period-3 vortex loses spatial symmetry, but the period-1 vortex maintains the spatial symmetry. The experimental evidence of multistability in a turbulent flow has been demonstrated by Ravelet et al. [57]. At high Reynolds numbers, because the global bifurcation between states is highly subcritical, multiple turbulent states that keep a memory of the system history coexist.

1.1.4. Multistability in optical systems

It was not until the beginning of the 80s, that multistability became a prominent phenomenon in laser physics. Clear experimental evidence of multistability in physical systems was first shown by Arecchi et al. in a modulated CO_2 laser [6]. They referred to the coexistence of oscillatory attractors as *generalized multistability* in order to distinguish it from the ordinary coexistence of stationary solutions [58], e.g. optical bistability, where two dc output amplitude values appear for a single dc driving amplitude [59]. Since then, multistability has been detected in other types of lasers, including a Nd:YAG (neodymium doped yttrium aluminum garnet) laser with intracavity second harmonic generation [60], semiconductor [61–64], and fiber [63,64] lasers.

A particular kind of multistability, *spatial multistability* has also been observed in a laser. This multistability appears in the transverse spatial patterns due to the interaction of the cavity modes [65]. To describe spatial multistability in optical patterns, Brambilla et al. [65] established a general connection between laser physics and hydrodynamics by reformulating the laser dynamical equations in a similar form of a compressible fluid hydrodynamical equations, i.e. the mass conservation law and the Bernoulli equation. Two-dimensional optical patterns can also appear as a consequence of phase-locking of several wave vectors with different lengths and orientations [66]. Multistability of the patterns is considered to be a very promising phenomenon for information processing, associative memories, and pattern recognition [67].

1.1.5. Multistability in semiconductor materials

Semiconductor superlattices are known to give rise to a variety of different dynamical regimes related to negative differential conductivity. The electric field domain formation in weakly coupled superlattices leads to a hysteresis in the current–voltage phase space that is associated with multistability in the current [68]. Experimentally, when the voltage is swept in a well-defined manner, coexisting stable current values have been obtained. This phenomenon has already been simulated by simple theoretical models that give a qualitative accurate description of the effects of electric field domain formation [69,70]. A THz radiation applied to such a superlattice leads to new regions of photo-induced multistability caused by the interplay of nonlinear properties of the semiconductor superlattice due to the Coulomb interactions and the photon-assisted channels [71].

It was shown that the negative differential conductivity, by inducing a current flow between a contact in the center and a circular ring electrode, often gives rise to the formation of multiple current filaments in n-GaAs Corbino disks [72] which mimic semiconductors without lateral boundaries. Both theoretical and experimental studies have demonstrated the coexistence of several different filamentary patterns for the same bias voltage [73].

Multistability also appears in nanometer-scale semiconductor heterostructures as differently quantized charge distributions and can be controlled by external laser pulses [74].

1.1.6. Multistability in chemical reactions

Several chemical reactions exhibit different dynamical behaviors; periodic, quasiperiodic, and chaotic orbits have been found in continuously stirred tank reactors [75,76], as well as in the transients of batch reactors [77]. Besides, bistability has been observed in several oxidation reactions [78]. The coexistence of more than two attractors has been reported for the steady state behavior of a circular and a linear array of three photosensitive biochemical reactor cells connected by diffusion [79]. In each of the reactors, a nonlinear photo-biochemical reaction takes place where nonlinearity arises from

two different processes, namely, the consumption of the substrate by the photochemical reaction and the light absorption by the substrate. The coexistence of several steady states in this reaction has been shown both theoretically and experimentally in certain parameter ranges. Furthermore, coexisting states have been found in arrays of diffusion coupled flow reactors, where in each reactor a bistable chemical reaction occurs [80].

Even more complicated behavior has been observed in the chlorite–thiosulfate [81] and chlorite–iodide reactions [82]. Both reactions are characterized by a remarkable irreproducibility in the behavior; despite the experimental care to ensure the same outcomes, for the same setup and experimental conditions, the long-term behavior varied from trial to trial. This apparently random behavior is related to *uncertain destination dynamics* [83] (cf. Section 2.1.5), the possible underlying mechanism for this irreproducibility may be an extreme sensitivity to initial conditions.

Multistability is not only be found in coupled reactor systems, but also in spatially extended reaction–diffusion systems. Coexisting spatially inhomogeneous states have been identified in hexagonal and square Turing superlattice patterns [84] in a photosensitive reaction–diffusion system [85]. This multistability can be employed to create multiple adjacent spatial domains with diverse geometries and stationary frontiers between them.

1.1.7. Multistability in ecosystems

Several ecosystems have been shown to possess two or more alternative states [86,87]. Studies of the emergence of such alternatives states and their consequences in terms of possible regime shifts or bifurcations in ecological systems, ranging from coral reefs [88,89] and deserts [90] to lakes [91] and tidal flats [92,93] have proliferated in the last decade. Ecological systems are networks of species organized in different trophic levels, where the interplay of species is basically determined by predator–prey interactions and food competition. Such alimentary webs usually possess a complicated interaction structure that yields a variety of equilibrium states related to sets of different proportions of coexisting species, i.e. different species community compositions corresponding to different levels of biodiversity. In the field, states with low biodiversity are usually considered undesirable and should be avoided. The coexisting species can be characterized by highly complicated fractal basins of attraction of the various equilibria; a minute perturbation is sufficient to cause a shift in biodiversity because of a transition to a state where some species have died out [94]. As a result, one has to deal with a fundamental long-term unpredictability of the species composition in multi-species ecosystems.

Since ecological systems often cannot be considered as spatially homogeneous, one has also to include influences like landscapes with different environmental conditions leading to heterogeneous forcing, as well as dispersal of the species in space. The corresponding pattern formation phenomena also lead to multiple patterns which are related to different relative abundances of the species in space. In some instances, such as biogeochemical models describing the degradation of organic matter by bacteria in marine sediments [95] or to the emergence of vegetation patterns in semiarid areas [96,97], inhomogeneous patterns can be explained by Turing instabilities.

1.1.8. Multistability in neuron dynamics

Multistability has been proposed as the basic mechanism for associative content-addressable memory storage and pattern recognition in both artificial [98] and living neural systems [99]. The coexisting attractors mimic different brain states representing particular objects of perception which can be selected by giving the neural network some input corresponding to an initial condition. This corresponds to a parameter-independent mode-switching mechanism with fixed parameter values, as opposed to a parameter-dependent one based on changing parameter values, such as synaptic couplings [100].

Based on the physiology of neural systems, various dynamical concepts, such as time delay [101], phase locking patterns [102], etc., have been introduced to explain their multistability. Delayed recurrent neural loops has been studied by Foss et al. [11] as a possible mechanism leading to a multistable behavior. They investigated the dynamics of a recurrent inhibitory loop consisting of two coupled neurons: an excitatory neuron that transmits a signal to an inhibitory neuron which in turn inhibits the excitatory neuron firing. This inhibitory effect depends on the delay time τ needed for the signal to travel along an axon and dendrites. Using both an integrate-and-fire model and a Hodgkin–Huxley type model, different kinds of multistability corresponding to different firing patterns have been found without a delayed feedback, depending on the nature of firing (excitatory or permanent firing). An experimental realization of this kind of multistability has been reported for slowly adapting periodically spiking *Aplysia* motoneurons [103].

On the level of a single neuron, multistability is represented by the coexistence of basic firing patterns, like silence, spiking, regular, and chaotic bursting [104]. When noise is imposed, neurons can switch between the different firing patterns which can be interpreted as a *dynamic short-term memory* [105]. A similar behavior was observed for coupled entire networks of integrate-and-fire neurons [106]. The analysis of multistable networks merits a significantly different treatment [107]. Noise-driven switching between oscillatory states with different low and high frequency firing rates has also been found in a globally coupled (excitatory and inhibitory) FitzHugh–Nagumo oscillators network [108]. The state selection depends on the external input applied as a forcing. By means of an optimal noise level, the system demonstrates a considerably improved coherence between the external forcing and the mean firing rate similar to the stochastic and coherence resonance phenomena [109,110].

In neural networks, multistability and particularly bistability play an important role in cell signaling and in neuronal interactions [34,35,111]. Communication between cells takes place at synaptic contacts, where an arriving action potential releases a neurotransmitter, thus affecting the post-synaptic potential of the target cell. Typically, each cell receives input

from thousands of cells mediated by many different neurotransmitters, and consequently modifying the post-synaptic potential by excitation or inhibition [55]. The role of multiple dynamical regimes in neuronal interactions has also been examined both theoretically and experimentally [111].

A dynamical model for the pattern of contour detecting neurons in the visual cortex has been developed by Wolf [112], who introduced a permutation symmetry which guarantees the emergence of contour detectors for all stimulus orientations. The theory predicts a novel discrete multistability of visual cortical pattern formation. It is intimately linked to the functional requirement of representing all stimulus orientations. This kind of multistability is suspected of having profound implications for visual development and plasticity. When it is encountered in visual cortical circuits, biological factors, such as genetic information, spontaneous activity patterns, and visual experience are the elements that help in the selection of structured orientation representation choosing from a discrete repertoire of stable patterns; this emergent collective property describes the cortical learning dynamics.

1.1.9. Multistability in climate dynamics

Since the climate is regulated by numerous natural parameters and characterized by various state variables, many previous studies support the idea of a multistable character of climate dynamics emphasizing that a climate change can appear as a shift in the preference of some coexisting attractors or climate regimes [113–116]. Transitions between different dynamical regimes and their corresponding critical thresholds for environmental parameters (sometimes called *tipping points*) are of increasing interest in climate studies [117,118]. Coexisting attractors, mostly alternative states related to bistability, have been obtained in deep ocean convection [119–121], atmosphere variability [122], ice sheet dynamics [123,124], and Sahara desertification [90]. In each of these phenomena, the sizes of the basins of attraction of the possible states may vary dramatically; a particular state is determined by initial conditions and may undergo a major change due to noisy environment, e.g. random fluctuations in wind direction, atmospheric pressure, and temperature.

Multistability with more than two different stable states has been observed in the thermohaline ocean circulation (THC) model [125–128]. The THC is a large scale circulation around the globe, that is particularly important in the Atlantic ocean. This circulation driven by density gradients between the Southern and the Northern hemispheres, accounts for the relatively warm climate in Northern and Western Europe compared to the climate in North America at the same latitude. The THC is responsible for a considerable heat transport to Northern latitudes. Simulations using a global ocean circulation model yield different stable states corresponding to different strengths of the overall circulation towards the North Atlantic [120,128,129]. These states are related to distinct sites in the ocean, where the heat is released into the atmosphere and deep ocean convection occurs. One of these stable states is associated with a breakdown of the THC, i.e., the interruption of the heat transfer to Northern latitudes will lead to a dramatic climate change in Europe. This can be regarded as one example of a multistable system, where at least one of the stable states is undesired and needs to be avoided at all costs.

1.1.10. Multistability in social systems

Nowadays, in the epoch of social networks, the understanding of dynamical processes in social–political systems is extremely important. Many researchers seek a comprehension of how societies move towards consensus in the adoption of ideologies, traditions, and attitudes. The dynamics of social networks explains how one individual adopts a new state in behavior, opinion, or consumption through the influence of others. Since opinions spread through social contacts, competing states are an intrinsic part of society.

A simple example of bistability in social competition is the naming game [130], where two words compete across an intermediate state and agents accept both words [131]. Multistability has been introduced in the network model [132], where the agents represented by vertices are allowed to have one of several opinions each. These opinions are updated by voter dynamics of the network. Moreover, agents accept connections with other agents provided they have equal opinions. When links are removed and disconnected agents are assigned to have new opinions randomly, the model has multiple solutions with a mixed metastable state of the disconnected agents, this corresponds to a dissolved society.

In the model introduced by Sneppen and Mitarai [133], states or species compete and exhibit multistability through combinations of antagonistic conversions. In the context of a society with antagonistic political fractions, the mixed metastable state may be associated with a representative democracy with many balanced interest groups, while the extreme states correspond to a one-party system.

2. Multistability emergence and control goals

As illustrated in the previous chapter, multistability is a widespread general phenomenon. Accordingly, there is a wide variety of reasons leading to the coexistence of multiple stable states in a complex system. In the following we will discuss the most important known mechanisms for multistability emergence in dynamical systems. These are weak dissipation, homoclinic tangencies, coupling, delayed feedback, and random perturbations. Each of these processes has particular properties which can partly be used to design a control strategy.

Controlling complexity of dynamical systems is a fascinating challenge that will prove to have many applications. Each application implies different difficulties to be solved. Before formulating control goals, it would be wise to take a closer look at the dynamics of multistable systems in reality.

2.1. Mechanisms for multistability

Though mechanisms for multistability emergence can be rather different, the overall behavior of systems with multiple coexisting attractors is quite similar. They are characterized by a high degree of complexity in their behavior due to the "interaction" among multiple states. Firstly, the dynamics of a multistable system is extremely sensitive to the initial condition; because of a large number of different coexisting attractors, very small perturbations in the initial condition may cause an enormous change in the final state. This final state sensitivity is especially pronounced when the basins of attraction are complexly interwoven. Secondly, the qualitative behavior of the system sometimes changes dramatically under a small variation of the system parameters; the parameter space where multiple states are stable can be so small that a slight change in a control parameter may cause a huge change in the number of coexisting attractors, i.e., attractors appear and disappear quickly when a system parameter is varied.

Such a behavior poses particular difficulties for the multistability control. While designing a control strategy, one has to ensure that the parameter variation due to the control does not drastically change the system, meaning that only small control impacts are desirable in many cases. On the other hand, the extremely high sensitivity to perturbations possibly leading to a different state needs a special care when designing an adequate control technique.

2.1.1. Weakly dissipative systems

One of the easiest ways to construct a class of multistable systems is to take a conservative system and add a small amount of dissipation. Conservative systems are characterized by two types of dynamics: regular motion and Kolmogorov–Arnold–Moser (KAM) tori in the hierarchy of islands which are embedded in a phase space chaotic sea. Introducing a small damping ν which turns the islands into sinks and the permanent chaotic motion into transient chaos [134], one can obtain systems with an arbitrarily large number of coexisting attractors since their number scales roughly with $1/\nu$ [135]. Dynamics in this system class is dominated by regular motion, i.e., almost all attractors are periodic orbits with mainly low periods. High-period orbits have very small basins of attraction and therefore it is very difficult to find them.

One of the simplest systems which exhibits coexistence of attractors is the dissipative standard map of a periodically kicked rotor without gravity. This map can be considered as a paradigm to explain the emergence of multistability in a weakly dissipative system. If there is no damping in the pivot of the rotor, this system displays infinitely many marginally stable periodic orbits. When a small amount of damping is added, the map is described by

$$x_{n+1} = x_n + y_n \bmod 2\pi, \tag{1}$$

$$y_{n+1} = (1-\nu)y_n + f_0 \sin(x_n + y_n), \tag{2}$$

where x is the phase variable and y is the angular velocity. The map dynamics depends on both the kick strength f_0 and the damping ν. When the damping is introduced, the marginally stable periodic orbits turn into sinks. As a result, though the number of marginally stable orbits is believed to be infinite in the conservative case, the number of attractors in the dissipative case is finite [135].

Another intriguing feature of this class of systems is that chaotic attractors are rare because their existence intervals and their small basins of attraction shrink to zero in the conservative limit along a certain path in parameter space [136]. For periodic orbits, another path can be found where the same behavior is encountered [137]. For sufficiently small dissipation, it is possible to obtain the coexistence of a very large number of attractors, which are mainly low-period periodic orbits. This phenomenon was found in the single and double rotors, optical cavity map, and Hénon map [135,138,139].

The coexisting stable periodic orbits have a complex interwoven structure of their basins of attraction with basin boundaries permeating most of the state space. In fact, when estimating the box dimension of the union of all basin boundaries, the result is very close to the state-space dimension, i.e., most of the state space is indeed filled with boundary points [135]. Although the attractors are mainly periodic orbits and hence correspond to regular motion, this does not preclude these systems from showing a chaotic behavior. The chaotic component of its dynamics manifests itself as transient chaos because it is found in chaotic saddles embedded in basin boundaries. Due to the complexly interwoven basins of attraction, such systems are highly sensitive to a small amount of noise [140,141].

In particular, weakly dissipative systems can be considered as an important class of highly multistable systems occurring in many mechanical systems, such as mechanical oscillators [142] and suspension bridges [143]. One can argue that the two attributes, namely, accessibility to many different states and high sensitivity, are an asset in the sense that they are suitable for easy control of the complex system. The transition between different stable states poses however a delicate problem in view of long chaotic transients in the basin boundary. This is the problem of migration between different coexisting states and their stability [144,145].

2.1.2. Gavrilov–Shilnikov–Newhouse sinks

Another important mechanism leading to multistability is the appearance of homoclinic tangencies and their stabilization by small perturbations or by coupling of systems possessing a large number of unstable invariant sets. Contrary to earlier conjectures that generic systems might have only finite number of attractors, Gavrilov, Shilnikov [146], and Newhouse [147–149] have proved that a class of diffeomorphisms in a two-dimensional manifold has infinitely many attracting periodic orbits (sinks), a result later extended to higher dimensions [150]. Models of such diffeomorphisms have been

constructed by Gambaudo and Tresser [151]. Later, Wang [152] has proved that the Newhouse set has a positive Hausdorff measure.

After publication of these results, intense studies have been devoted to the unfolding of homoclinic tangencies and the essential question arose: whether in addition to infinitely many sinks, there would also be infinitely many strange attractors near the homoclinic tangencies. The positive answer to this question was given by Colli [153]. Having established the existence of infinitely many sinks and infinitely many strange attractors near homoclinic tangencies, the important practical problem that presented itself has been the stability of these attractors under small random perturbations. Scientists are still looking how to give robustness to the system subject to small noise, so that the set of attractors remains infinite.

The complexity of weakly dissipative systems has been studied in detail by Goswami [154], who showed that the appearance of period-n solutions in a periodically forced system can be explained in terms of harmonic and subharmonic resonances. This phenomenon is related to the emergence of Gavrilov–Shilnikov–Newhouse sinks in the neighborhood of homoclinic bifurcations. If a control parameter is varied in the neighborhood of a homoclinic tangency of a first-order (e.g. period-1) saddle, first-order secondary Newhouse sinks are born. In a similar way, higher-order secondary Newhouse sinks around the first-order secondary sinks appear. As a result, the whole bifurcation structure exhibits self-similarity in parameter space [155,156]. Moreover, the basins of attraction of these higher-order Newhouse sinks are organized so that they are progressively intertwined with the basins of attraction of lower-order sinks.

2.1.3. Coupled systems

Multistability often arises in coupled systems due to an increase in complexity when two or more systems are joined. The emergence of multistability depends strongly on the kind of coupling (linear or nonlinear, unidirectional or mutual) and on the coupling strength. As expected from the consideration in Section 2.1.1, coupling of weakly dissipative systems leads to a very large number of coexisting attractors [135].

Multistability in coupled systems is often accompanied by the loss of synchronization. This was observed in the coupled logistic maps [157], Hénon maps [158,159], genetic elements [45], mutually coupled semiconductor lasers [160], and ensembles of coupled oscillators where cluster formation was demonstrated [161,162]. In the latter, the number of attractors increases drastically as the number of oscillators increases, resulting in *attractors crowding* in phase space. In their study of coupled Josephson junctions and coupled circle maps, Wiesenfeld and Hadley [163] found out that in both cases the number of stable limit cycles scales as $(N-1)!$, where N is the number of oscillators. The attractor crowding makes these systems extremely sensitive to noise-driven hopping among many coexisting states.

Multistability is also found in spatially extended coupled systems, including both, dynamical systems containing diffusively nearest-neighbor coupled identical elements and systems with global coupling where each element is coupled to any other. A high degree of multistability exists even in very simple models, namely, coupled map lattices [164] in which the coupling forms clusters where all elements exhibit the same dynamics, thus resulting in a multitude of coexisting attractors. The classification of emerging patterns in the globally coupled map lattice includes coherent, ordered, partially ordered, and turbulent phases [164] according to the number of clusters and their basins of attraction. It has been shown that the number of attractors is larger when the coupling strength between the elements in the lattice is small, that is again the consequence of weak dissipation.

A particular type of multistability, *phase multistability*, when stable synchronous regimes with different phase relationships between oscillations coexist, has been found in coupled oscillators. Phase multistability was first observed for diffusively coupled oscillators which individually follow a period-doubling route to chaos [165,166]. The number of coexisting regimes at the chaos threshold inside the synchronization region for a weak coupling may be huge. The coexistence of periodic regimes with different phase shifts has also been found in two coupled Rössler oscillators [167]. Some period-doubling bifurcations are replaced by torus (Neimark–Sacker) bifurcations leading to the emergence of new, non-symmetric families of attractors [168].

2.1.4. Delayed feedback systems

Multistability often appears in systems with time-delayed feedback. This mechanism predicted by Ikeda [169,170] was experimentally confirmed, first in an electro-optical bistable device with a computer delay [171], and then in a laser diode-pumped hybrid bistable system, where a very large number of multistable self-oscillatory modes have been observed at a long delay time [172]. These systems are commonly described by delay differential equations $\dot{x} = f(x(t), x(t-\tau))$. While without delay in the feedback the system is monostable, the system with delayed feedback becomes multistable. The number of coexisting attractors, usually periodic orbits, depends on the delay time. The necessary condition for the emergence of new stable periodic orbits is that the delay time τ has to be larger than the system response time [170,173].

This type of multistability was found in the Rössler oscillator [174], electronic circuits [175], CO_2 [176] and semiconductor [177] lasers, and in neuron models [11]. Multistability induced by delayed feedback was also studied in discrete-time dynamical systems, such as the logistic and Hénon maps [176,178,179]. Besides, locally coupled maps and globally coupled systems with time delay also exhibit the coexistence of attractors [180].

2.1.5. Extreme multistability

The phenomenon of extreme multistability or the coexistence of infinitely many attractors for a given set of parameters has been found in two system classes, namely, in forced systems, where a dissipative system is forced by a conservative

system [181], and in coupled systems with a specific type of coupling [83,182]. In both cases, multistability does not arise due to bifurcations, where new attractors are born as a control parameter is varied, but infinitely many attractors appear suddenly.

To show how one can get a forced system exhibiting infinitely many attractors, Lai and Grebogi [181] considered skew product dynamical systems in which a conservative (Hamiltonian) system acts as a driver for a dissipative system. They called such systems *Hamiltonian-driven dissipative dynamical systems* and showed that in this class of systems an infinite number of distinct attractors coexist. The attractors can be either quasiperiodic, strange non-chaotic, or chaotic with different positive Lyapunov exponents. Specifically, they studied the following general class of N-dimensional discrete maps in $\mathbf{R}^N$:

$$\begin{aligned}\mathbf{x}_{n+1} &= \mathbf{f}(\mathbf{x}_n),\\ \mathbf{y}_{n+1} &= \mathbf{F}(\mathbf{x}_n, p)\mathbf{G}(\mathbf{y}_n),\end{aligned} \tag{3}$$

where $\mathbf{x} \in \mathbf{S} \subset \mathbf{R}^{N_S}$, $\mathbf{y} \in \mathbf{T} \subset \mathbf{R}^{N_T}$, $N_S \geq 1$, $N_T \geq 1$, $N_S + N_T = N$, and p is a parameter. The conservative dynamics of the area-preserving map $\mathbf{x}$ takes place in the invariant subspace $\mathbf{S}$. Therefore, every initial condition starting in $\mathbf{S}$ results in the trajectory which remains in $\mathbf{S}$ forever.

The dynamics of $\mathbf{y}$ occurs in the subspace $\mathbf{T}$ that is transverse to $\mathbf{S}$. The functions $\mathbf{F}(\mathbf{x}_n, p)$ and $\mathbf{G}(\mathbf{y}_n)$ were chosen so that the magnitude of the determinant of the Jacobian matrix $|DJ_y| \equiv |\partial \mathbf{y}_{n+1}/\partial \mathbf{y}_n|$ is less than one, in some phase–space regions. Thus, the dynamics in the transverse subspace is dissipative and hence the whole system is also dissipative. The driving variable $\mathbf{x}$ exhibits different kinds of dynamics, e.g. quasiperiodic motion on KAM tori or chaotic motion, so that every initial condition in $\mathbf{x}$ gives rise to a different forcing and, due to the skew product structure, to a different attractor in the full phase–space. This is a way to obtain a system with infinitely many attractors.

While the observed complexity in the Hamiltonian system is a direct consequence of the Hamiltonian phase–space structure that typically contains chaotic components and hierarchies of KAM islands, the introduction of dissipation in the transverse direction gives rise to much richer dynamics. The quasiperiodic motion on KAM surfaces in the invariant subspace can lead to quasiperiodic, strange non-chaotic, and chaotic attractors in the full phase space. Moreover, chaotic motion in the invariant subspace can induce chaotic attractors with different positive Lyapunov exponents.

Another kind of extreme multistability has been discovered by Sun et al. [83] who demonstrated that two identical coupled systems, e.g. Lorenz systems coupled in a determined way, exhibit an infinite number of coexisting attractors. One such coupling for the Lorenz systems has been designed as follows

$$\dot{x}_1 = \sigma(y_1 - x_2), \tag{4}$$
$$\dot{y}_1 = rx_1 - y_1 - x_1 z_1, \tag{5}$$
$$\dot{z}_1 = x_1 y_1 - b z_1, \tag{6}$$
$$\dot{x}_2 = \sigma(y_2 - x_2), \tag{7}$$
$$\dot{y}_2 = rx_1 - y_2 - x_1 z_2, \tag{8}$$
$$\dot{z}_2 = x_1 y_2 - b z_2. \tag{9}$$

Note that the x variable from the second system enters the first equation of the first system, while the x variable from the first system enters both the second and the third equations of the second system. This leads to a somewhat unusual coupling which gives rise to a rather complicated dynamics.

The two coupled systems exhibit generalized synchronization in the long-term limit in such a way that the y and the z components are completely synchronized, while the x components of the two oscillators keep a certain distance c. The value of c is an arbitrary real number which is determined by the initial conditions in an intricate way. The dynamical problem is better solved in terms of error variables which measure the distance from the synchronization manifold: $e_1 = x_1 - x_2$, $e_2 = y_1 - y_2$, and $e_3 = z_1 - z_2$. The error dynamics is then written as

$$\dot{e}_1 = \sigma e_2, \tag{10}$$
$$\dot{e}_2 = -x_1 e_3 - e_2, \tag{11}$$
$$\dot{e}_3 = x_1 e_2 - b e_3, \tag{12}$$

where the phase–space trajectory converges to the fixed point $(e_1^*, e_2^*, e_3^*) = (c, 0, 0)$, whose stability can be proven using the Lyapunov function $V = e_2^2 + e_3^2$. To be more specific, this describes a continuous set of fixed points, depending on the real value of the constant c. The constant c is a conserved quantity that determines the synchronization manifold in which the long-term limit dynamics takes place. In fact, as $t \to \infty$ the state space is foliated into infinitely many such synchronization manifolds, each with at least one attractor. The dynamics of such a system reminds us a lot of the conservative systems dynamics, where for each value of the conserved quantity, e.g. energy, another behavior appears. However, it is important to underline a fundamental difference; in the case of extreme multistability this conserved quantity is not given at very beginning, but does evolve in time as the two systems are synchronized. This kind of complex dynamics is observed in chemical models [183] and in two coupled autocatalator systems with generalized synchronization [182].

The general approach to designing a coupling which leads to extreme multistability has been recently developed by Hens et al. [184] who explored two Rössler oscillators. They have shown that extreme multistability is possible in any two identical chaotic systems with a specific type of coupling.

2.1.6. Multistability induced by parametric forcing

Another mechanism for multistability emergence is a weak periodic perturbation imposed to one of the system parameters. This route to multistability can be observed in a wide class of nonlinear driven systems which display a Feigenbaum cascade to chaos via period-doubling bifurcations. A classical example is the quadratic map $x_{n+1} = \lambda - x_n^2$ (λ being the map parameter and $n = 0, 1, 2, \ldots$), in which Sanju and Varma [185] demonstrated the appearance of bistability when the additive forcing $\epsilon \cos(2\pi j/p)$ (ϵ being the amplitude of forcing and $j = 0, 1, \ldots, p-1$) with period $p = 2$ was added. Furthermore, they found that the forcing with $p > 2$ can induce multistability. If the map is in the period n, it will possess k complementary n/k-period attractors, where k is the highest common factor of p and n.

Dynamical bistability induced by harmonic parametric forcing was demonstrated in the logistic map [186], the Hénon map [187], and a loss-driven CO_2 laser with modulated cavity detuning [188,189]. It was shown that the parameter modulation stabilizes unstable periodic orbits by shifting period-doubling bifurcation points. The new, shifted positions of the bifurcation points depend on the parameters of the external modulation or forcing, in particular, on its frequency and amplitude. Bistability induced by a resonant perturbation at the first subharmonic frequency has been observed in a loss-modulated CO_2 laser [190,191] and in a fiber laser with dual-frequency modulated pumping [192]. Chizhevsky [193] has shown that in the laser driven at frequency f_d, an additional weak modulation at frequencies f_d/n ($n = 3, 4, 8, 16, \ldots$) induces up to n coexisting attractors for certain system parameters. The external periodic forcing increases the system dimension by one leading to the appearance of multistability. Since the modulated CO_2 laser can be considered as a nonautonomous system with a Toda potential [194], a similar behavior is expected in a large class of periodically forced asymmetric nonlinear oscillators.

2.1.7. Noise-induced multistability

Some studies demonstrate that multistability can be induced by noise. Such an effect has been found in systems of coupled oscillators [101] and in a field-dependent relaxation model [195,196]. The oscillations created by noise have statistical noise-dependent properties and can be considered as a motion on a stochastic limit cycle with the corresponding noise-induced eigenfrequency. In a globally coupled oscillator system, noise with a critical intensity induces a subcritical saddle–node bifurcation from an asymmetric state to a symmetric state leading to multistability. It was observed [101] that the system subject to noise with a finite correlation time exhibits not only ordered and disordered phases but also a multistable phase of ordered and disordered states. The number of transition points for triple transitions, disordered phase → ordered phase → multistable phase → disordered phase, increases as both the correlation time and the coupling strength increase.

This phenomenon may well awaken a renewed interest linked to memristive systems, like resistors with memory, called memristors, whose resistance varies according to the voltage applied to them or the current flowing through them [197]. The distinctive feature of all memristive systems is the frequency-dependent pinched hysteresis loop. Recent studies show that such dynamical bistability (stochastic memory) can be induced by white noise of appropriate intensity [198].

Noise-induced bistability has also been found in a system of mutually coupled semiconductor lasers where random spontaneous emission stabilizes an unstable fixed point which coexists with a chaotic regime [160].

2.2. Why we need to control multistability

Experimental and real-life systems are always subject to different kinds of noise. These random perturbations which are inevitable can be either intrinsic fluctuations or externally imposed random signals. Due to the noise influence, a multistable system becomes metastable, because the random perturbations kick the system out of the neighborhood of attractors and initiate a transition to another coexisting state. This noise-induced attractor hopping leads to an overall motion of the system which consists of two phases: a regular one in the neighborhood of attractors and a chaotic one which corresponds to the transitions between attractors taking place on the chaotic sets embedded in the fractal basin boundaries. The time needed for the transition depends crucially on the structure of the basin of attraction; in particular, for fractal basins only very small perturbations are sufficient to initiate a jump to another metastable state. Moreover, in highly multistable systems this hopping dynamics often includes only a small fraction of all possible attractors [140,141]. The ones with the smaller basins of attraction are usually "buried" under the noise, i.e., the trajectory will not stay in their neighborhood forever. This high sensitivity to perturbations enriches the system dynamics and plays an important role in formulating various control aims.

First, for some applications multistability is an undesirable behavior of a system. If the system is designed to remain at a certain dynamical state, a perturbation-induced jump to a coexisting state may change the performance and spoil the reproducibility and hence reliability. Furthermore, as previously mentioned, the control problem very often becomes even more involved when the basin boundaries are fractal [199]. In this case, two control strategies are possible. On the one hand, a control is needed to stabilize the system against noise and keep it in a particular preselected attractor. On the other hand, an external forcing can be applied with the aim of making the system monostable with only one global attractor conveniently chosen in advance.

Second, for a system that has to preform different tasks it is highly advantageous that it possesses a multitude of coexisting states assuming that each state corresponds to a particular task. In that case, the control aim is to enable the system, without changing the setup, a well-defined switching between different states (tasks) on demand. Two different goals, closely related with the problem of attractor switching, can be formulated: (i) attractor selection, i.e. choosing a desired attractor to which the system should converge, and (ii) attractor avoidance, i.e. the exclusion of certain undesired attractors

from the dynamics. It should be noted that multiple coexisting attractors can be created or destroyed simultaneously in multiple choice bifurcations [200]. These bifurcations are so sensitive to noise that the trajectories are unpredictable when a system parameter is slowly varied through the bifurcation point. This dynamical determination demands an appropriate control of the system.

Like in any other control theories (e.g. conventional linear and nonlinear control), we can distinguish two types of control: feedback and nonfeedback control. Also, stochastic control of multistability will be considered separately as a particular type. The control of multistability may have different goals: (i) stabilization of particular attractors in the presence of noise, (ii) directing a system to a desired attractor (targeting methods) or control of switches between attractors, (iii) destabilization of undesirable attractors to transform a multistable system into a monostable one (attractor annihilation), (iv) a change in the attractor character, e.g. converting a fixed point into a periodic orbit with different stability, (v) a change in the attractor preference, i.e. a change in the volume of basins of attraction of coexisting states or the probability of their appearance (statistical stability) in the presence of noise.

Next, we outline very briefly some important applications where the control of multistability could be useful.

2.2.1. Laser technology

Fast development of laser technology faces important technological problems which require multistability control. One famous example is the so-called "green problem" [60] present in the operation of an intracavity frequency-doubled Nd:YAG laser. Usually, this laser emits infrared light, that can be converted into visible green light by using a nonlinear optical crystal. The nonlinear coupling between modes in the crystal gives rise to irregular fluctuations in the optical cavity, that are amplified by the quality factor Q of the laser cavity and by the presence of the laser amplifier media. For practical applications, this clearly undesirable for the laser performance. The irregular behavior of the intensity of this laser has been widely investigated and has been associated with the destabilization of relaxation oscillations, always present in this kind of systems. Such a behavior is attributed to the coexistence of multiple attractors which often appear in a system with many degrees of freedom. The irregularity in the laser intensity results from involuntary switches between the coexisting states, so that additional stabilization mechanisms like a feedback control need to be applied to obtain a stable output [201]. However, the feedback signal itself induces multistability that has to be tackled by a control strategy to reach monostability.

2.2.2. Optical communication

In modern fiber communication technology, to transmit a signal through a lightwave carrier semiconductor and fiber lasers are used. These lasers are nonlinear systems which can exhibit multistability when coupled or subject to external driving [63,64,202–206]. This again is an example, where multistability is undesirable because it hinders efficient communication and therefore it has to be avoided.

2.2.3. Cardiology

Deterministic nonlinear dynamics approach has entered in various medical disciplines. Particularly, in physiology the transition from normal cardiac rhythm to arrhythmia has been observed to follow a period-doubling route to chaos [207]. Cardiac alternation of period-1 with period-2 rhythms could be a precursor to arrhythmia and therefore, efforts have been made to design some kind of control [208]. Indeed, chaos control [209] and tracking technique [210] have been successfully applied to suppress cardiac alternance and thus stabilize the cardiac rhythm in the period-1 state [211]. Moreover, cardiac dynamics is known to exhibit multistability in some pathologies. As the cardiac rhythm increases, the probability of emergence of higher periodic orbits, including a chaotic one, also increases. Notably, under certain circumstances, a stable period-2 rhythm coexists with a stable period 1 [212]. It is evident that bistability and multistability in cardiac rhythm are undesirable, in such cases forwarding the trajectory of the cardiac rhythm back to the stable period 1 is an attractive proposition.

2.2.4. Brain diseases

In diseases like Parkinson and epilepsy, it is quite possible that undesirable dynamical states coexist. If that is so, the objective in brain medicine would be to switch the brain dynamics from those undesirable sick states to a normal one, even better would be the avoidance of such undesired states before a crisis happens. Since in biological systems it is hardly possible to change system parameters, the application of the control techniques using, for instance, short pulses or periodic forcing may be a good solution. Therefore, we suspect that to control brain multistability only external signals will have to be used.

Theoretically, a proper change in initial conditions is sufficient to change an attractor. Such a change can be realized, for example, by the nonfeedback control method of a short external impact proposed by Chizhevsky et al. [213,214] that will be described in Section 3. However, a direct implementation of this method for medical systems is a dangerous task. The situation gets worse because the lack of sufficient information about the true nature of brain multistability makes difficult the construction of a good theoretical model.

2.2.5. Genetics

As outlined in Section 1.1.2 multistability is considered to play an important role in genetic circuits. The capability of cells to present different stable expression states while maintaining identical genetic content plays a significant role in

differentiation, signal transduction and molecular decision-making. These epigenetic phenotypes are partly associated with changes in genomic structural features, including several types of chromatin and DNA modifications [215]. In some cases they are induced by the action of underlying genetic regulatory circuits, exhibiting a positive feedback loop configuration. The molecular circuits with positive feedback can induce two different gene expression states (bistability) under the same cellular conditions [216,217] and in addition, the circuits display some degree of nonlinearity, i.e. sigmoidality, on their constituent interactions [55,218,219]. Both the positive feedback and sigmoidality endow these genetic modules interpreted as multistable dynamical systems with the possibility to find the system in alternative steady states under conditions in which all its biochemical parameters are fixed. These different stable expression states are regulated by molecular loops. The process by which the cells take advantage of the coexistence of many stable states (attractors) is today largely unknown. Many such decisions have been directly linked to survival, as the sporulation/competence choice in the bacterium *Bacillus subtilis*, and are probably involved in the establishment of developmental programs from pluripotent stem cells. The crucial question is: How are these decisions controlled at the molecular level?

Small gene networks, either synthetic [216,220] or natural [217,221], with mutual regulation of genes have recently been studied and shown to be able to generate multiple attractor states. Some attractor states appear to provide an optimal gene expression program for the cell adaptation to a particular, rare environment, yet no specific signaling pathway to connects this rare external condition with the appropriate genetic program has been found. Kashiwagi et al. [222] showed that cells can select the adaptive attractor and proposed that this selection process was a general consequence of the stochastic nature of gene network dynamics. The challenge is now to understand the control mechanisms of the cells that switch to the adaptive attractor state of the network to express the appropriate genes in the case of rarely occurring environmental changes. The external control has to be written in form of some input that would lead to attractor selection and a defined switching. Even for frequently occurring environmental changes, attractor selection can be beneficial for cells since it requires no specific signal transduction apparatus. Due to its stochastic nature, attractor selection may prevent cells from dying in fluctuating environments. Attractor selection may facilitate the design of a network that can robustly respond in an adaptive manner to unknown environmental changes without requiring a large number of specific sensors and transducers. It may also be viewed as a sort of Darwinian preadaptation for the evolution of signal-specific transduction pathways when a particular new environmental condition becomes dominant and hence contributes to evolvability [222].

2.2.6. Ecology

There are also situations when only some of the coexisting states of a system correspond to a desired behavior while others do not. The latter ones might be harmful or even fatally dangerous, hence they should be avoided under any circumstances. To exemplify such a situation let us take an ecosystem where different species compete for the same resources [223], then only a few states or even worse, only one state allows the system to be permanent, i.e., enables all occurring species to coexist on the resources provided by nature. In most alternative states, some species die out meaning that these states relate to a lower degree of biodiversity. Any anthropogenic manipulation of our natural environment should avoid perturbations leading to such states.

In case that an undesired state has already occurred, the control problem is to switch back to the original state if possible. Such control strategies have been implemented in the case of shallow lakes exhibiting two states [91]: a clear water state with large water plants (macrophytes) on the bottom of the lake and a turbid phytoplankton dominated state. Based on a theoretical investigation of the system feedbacks, a bio-manipulation scheme has been developed and successfully applied to several lakes in the Netherlands [93].

3. Nonfeedback control of multistability

Several methods have been developed to perform the various control tasks mentioned in Section 2. We start with nonfeedback control techniques as the simplest approach, since it requires neither a feedback loop nor a permanent tracking of the phase–space trajectory as feedback control does. Also, nonfeedback control is particularly appealing in systems where feedback control is not feasible, especially, for biological and chemical systems. In this section, several nonfeedback control methods will be discussed, namely, pulse control, where short pulses are used to select particular attractors in a multistable system and parametric forcing leading to annihilation of attractors and thereby turning the multistable system to a monostable one.

3.1. Attractor selection by short pulses

One of the simplest ways to control multistability is to apply a particular external perturbation to direct the trajectory from one basin of attraction to another one and wait until the trajectory relaxes to the desired state. Attractor selection by a short external input has been pursued for both discrete [164,224] and continuous systems [214,225].

3.1.1. Attractor selection in a coupled map lattice

Different types of multistability have been found in a globally coupled map lattice given as [164,224]

$$x_{n+1}(i) = (1-\epsilon)f(x_n(i)) + \frac{\epsilon}{N}\sum_{j=1}^{N} f(x_n(i)), \tag{13}$$

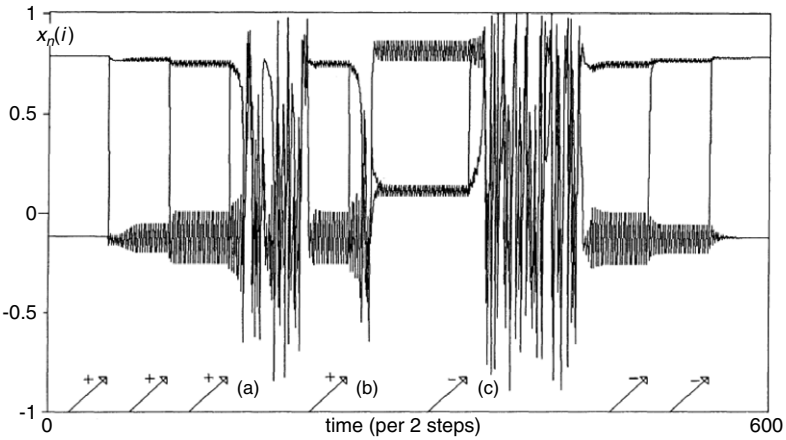

Fig. 2. Time series showing switches among coexisting attractors. The arrows indicate the inputs $\delta = -0.7$ on a site belonging to the $+/-$ cluster. After each input, the system either changes the attractor or returns to the same attractor, sometimes, after chaotic transients (a), (b), and (c). $a = 1.9$, $\epsilon = 0.3$, and $N = 50$. $N_{th} = 30$.
Source: From Ref. [224].

where n is a discrete time step, i is the index of an element ($i = 1, 2, \ldots, N$), and $f(x)$ is a nonlinear mapping. The model has been first introduced as a prototype of chaotic spatially extended systems, and then extended to a higher-dimensional lattice, different functions, and different types of couplings. Kaneko [164] has shown that an input $\delta_n(j)$ applied on a single site j at a single time step n can result in a system jump from one attracting state to another. This input changes only the value of element j from $x_n(j)$ to $x_n(j) + \delta_n(j)$. After the input, the map is iterated without the input till the system trajectory is attracted to another or return to the original attractor after transients. If $|\delta|$ is small, the system goes back to the same attractor after a few iterations, otherwise the system jumps from one attractor to the other.

Fig. 2 shows the switches between coexisting clusters in globally coupled logistic maps $f(x) = 1 - ax^2$ for successive inputs. The switches between attractors is often accompanied by intermittent chaotic transients, after which the system either come back to the original attractor (a) or goes to another attractor [(b) and (c)]. Thus, the attractors can be controlled by the input.

Kaneko [164,224] supposed that the switches between attractors can explain biological information processing if a neural network is considered as a network of globally coupled oscillators. Kaneko's model equation (13) can capture some of essential features of neural dynamics.

3.1.2. Attractor selection in a laser

A similar technique for attractor selection in a multistable system has been developed by Chizhevsky and his colleagues [190,191,213,214,225–228], who proposed to apply a short-pulsed perturbation to a system variable. The short (compared to characteristic times in the system) perturbation is equivalent to a change in the initial condition, i.e., an external pulse in the form of a δ-function switches the system off for a very short time and then switches it on again, so that the system starts from a different initial condition and hence can be sent instantaneously (compared again to the characteristic times) onto the basin of attraction of another coexisting attractor. The important advantage of this method is that it can be easily employed for the experimental search of coexisting attractors, because it does not require any preliminary knowledge of the system's model. Since the pulse is very short, this technique allows one to switch the attractor without any changes in the system parameters, so that the global structure of attractors in phase space remains unaltered. Moreover, the short-pulsed perturbation is a well controllable deterministic process, so that the system's response is experimentally reproducible with a very high accuracy.

The experimental setup for the short-pulsed control technique is shown in Fig. 3. It contains a continuous wave (cw) single-mode CO_2 laser, a pulsed Nd:YAG laser, and an acousto-optical loss modulator inside the CO_2 laser cavity. The short-pulsed loss perturbation is caused by absorption of the CO_2 laser emission on non-equilibrium charge carriers in a semiconductor GaAs plate. These carriers are excited by 15-ns pulses of a Q-switched Nd:YAG laser in the impurity band of the absorption; the rise time of the pulse losses do not exceed the duration of the excitation pulse of the Nd:YAG laser. The back edge of the induced losses is determined by the lifetime of non-equilibrium charge carriers in GaAs which do not exceed 300 ns. Both time constants are significantly shorter than the modulation period that is larger than 10 μs.

To meet attractor targeting conditions, two parameters (pulse amplitude and phase) should be matched at the moment of switching on. The following procedure for the attractor selection is used: for fixed driving and perturbation amplitudes, the perturbation phase (the instant of switching the pulse on) is varied with respect to the phase of the laser intensity modulation. The longer the transients duration in the laser response, the closer to a subharmonic attractor the trajectory approaches. Since this strong correlation between the transients duration and the modulation phase, one can quickly find all

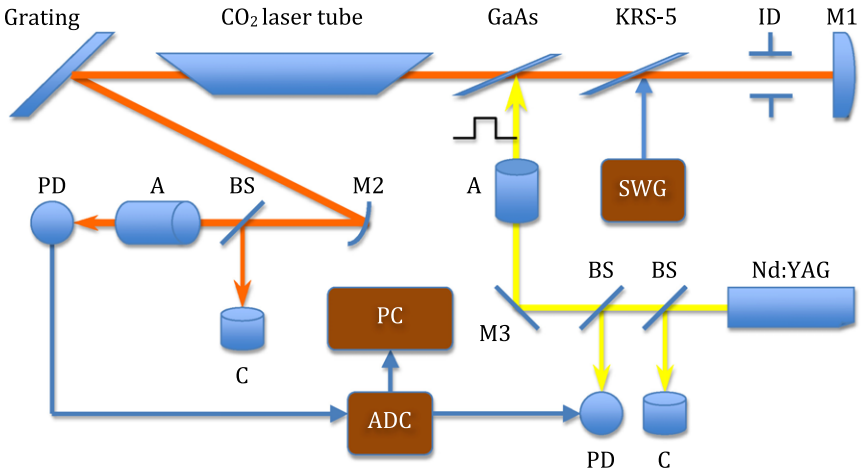

Fig. 3. Experimental setup for short-pulsed control of multistability. The cw CO_2 laser contains an active medium in a laser tube and a cavity formed by a grating and a totally reflecting mirror (M1). The cavity losses are modulated by a harmonic signal applied from a sine wave generator (SWG) to an acousto-optical modulator (KRS-5). Switches between coexisting attractors are realized by short pulses of the Nd^{3+}:YAG laser applied to a GaAs plate. M2 and M3 are mirrors, ID is an iris diaphragm, BS are beam splitters, PD are photodetectors, A are optical attenuators, C are calorimeters, ADC is an analog-to-digital converter, and PS is a computer.

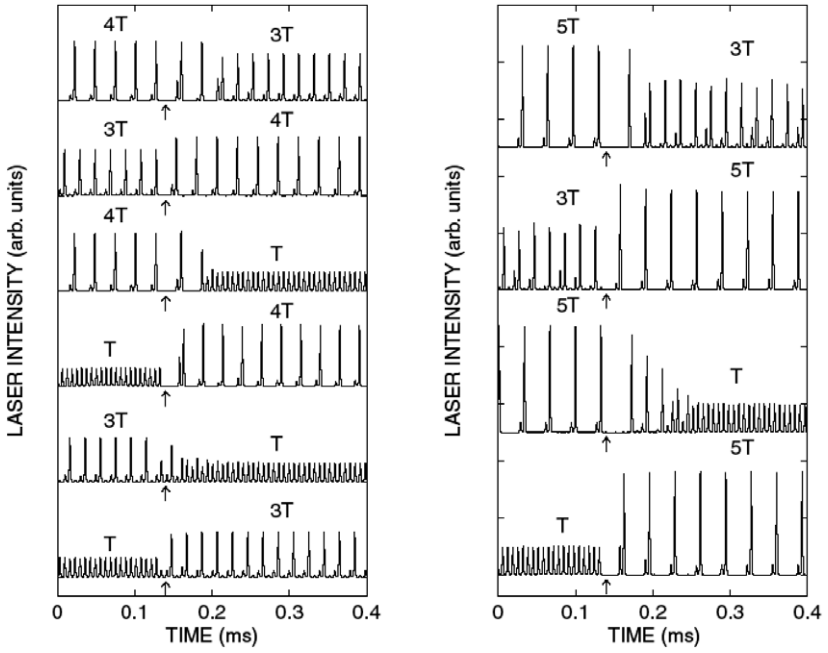

Fig. 4. Experimental switches between coexisting attractors in a multistable loss-modulated CO_2 laser. The arrows indicate the instants of the pulse action.

coexisting attractors. Specifically, the phase is fixed to correspond to the maximum transient duration, and then the pulse amplitude is slowly increased until the system switches to a selected attractor.

In the CO_2 laser, four different attractors, namely, period 1 (T), period 3 (3T), period 4 (4T), and period 5 (5T) have been found to coexist for the same laser parameters. Fig. 4 illustrates the effect of short-pulsed switching between the coexisting attractors. The efficiency of this type of multistability control is determined by a correct choice of both the phase and the amplitude of the short-pulsed perturbation. It is important to note, that this method can be used for targeting not only stable but also unstable orbits. Indeed, using this technique many stable and unstable periodic orbits have been found in a loss-modulated CO_2 laser [190,191,214,225–229].

It should be noted that the method of short-pulsed attractor switching has long been intuitively used in medical practice for heart defibrillation to initiate a normal heart beating by a high-voltage pulse. However, there is still no known method to take into account the strong phase dependence of the defibrillation effect, and hence the results are still somewhat unpredictable, and more research has to be done.

3.2. Eliminating multiple attractors using a pseudo-periodic forcing

It is old knowledge that identical nonlinear systems driven with the same periodic signal can exhibit the coexistence of stable periodic orbits with a period n which is a multiple of the period of the driving signal [230–232]. To control multistability in such systems, Pecora and Carroll [233,234] have suggested to add either chaotic or random components to the periodic drive. Alternatively, the control can be realized by modulating (chaotically, quasi-periodically, or randomly) a system parameter. In the following, we will show how this method can be applied to simplify the basin of attraction of a period-n orbit.

When we change a driving signal v slightly to a new value v', the dynamical system $\dot{w} = f(w, v)$ (w and f being n-dimensional vectors and functions) will evolve according to

$$\Delta \dot{w} \equiv \frac{d(w' - w)}{dt} = f(w', v') - f(w, v), \tag{14}$$

which by adding and subtracting $f(w, v')$ can be rewritten as

$$\Delta \dot{w} = D_w f(w, v')\Delta w + B(t), \tag{15}$$

where $D_w f(w, v')$ is the Jacobian of the vector field, $B(t) = f(w, v') - f(w, v)$, and the higher-order terms are dropped. The solution of the linear equation (15) can be given in terms of transfer function $\Phi(t, t_0)$ (t_0 being the initial time) for the homogeneous version of Eq. (15):

$$\Delta w(t) = \Phi(t, t_0)\Delta w(t_0) + \int_{t_0}^{t} \Phi(t, \tau)B(\tau)d\tau \tag{16}$$

and it will have negative Lyapunov exponents if the original system is stable. This means that there are two positive constants, c_1 and c_2, such that $\|\Phi\| \le c_1 e^{-c_2 t}$. If $B(t)$ is bounded by a constant $b_1 > 0$, then $|\Delta w(t)| \le c_1 b_1/c_2$ for large t. For a small deviation $\Delta v \equiv v' - v$ from the original periodic forcing (b_1 is small), the trajectory will always remain close to the original trajectory and hence multistability will still remain. For a larger Δv, the above analysis will not be valid for long times, since the higher-order terms cannot be neglected and b_1 will be so large that $\Delta w(t)$ can become on the order of the attractor size. Therefore, a threshold value of Δv above which the system behavior will cease to be close to the original orbit $w(t)$ has to be taken into account, so that Δw will be always small. Above the threshold, the new behavior will likely resemble the original dynamics if the new motion remains stable with respect to the new driving signal v' which is still not too different from the original drive. If v' has a chaotic component, the periodicity will be lost and the coexistence of multiple domains may not be possible.

The elimination of multiple domains using pseudo-periodic driving has been tested numerically with the Duffing system and demonstrated experimentally using the corresponding electronic circuit [233]. The Ueda version of the Duffing oscillator is written as

$$\frac{dw_1}{dt} = w_2, \tag{17}$$

$$\frac{dw_2}{dt} = -kw_2 + w_1^3 + \alpha v' + \beta, \tag{18}$$

where $k = 0.05$, $\alpha = 0.21$, $\beta = 0.15$. Eq. (18) contains a pseudo-periodic driving $v'(t) = \cos(t) + \varepsilon x(t)$ with a chaotic component $x(t)$ taken from the Rössler system and an adjustable parameter ε. For $\varepsilon = 0$, the system equations (17) and (18) exhibit the coexistence of period-1, period-2, and period-3 attractors shown in Fig. 5(a). When the chaotic component is added for $\varepsilon = 0.129$, the period 3 disappears, while the period 1 remains stable and the period-2 attractor is converted to a chaotic one, as shown in Fig. 5(b).

For the parameters used in the simulation, the threshold value $\varepsilon = \varepsilon_c = 0.0154$ has been found, above which the period 3 becomes unstable and simultaneously the period-2 orbit is converted into a chaotic attractor, i.e., the addition of only a small portion of chaos to the harmonic driving eliminates multistability. The threshold behavior indicates that the main mechanism for the attractor destruction is related to a crisis, similarly to the method of attractor annihilation by periodic modulation which will be considered in the next section.

We should note that there is a big difference between a pseudo-periodic driven system and a randomly driven system [235–239]. Although both drives can induce a crisis, the former system is deterministic, while the latter is stochastic and hence its study requires a probabilistic approach. The methods for stochastic control of multistability will be discussed in Section 5.

3.3. Attractor destruction by harmonic perturbation

As we already mentioned above, in some practical situations, it is not good if a system has many attractors. A practical technique allowing attractor annihilation is a slow harmonic modulation applied to a system parameter or a variable. In this

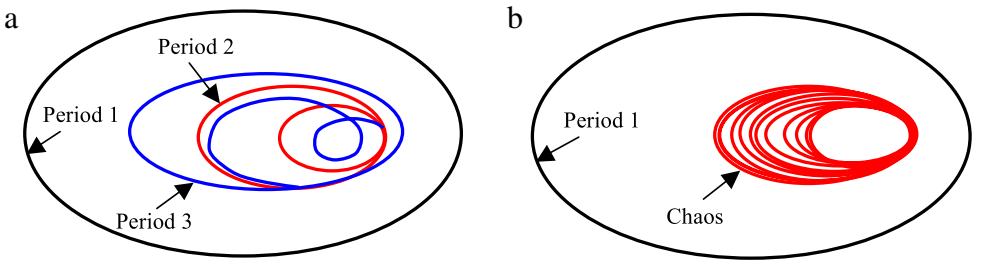

Fig. 5. Schematic representation of coexisting attractors for (a) periodically and (b) pseudo-periodically driven Duffing system.

case, the important control aim is to destroy undesirable attractors. The method of attractor annihilation has been proposed in Refs. [240,241] and experimentally realized, first in CO_2 [240,242] and fiber lasers [243] and later in an electronic circuit mimicking the Lorenz system [244]. Although the method is powerful, not every attractor can be annihilated by this control technique. The necessary requirement for the attractor to be destroyed is that it has to be a focus type, i.e., it should possess complex conjugate eigenvalues [241]. The dynamics in the neighborhood of the attractor is then characterized by damped relaxation oscillations with a certain frequency f_r close to the attractor's own characteristic frequency (eigenfrequency). For a fixed point or a periodic orbit (to be annihilated) with more than two eigenvalues, the method works as well if at least one pair of the eigenvalues is complex conjugate [241,245].

The idea of the annihilation method is the following. Suppose that p is the control parameter governing the bifurcations which lead to the attractors appearance or disappearance. Then, a modulation of this parameter in form of $p = p_0 + p_c \sin(2\pi f_c t)$ (p_c and f_c being the amplitude and the frequency of the control) is applied to the system. We assume that the amplitude p_c is so small that no changes in the qualitative behavior are induced as $p = p_0 \pm p_c$. Even though large-amplitude modulation is also known to produce good results [246], in some applications, for example, in biological or medical systems only small parameter changes are allowed. Since the parameter modulation with properly chosen frequency leads to attractors annihilation, the control may be optimized in the sense that the modulation amplitude can be minimized by adjusting f_c to be close to f_r of the attractor to be annihilated.

The same approach has been used for attractor annihilation in a multi-attractor system with more than three coexisting attractors. According to the Gavrilov, Shilnikov and Newhouse (GSN) prediction, the number of coexisting attractors increases as dissipativity of the system reduces (see, for example, [246] and references therein); these attractors, referred to as GSN sinks are created in various period n-tupling processes and organized in phase and parameter spaces in a self-similar order. The main mechanism for attractor annihilation in such systems lies in the destruction of the GSN sinks by a small-amplitude slow parameter modulation so that the system can be suitably converted again to a controlled monostable system. Such a control is robust against small noise as well [246].

The underlined process behind this annihilation scenario leading to a system possessing less attractors or even only one, can be explained in terms of basins of attraction. An additional harmonic perturbation converts periodic attractors to tori with different stability and different basins of attraction, so that the global basin structure changes [241,246]. Due to these overall changes in the qualitative behavior, the periodic orbits move towards boundaries of their own basins of attraction when the modulation amplitude is increased. During this movement they can undergo other bifurcations, such as a cascade of period-doubling bifurcations leading to chaos, to collide finally with their own basins of attraction boundaries and disappear in boundary crisis.

The control of multistability by attractor annihilation has been successfully realized in lasers [63]. Since in laser experiments only one variable (output intensity) is usually available for measurements with no access to any other variable (inversion population), experimental control of initial conditions is hardly possible. Therefore, one cannot find basins of attraction of coexisting states to definitely confirm whether or not an attractor completely disappears. Neither one can study probability properties of basins of attraction in the presence of noise. Nevertheless, the basins of attraction can be found numerically. The numerical analysis of the phase space structure is crucial to insure that the attractor annihilation effectively takes place. In the following few pages we will show how small periodic or random modulation applied to a control parameter modifies basins of attraction of coexisting states in a paradigmatic multistable system.

3.3.1. Attractor annihilation in the multistable Hénon map

As was already shown above, a parameter modulation with properly chosen frequency and amplitude can annihilate one of coexisting attractors in a bistable system. Under such a modulation, the attractor undergoes a crisis that leads to its destruction. In this regard, a more global question arises: Is it possible to control attractors selectively in order to annihilate a particular attractor or simultaneously various attractors thus transforming a multistable system to a monostable one? To answer this question, we will first consider how multistability emerges in the Hénon map [247], the popular example of a discrete-time two-dimensional dynamical system. Then, we will demonstrate how multiple attractors can be selectively destroyed by harmonic parameter modulation. And finally, we will discuss conditions for the best performance of this method.

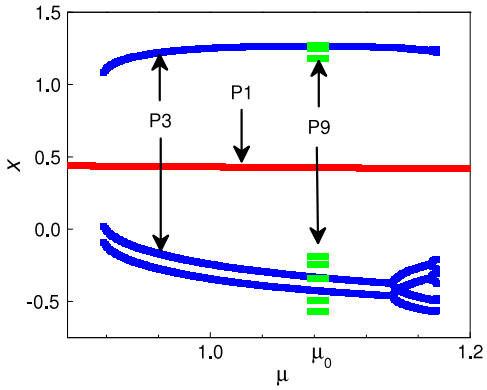

Fig. 6. Bifurcation diagram of x variable of the Hénon map demonstrating the coexistence of period-1 (P1), period-3 (P3), and period-9 (P9) attractors indicated by the arrows. $\mu_0 = 1.083$ is the initial value of the control parameter.

The study using the two-dimensional Hénon map is very important, since the results obtained with this simple discrete system can be generalized to more complex continuous-time dynamical systems due to the fact that a three-dimensional flow can be represented as a two-dimensional Poincaré map. Also, a large number of driven nonlinear systems, including Duffing and Toda oscillators, exhibit qualitative similarity in their bifurcation structures in parameter space [248].

The Hénon map is given as

$$x_{n+1} = 1 - \mu x_n^2 + y_n, \tag{19}$$

$$y_{n+1} = -Jx_n, \tag{20}$$

where parameter J is related to dissipation and μ is an externally controllable parameter. Multistability in this map equations (19) and (20) occurs due to small dissipation, i.e., when J is close to zero ($J > 0$) [249]. The fixed points for the period-1 regime of the Hénon map are given by

$$(x^*_{1,2}, y^*_{1,2}) = \left(-\frac{J+1}{2\mu} \pm \sqrt{\left(\frac{J+1}{2\mu}\right)^2 + \frac{1}{\mu}}, -Jx^*_{1,2} \right). \tag{21}$$

These two equilibrium points possess four eigenvalues (two real and two complex conjugates):

$$\lambda_{1-4} = -\mu x^* \pm \sqrt{(\mu x^*)^2 - J}. \tag{22}$$

There is only one stable fixed point (period-1 attractor) $x^* > 0$ ($x^* = 0.426$ for $\mu = 1.05$). For this attractor there exists a range of parameter values μ, where λ are complex, i.e., the system undergoes damped oscillations and the corresponding equilibrium point is a focus.

A similar analysis can be performed for the period-3 attractor. Though the period-3 solution is impossible to obtain analytically, because the characteristic polynomial is of 8th order, one can find it and analyze its stability only numerically. The numerical results show that the period-3 orbit is stable within the range $0.915 < \mu < 1.171$.

Fig. 6 shows the bifurcation diagram of the variable x with μ as a control parameter at $J = 0.9$. One can see the coexistence of as many as three attractors, period 1 (P1), period 3 (P3), and period 9 (P9), in the parameter range of $\mu \in [1.077, 1.089]$, whereas only two attractors (P1 and P3) coexist for $\mu \in [0.915, 1.171]$.

Each coexisting attractor is characterized by different eigenvalues, some of them are complex with different eigenfrequencies. This means that every attractor i of the focus type has its own relaxation oscillation frequency $f_r^{(i)}$ that depends on μ and can be measured from the time series as a frequency of damped oscillations during transients after a small disturbance from the equilibrium. Fig. 7 shows how $f_r^{(i)}$ depends on μ for every coexisting attractor. One can see that in the range of the coexistence of three attractors (e.g., at $\mu = 1.083$), the P3 and P9 attractors are foci with relaxation oscillation frequencies $f_r^{(3)} = 0.106$ and $f_r^{(9)} = 0.0275$, respectively, and the P1 attractor is a node (no damped oscillations occur).

Next, to control multistability, a slow harmonic modulation is applied to μ as

$$\mu = \mu_0 + \mu_c \sin(2\pi f_c n), \tag{23}$$

where μ_c and f_c are the control amplitude and frequency and $\mu_0 = 1.083$ is the initial value of the control parameter. Let $\delta\mu$ expresses the dynamical range of μ_c to be used, so small that no qualitative changes in the asymptotic stability of the coexisting attractors occur for the uncontrolled case, i.e. when μ is varied adiabatically ($t \to 0$) within the range $\mu_0 \pm \delta\mu$. Impressively, such a weak modulation is capable to destroy either P9 or simultaneously both the P9 and P3 attractors.

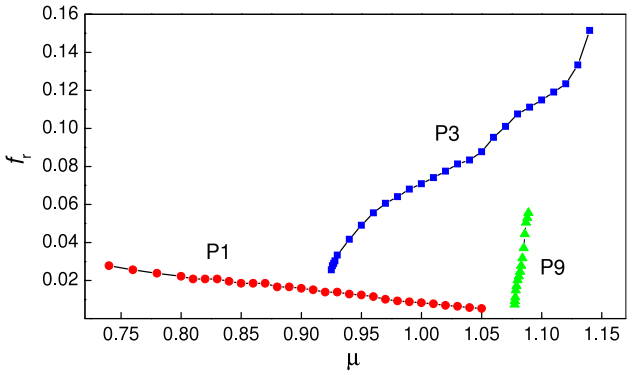

Fig. 7. Relaxation oscillation frequencies of period-1 (P1) (dots), period-3 (P3) (squares), and period-9 (P9) attractors (triangles) as a function of μ.

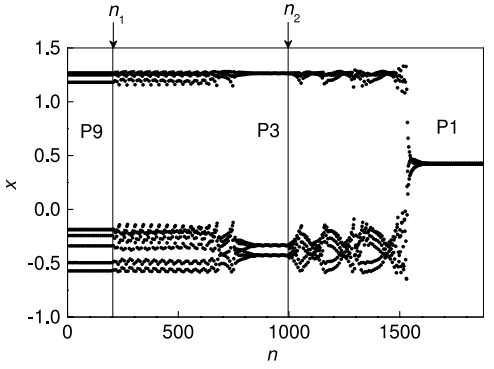

Fig. 8. Temporal evolution of the Hénon map with coexisting attractors under control harmonic modulation. Prior to the control ($n < n_1$), three attractors (P1, P3 and P9) coexist while the system is initially in P9. The control is applied successively at $n = n_1$ ($\mu_c = 0.0029$ and $f_c = 0.0275$) and $n = n_2$ ($\mu_c = 0.023$ and $f_c = 0.106$). The arrows show the instant when the control parameters are changed. P9 and P3 are destroyed after some transients.

The effect of the control modulation on the destruction of the coexisting attractors is demonstrated with the time series in Fig. 8, that illustrates the consecutive annihilation of the coexisting attractors. Initially, prior to the control ($n < n_1$) all three periodic attractors coexist at $\mu_0 = 1.083$. Starting from the initial conditions for P9, the control modulation equation (23) with $\mu_c = 0.0029$ and $f_c = 0.0275$ is applied at $n = n_1$.

The mechanism underlying the attractor annihilation is the following. The external harmonic modulation converts the P9 attractor into a torus, whose stability depends on the modulation parameters. When the control frequency is close to $f_r^{(9)}$ the torus undergoes a period-doubling cascade of bifurcations followed by chaos which disappears in crisis, when the modulation amplitude is increased. After the P9 attractor destruction, the system goes to P3. Note, the control modulation is almost invisible in the P3 regime, because $f_r^{(9)}$ and $f_r^{(3)}$ are very different. Next, to annihilate the P3 attractor one needs either to shift f_c closer to $f_r^{(3)}$ or to increase the modulation amplitude μ_c. Even if the control modulation presents, the oscillations in the P1 regime are indistinguishably small because this attractor is of a node type for $\mu_0 = 1.083$.

Fig. 9 shows the stability boundaries of the P9 and P3 attractors (annihilation curves) in the space of the control parameters μ_c and f_c. For the control parameters above the annihilation curve, the corresponding attractor loses its stability.

Basins of attraction. The physical mechanism underlying the annihilation phenomenon can be clearly understood from the analysis of the basins of attraction of the coexisting states shown in Fig. 10. The dots inside the basins have three different colors for each attractor: yellow for P1, blue for P3, and gray for P9. The parameter modulation creates invariant curves in the vicinity of every periodic point, thus forming a quasiperiodic orbit. For the P9 orbit, these are the red lines near the white triangles in Fig. 10(b)]. One can see that when f_c is very different from $f_r^{(9)}$, the amplitude of the system's response is relatively small and the corresponding basins of attraction remain almost the same as without modulation. However, when f_c approaches $f_r^{(9)}$ or its subharmonics, this frequency gets in resonance with the relaxation oscillations, that makes the system's response so strong that the attractor loses its stability. The control modulation may induce a torus-doubling route to chaos terminated in boundary crisis. Beyond the crisis, the trajectory approaches another attractor along the arrows and black dots shown in Fig. 10. The modulation amplitude also plays a significant role in the attractor annihilation; it should be large enough for the resonant trajectory to collide with the boundary of its own basin of attraction.

Of course, the diagram shown in Fig. 10 is a very rough illustration of the dynamical processes responsible for the attractor annihilation. We recall that the basins shown in Fig. 10 belong to the uncontrolled system. Strictly speaking, the parameter modulation not only creates quasiperiodic orbits, but also changes whole basins' structure [241]. However, even though the

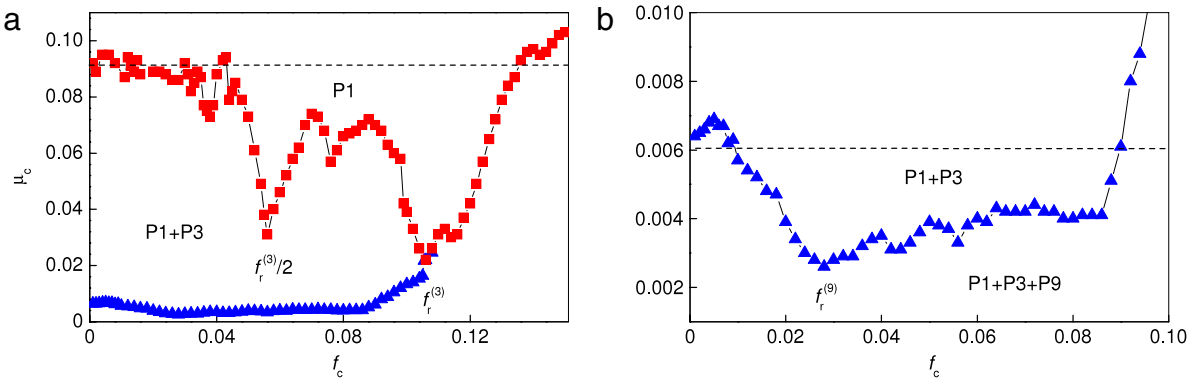

Fig. 9. Annihilation curves for P3 (squares) and P9 (triangles) in space of modulation frequency and amplitude for $\mu_0 = 1.083$. The best conditions for annihilation of P3 and P9 are realized, respectively, for (a) $f_c = f_r^{(3)} = 0.106$ or $f_c = f_r^{(3)}/2 = 0.053$ and (b) $f_c = f_r^{(9)} = 0.0275$. The corresponding attractor is destroyed for the parameters above the annihilation curve, while below both curves the three attractors coexist. The dashed lines indicate the maximum control amplitude at which the system changes the attractor when $f_c \to 0$.

new attractors created by the parameter modulation have different basins of attraction, the changes in the basins' volumes have no effect on general interpretation of the observed phenomenon [245].

Effect of modulation phase. In addition to the control frequency and amplitude, the modulation phase also plays an important role in attractor annihilation. Egorov and Koronovskii [250] have shown that the structure of the basins of attraction of the residuary states depends crucially on the initial modulation phase ψ_0, that was considered in the following modulation form

$$\mu = \mu_0 + \mu_c \sin(2\pi f_c n + \psi_0). \tag{24}$$

The control modulation equation (24) with $f_c = 0.11$ and $\mu_c = 0.05$ applied at $\mu_0 = 1.083$ destroys the P3 and P9 attractors. Although the basins of attraction of the remaining P1 and the infinity attractor are very similar (prima facie) for different ψ_0, a closer inspection of the basins structure revealed riddles in the phase space regions where the P3 attractor was located prior to its annihilation. Therefore, small changes of the initial phase (or noise) will determine the residuary attractors.

Thus, the method of attractor annihilation can be applied to a multistable dynamical system to selectively control coexisting attractors of a focus type. The best performance of this kind of control is achieved when the control frequency is close to the relaxation oscillation frequency of the attractor to be annihilated or its subharmonics. Theoretically, this method has been verified in the Lorenz system [244], lasers [240,243,251,252], and coupled Duffing oscillators [253,254]. Experimentally, the attractor annihilation has been realized in laser experiments, that we will describe below.

3.3.2. *Control of bistability in a CO_2 laser by modulating the cavity length*

From the experimental point of view, a laser with modulated parameters is a very convenient system for studying nonlinear dynamics. The advantages of the laser resides in its relative stability under a wide range of operating conditions and its fast response when compared with other systems, for example, mechanical or fluids. In particular, the first experimental control of bistability by attractor annihilation using a periodic parameter modulation has been performed in a laser [240].

Theory. The dynamics of a class-B laser can be described by the simple two-level model [190,240]

$$\dot{u} = \tau^{-1} u \left[y - k_0 - k_d \sin(2\pi f_d t) \right], \tag{25}$$

$$\dot{y} = (y_0 - y)\,\gamma - uy, \tag{26}$$

where u is proportional to the radiation density, y and y_0 are the gain and the unsaturated gain in the active medium, respectively, τ is half round-trip time of light in a resonator, γ is the gain decay rate, k_0 is the constant part of the resonator loss, and k_d and f_d are the driving amplitude and frequency of the cavity loss modulation.

The laser equations (25) and (26) exhibit the coexistence of a period-1 and a period-2 stable limit cycles for the following parameters: $\tau = 3.5 \times 10^{-9}$, $\gamma = 8.5 \times 10^5$, $k_0 = 0.173$, and $f_d = 160$ kHz. The state diagram in the space of the laser gain y_0 and the driving amplitude k_d is shown in Fig. 11. The minimum k_d corresponds to the case when the modulation frequency is twice the laser relaxation frequency, i.e. $f_d = 2f_r$. The period-doubling (PDB) and saddle–node bifurcation (SNB) lines are marked by squares and dots, respectively. Bistability exists for $y_0 > 0.1835$ and $k_d > 3 \times 10^{-4}$, i.e. at the right-hand side of the SNB line.

Fig. 12 shows the bifurcation diagram of the laser radiation density u with respect to the laser gain y_0 for $k_d = 3 \times 10^{-4}$. The control modulation affects the laser gain as $y_0' = y_0 + y_c \sin(2\pi f_c t)$, where y_0 is the gain of the uncontrolled laser, and y_c and f_c are the amplitude and frequency of the control modulation. It is assumed that this additional modulation is slow ($f_c \ll f_d$) and weak ($y_c \ll y_0$) and y_0 is fixed at 0.1855 (shown by the arrow in Fig. 12) to keep the modulation in the bistable

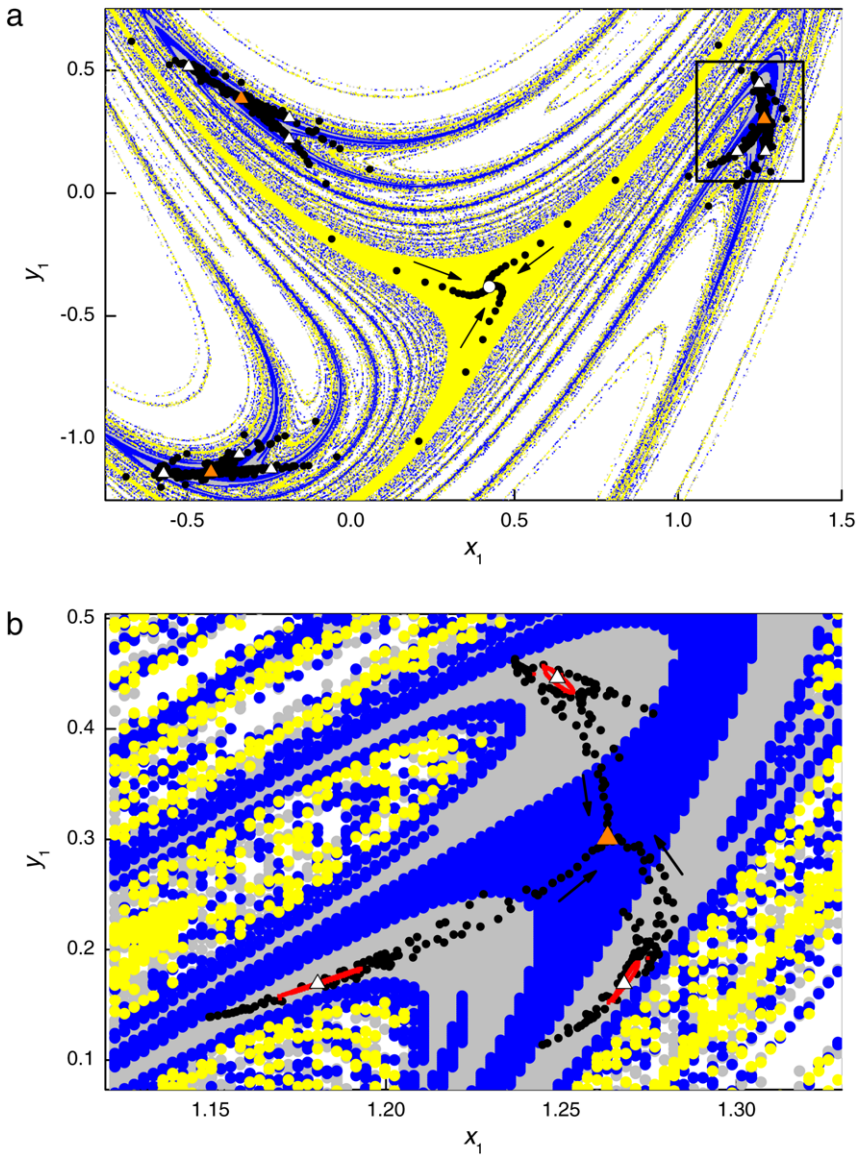

Fig. 10. Basins of attraction of P1 (yellow dots), P3 (blue dots), and P9 (gray dots). (a) Annihilation of P3 at $\mu_c = 0.023$ and $f_c = 0.106$. (b) Enlarged diagram of the rectangular box showing the annihilation of P9 at $\mu_c = 0.0029$ and $f_c = 0.0275$. P1, P3, and P9 are shown respectively by the white dot, red triangles, and white triangles. The P9 torus induced by modulation at $\mu_c = 0.0029$ and $f_c = 0.01$ are shown by the red lines. The arrows indicate the directions of the trajectories (black dots) leading to another attractor. (For interpretation of the references to color in this figure legend, the reader is referred to the web version of this article.)

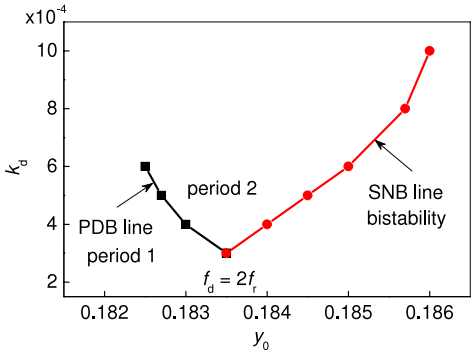

Fig. 11. State diagram of loss-modulated CO_2 laser equations (25) and (26) in parameter space of driving amplitude k_d and laser gain y_0.

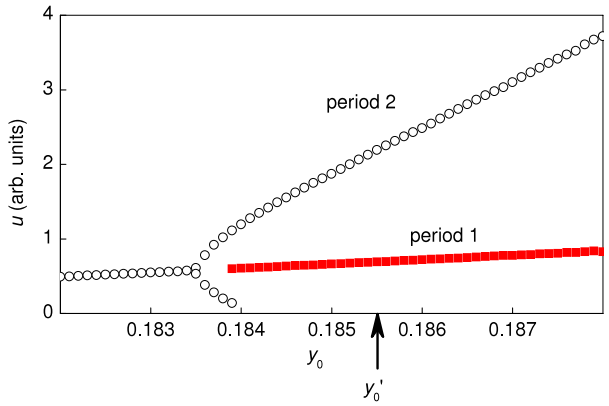

Fig. 12. Bifurcation diagram of laser radiation density versus gain factor demonstrating the coexistence of period-2 and period-1 attractors marked respectively by open dots and red squares.

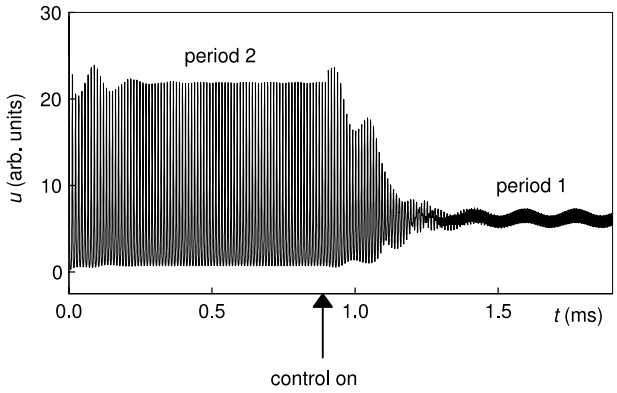

Fig. 13. Annihilation of the period-2 attractor in a loss-driven CO_2 laser. As an additional weak harmonic modulation is applied to the cavity losses, the period 2 is destroyed and the trajectory after transients is attracted to the remaining period-1 state.

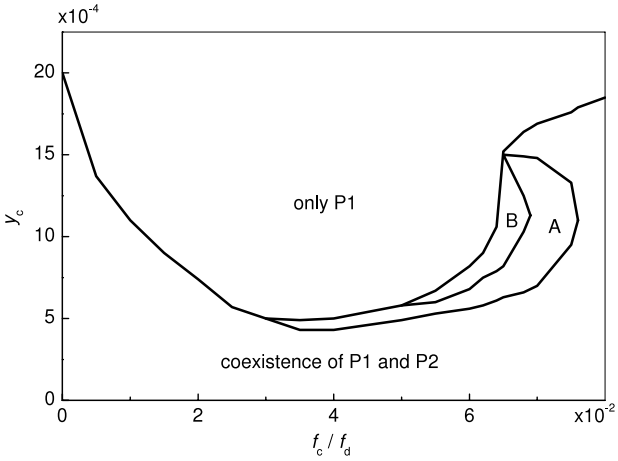

Fig. 14. Stability boundary of period-2 attractor in $(f_c/f_d, y_c)$ space for $y_0 = 0.1855$. Region A: period 2 in control frequency. Region B: higher periodic orbits and chaos in control frequency.

region. Under the control modulation, both P2 and P1 orbits are converted into tori. It is note worthy, that when the laser initiates in P2, as the control amplitude is increased the P2 torus undergoes a period-doubling route to chaos to be destroyed in a crisis. As a result, the laser has to jump into the remaining P1 torus, as shown in Fig. 13.

The attractor destruction is observed over a wide range of the control frequency as illustrated in Fig. 14 which shows the stability (annihilation) curve for the P2 attractor.

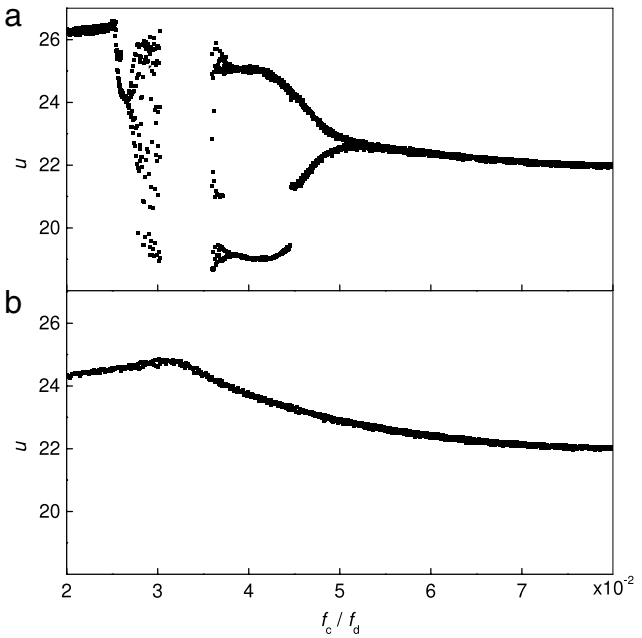

Fig. 15. Bifurcation diagrams of laser peak intensity with respect to the normalized control frequency f_c/f_d in the vicinity of the annihilation curve for different control amplitudes: (a) $y_c = 5 \times 10^{-4}$ and (b) $y_c = 3 \times 10^{-4}$. Within the range of $0.030 < f_c/f_d < 0.036$ the period-2 attractor does not exist anymore.

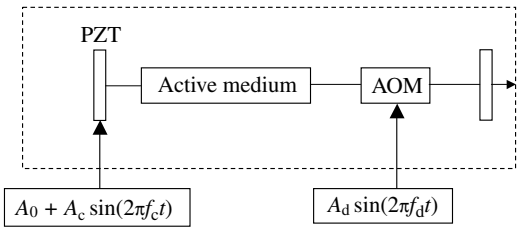

Fig. 16. Experimental setup demonstrating attractor annihilation in a CO_2 laser with modulated losses. AOM is an acousto-optical modulator and PZT is a piezo-transmitter.

Fig. 15 shows typical bifurcation diagrams with f_c as a control parameter for different control amplitudes y_c. These diagrams are obtained by sampling the laser intensity at interval $1/f_c$. In Fig. 15(a) one can see a bubble cascade of period-doubling bifurcations (period $1 \to 2 \to 4 \ldots$chaos$\ldots \to 4 \to 2 \to 1$) in the P2 torus, where the periodicity is related to the control frequency. The chaotic orbit, in the interior of the cascade, gets destroyed in the range of 4.8 kHz $< f_c <$ 5.7 kHz. Such a destruction is expected due to the collision of the attractor with the regular P2 (with respect to f_d) saddle orbit. After a boundary crisis, the system jumps into the remaining P1 attractor. Evidently, these features are very similar to dynamics of the Hénon map under harmonic modulation, described in the previous section.

Experimental verification. The method of attractor annihilation has been experimentally verified in a single-mode CO_2 laser with an intracavity acousto-optical modulator. The experimental setup is shown in Fig. 16. The electric driving signal $V_d = A_d \sin(2\pi f_d t)$ with frequency $f_d = 105$ kHz and amplitude A_d is applied to the modulator providing time-dependent cavity losses. The output laser intensity is detected with a $Cd_xHg_{1-x}Te$ detector and displayed on a Digital Signal Analyzer. Bistability in this laser reveals itself via hysteresis observed when the cavity mirror connected with a piezo-transmitter PZT is moved forth and back changing the cavity length; this resulted in the laser gain contour asymmetry shown in Fig. 17. The coexistence of two attractors is observed for 30 V $< |A_0| <$ 60 V.

The laser intensity is stroboscopically sampled at intervals of $1/f_d$. The bifurcation diagram of the peak laser intensity in Fig. 17 is obtained by linearly increasing the bias voltage A_0 from negative to positive values with no control (i.e. $A_c = 0$). One may notice that the period-2 bubbles at the negative and positive detunings appear at different values of $|A_0|$, that can be interpreted as evidence of bistable behavior. The electric control signal $V_c = A_0 + A_c \sin(2\pi f_c t)$ with a constant bias voltage A_0 and modulation amplitude A_c is used to tune the output mirror with PZT in the middle range of bistability, i.e. at $A_0 = -45$ V and $A_c = 5$ V. The modulation of cavity detuning leads to appropriate changes in the gain factor. If the small amplitude of the detuning modulation is not at the line center, the detuning is almost proportional to the gain.

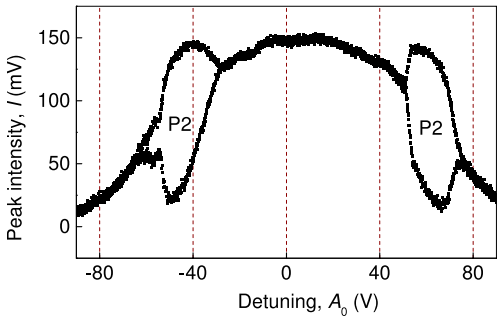

Fig. 17. Gain contour of a CO_2 laser with modulated losses.

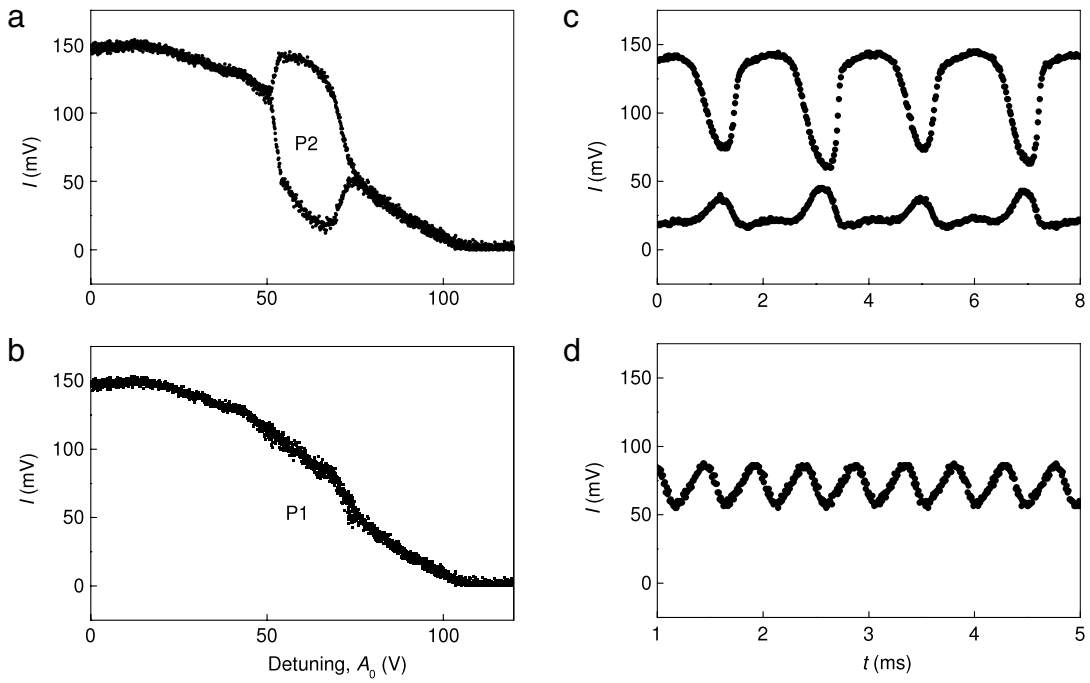

Fig. 18. Experimental stroboscopic measurements of laser intensity sampled with a period $T = 1/f_d$ driving modulation. (a) Bifurcation diagram without control with respect to cavity detuning. Period-1 orbit coexists with period-2 orbit for detuning 30 V $< A_0 <$ 50 V. The control with $A_c = 5$ V is applied at $A_0 = -45$ V. (b) Time series at $f_c = 200$ Hz, (c) 500 Hz, and (d) 2 kHz. The envelope is modulated with f_c. The period-2 orbit disappears and only the period-1 orbit remains.

Fig. 18 illustrates the P2 attractor annihilation by modulating the cavity detuning. While without control the P2 exists for certain detuning (Fig. 18(a–b)), the control modulation annihilates it (Fig. 18(b–d)). The laser intensity is periodically modulated with both the carrier $f_d/2$ and the control f_c frequencies thus forming a torus. As the control frequency f_c is increased, the torus undergoes a period-doubling bifurcation (Fig. 18(c)). As f_c is further increased, the laser jumps to the P1 torus (P1 torus) (Fig. 18(d)). One can see that the experimental results are in a good agreement with the above theory.

Other types of lasers. Attractor annihilation by periodic parameter modulation has also been realized in multistable semiconductor lasers [251]. The method is particularly suitable for this type of lasers because their oscillations are typically accompanied by high intensity noise that may cause spontaneous switches between coexisting states.

The technique reported for a semiconductor laser presents some differences with the previously described in the CO_2 laser. Whereas in the latter, the driving and the control modulations are applied to distinct parameters (cavity loss and cavity detuning), in the former the same parameter (pump current) is simultaneously modulated by two frequencies. In the semiconductor laser, coexisting period-4 and period-3 attractors are destroyed by an additional weak harmonic modulation applied to the injection current so that only a period-1 attractor remains. This points out a simpler way to manipulate the system dynamics that can be more easily realized in practice. Later, the attractor annihilation method using one-parameter modulation has been successfully realized in an erbium-doped fiber laser [243,252].

4. Feedback control of multistability

In the previous section we have discussed nonfeedback control strategies which act via an external perturbation such as a short pulse, a pseudo-periodic and harmonic forcing. Although these methods are in general easy to apply, since they do not require a knowledge of system dynamics, this control is usually not small in the sense that the amplitude of the external signal is relatively large. Another very successful way to control multistable systems is a feedback technique, where the internal state of the system is fed back into the system either instantaneously or with a time delay. In this section, we consider several feedback methods for controlling multistability.

4.1. Attractor stabilization and controlled switching

When designing a control strategy, the presence of external noise has to be taken into account, because due to the high sensitivity to perturbations, one has to expect the emergence of an attractor hopping process in which the trajectory is kicked out of the open neighborhood of the attractor. Therefore, one needs to apply a permanent control for stabilizing the selected attractor. The strength of this control depends mainly on the size of the open neighborhood. For sake of simplicity, we suppose that the chosen state is a fixed point $\mathbf{x}^*$ of the map

$$\mathbf{x}_{k+1} = \mathbf{F}(\mathbf{x}_k), \tag{27}$$

where $\mathbf{x}$ and $\mathbf{F}$ are n-dimensional quantities. Since without noise the desired attractor is stable, all eigenvalues of the Jacobian matrix $\mathbf{DF}(\mathbf{x}^*)$ evaluated at the fixed point are inside a unit circle. When noise is introduced, the stabilization of this fixed point can be done by applying a feedback control originally developed by Poon and Grebogi [138]. The control scheme assumes that the trajectory is already near the desired attractor, so that the system can be linearized as

$$\mathbf{F}(\mathbf{x}^* + \boldsymbol{\varepsilon}) = \mathbf{x}^* + \mathbf{DF}(\mathbf{x}^*)\boldsymbol{\varepsilon}, \tag{28}$$

where $\boldsymbol{\varepsilon}$ denotes the distance from the fixed point. The influence of noise is modeled by adding noise vector $\boldsymbol{\delta}$ to the map

$$\tilde{\mathbf{F}}(\mathbf{x}) = \mathbf{F}(\mathbf{x}) + \boldsymbol{\delta}, \tag{29}$$

assuming the noise is bounded by $\delta = |\boldsymbol{\delta}|$. We now define a spherical neighborhood of radius ρ around the attractor. As soon as the trajectory falls into this neighborhood, the control is switched on to keep the system close to this attractor despite the noise. Suppose the system enters this ρ-neighborhood at the ith iteration, then $\mathbf{x}_i = \mathbf{x}^* + \boldsymbol{\varepsilon}$ with $|\boldsymbol{\varepsilon}| \leq \rho$. After the next iteration, the system will land at

$$\mathbf{x}_{i+1} = \tilde{\mathbf{F}}(\mathbf{x}_i) = \mathbf{F}(\mathbf{x}_i) + \boldsymbol{\delta}. \tag{30}$$

Assuming that the ρ-neighborhood is small enough so that the linearization is valid, we can control the trajectory by adding a control term in the form of

$$\hat{\mathbf{x}}_{i+1} = \mathbf{x}_{i+1} + \mathbf{C}\boldsymbol{\varepsilon}. \tag{31}$$

Since this control scheme can be used for both stabilization and destabilization, the control matrix $\mathbf{C}$ must reflect the control's aim. To stabilize an attractor, a good candidate is the Jacobian matrix $\mathbf{DF}(\mathbf{x}^*)$ since all its eigenvalues moduli are smaller than 1. If one wishes the system to go to another attractor, it is enough to turn the stabilization off and wait until the noise ejects the trajectory from the original open neighborhood to the desired one. The motion on the complexly interwoven basin boundaries, more specifically, on the embedded chaotic saddles, brings the trajectory close to the other selected attractor where the stabilization is again turned on.

In the same line of thought, to destabilize an attractor, but contrary to stabilization, one may use the inverse of the Jacobian matrix $\mathbf{DF}^{-1}(\mathbf{x}^*)$ as the control matrix [139]. This ensures that all eigenvalues moduli are larger than one. Combining these two control strategies one can perform stabilization as well as destabilization on demand. This yields a controlled switching between attractors.

However, there is one drawback of the above control scheme, mainly, that one has to wait for the trajectory to reach an appropriate ρ-neighborhood of the attractor, and the waiting time can be arbitrarily long. Therefore, special targeting strategies have been developed to allow rapid switching between different regimes [255–257]. Some of these methods will be described in Section 4.2.

Not only switching between attractors can be achieved using a linear feedback control, but also attractor avoidance. To avoid a specific attractor, destabilization can be turned on as soon as the trajectory enters the predefined ρ-neighborhood of the respective attractor.

4.2. Targeting a desired attractor

As outlined in Section 4.1, to keep the control within a certain boundary, the desired state feedback stabilization of metastable states in a noisy multistable system has to act only in a prescribed neighborhood. We recall that switching from one state **A** to another (say, **B**) relies on the dynamics of the chaotic saddles embedded in the basin boundary. Only when the trajectory arrives in the predefined neighborhood of the desired attractor, stabilization can be switched on to keep the

trajectory in the neighborhood of this selected state **B**. To approach the selected attractor **B** in a reasonable finite time, three different methods have been proposed. The first one [256] is based on the targeting technique for chaotic systems [258]. The idea is basically to exploit the inherent exponential sensitivity of the chaotic time evolution on the basin boundaries to small perturbations to direct the trajectory to some desired accessible state in a shortest possible time. The second method [255] uses particular perturbations to drive more trajectories to state **B**, i.e. to enlarge substantially its basin of attraction. The third method [257] is based on *reinforcement learning*, also known as *neurodynamic programming* [259]. While the two previous approaches are based on the knowledge of the model equations, the reinforcement algorithm does not require any mathematical model, but relies entirely on data.

4.2.1. Modified targeting method

Before describing how to switch from one metastable attractor **A** to another metastable attractor **B** in a noisy multistable system, let us recall briefly the basic steps of the targeting algorithm in chaotic systems [258]. Suppose that there is a source point **S** and a target point **T** both located on the basin boundary. Around each point we consider small regions r_S and r_T, respectively. The goal is to get from a point $p_S \in r_S$ to a point $p_T \in r_T$ in a shortest possible time. To find such a pathway, the region r_S is iterated forward in time, while the region r_T is iterated backward in time until both iterated regions intersect each other in point p_I in phase space. If such an intersection can be found, there exists a trajectory from p_S to p_T via p_I. The point p_S is then used to design a perturbation that when applied to **S** will bring the system to point p_S. Then it will follow its original trajectory to reach p_T.

To gear a noisy multistable system from the metastable state **A** to the metastable state **B**, Macau & Grebogi [256] suggested two modifications of this targeting technique and illustrated their efficiency using the dissipative standard map (cf. Section 2.1.1) as a paradigm. The first modification concerns the computation of the intersection p_I using forward and backward iterations of the regions r_A and r_B, respectively. $\mathbf{x}_{i+1}$ is calculated as the variable mean value obtained from each of the n different forward iterations, starting from the same initial condition $\mathbf{x}_i$ but using n different noise realizations. This procedure acts like an efficient filter reducing the noise. The second modification in the algorithm is made to arrive at point $p_A \in r_A$ from where the targeting is started. While in the noiseless chaotic system to brings the trajectory from **S** to p_S it is sufficient to apply a certain perturbation, in the noisy system a special control technique should be applied. A good solution is the traditional linear control method, such as the *discrete linear quadratic regulator* (DLQR) [260].

Thus, the combination of the original targeting procedure with classical control methods enables to switch, on demand, from one metastable state to another in the shortest possible time. This offers a great flexibility in switching between distinct system performances associated with different coexisting states.

4.2.2. Bush-like paths to a preselected attractor

Another algorithm to steer most trajectories to a desired attractor by using small feedback control has been designed by Lai [255] who proposed to build a hierarchy of paths towards the desirable attractor and then stabilize a trajectory around one of the paths. In the case of fractal basin boundaries, the probability for a random trajectory to asymptotically reach the desirable attractor increases significantly.

To explain how this method works, we again consider a dynamical system with two coexisting attractors, **A** and **B**. For a given region $\mathbf{\Sigma}$ of the phase space that contains a part of the basin boundary, a fraction of initial conditions $f_{\mathbf{A}}$ will yield trajectories that asymptotically go to the attractor **A**, and the remaining initial conditions, i.e. a fraction of $f_{\mathbf{B}} = 1 - f_{\mathbf{A}}$, send the trajectory towards the attractor **B**. Suppose, that one of the two attractors yields a much better system performance than the other. The goal of this control is to increase substantially the fraction of initial conditions $f_{\mathbf{B}}$ that will push the system to the attractor with better performance. For this purpose, a system parameter p should be delicately adjusted around its nominal value p_0, so that $p \in [p_0 + \Delta p, p_0 - \Delta p]$, where $\Delta p/p_0 \ll 1$.

Lai's [255] main idea is to construct a "tree-like" path structure which allows us to reach the desirable attractor. In particular, if we suppose that **B** is the desirable attractor, then an initial condition in $\mathbf{\Sigma}$ is randomly chosen to generate a trajectory to **B**, referred to as "root" path 1 to **B** and denoted by $\mathbf{X}_0, \mathbf{X}_1, \ldots, \mathbf{X}_{\mathbf{B}}$, where $\mathbf{X}_{\mathbf{B}}$ is a point on **B** (or a point in the vicinity of **B**). We then choose a second trajectory to **B** from an arbitrary initial condition $\mathbf{Y}_0$ in $\mathbf{\Sigma}$. If this second path approaches **B** directly without coming close to root path 1, we call it root path 2. It can also happen that a point on this trajectory $\mathbf{Y}_n$ falls into a suitably small neighborhood of some point along root path 1 before it comes close to **B**. In this case, we store $\mathbf{Y}_n$ together with the path of $n - 1$ points leading to $\mathbf{Y}_n$. The path $\mathbf{Y}_0, \mathbf{Y}_1, \ldots, \mathbf{Y}_n$ is referred to as the secondary path of the root path 1. This procedure can be repeated for initial conditions chosen on a uniform grid of size δ in $\mathbf{\Sigma}$. With a suitably chosen δ, a hierarchy of paths to **B** in $\mathbf{\Sigma}$ can be built with N_R root paths. To each root path i, some secondary path can be attached, to each secondary path, third-order path may be connected, and so forth, giving rise to a path tree **B** in the phase space region that contains the basin boundary.

In order to direct a trajectory to the desirable attractor after it comes close to a path on the bush, a targeting feedback scheme is employed. Let us take, for example, an N-dimensional map $\mathbf{x}_{n+1} = \mathbf{F}(\mathbf{x}_n, p)$. Suppose a trajectory originated from a random initial condition $\mathbf{x}_0$ falls at some later time n into an ε-neighborhood of a point $\mathbf{y}_n$ on the bush, i.e. $|\mathbf{x}_n - \mathbf{y}_n| \le \varepsilon$. Let $\mathbf{y}_n, \mathbf{y}_{n+1}, \ldots, \mathbf{y}_{\mathbf{B}}$ be the path on the bush that starts at $\mathbf{y}_n$ and ends at $\mathbf{y}_{\mathbf{B}}$ which is in the ε-neighborhood of the desirable attractor. In the vicinity of $\mathbf{y}_n$, we have the following linearized dynamics: $\Delta\mathbf{x}_{n+1} = \mathbf{DF}(\mathbf{x}_n, p)\Delta\mathbf{x}_n + (\partial\mathbf{F}/\partial p)\Delta p_n$, where $\Delta\mathbf{x}_n = x_n - y_n$, $\Delta p_n = p_n - p_0$, and both the Jacobian matrix $\mathbf{DF}(\mathbf{x}_n, p)$ and the vector $\partial\mathbf{F}/\partial p$ are evaluated at $x_n - y_n$ and $p_n - p_0$. Choosing a unit vector $\mathbf{u}$ in the phase space and letting $\mathbf{u} \cdot \mathbf{\Delta x}_{n+1} = 0$, we obtain for the required parameter

perturbation

$$\Delta p_n = \frac{-\mathbf{u}\cdot\mathbf{DF}(\mathbf{x}_n, p)\cdot\Delta\mathbf{x}_n}{\mathbf{u}\cdot\partial\mathbf{F}/\partial p}. \tag{32}$$

The unit vector $\mathbf{u}$ is arbitrarily chosen provided that it is not orthogonal to $\mathbf{x}_{n+1}$, and that the denominator in Eq. (32) does not approach zero. In practice, the maximum magnitude allowed for the parameter perturbation is $\Delta p_{\max} \sim \varepsilon$. If the computed $|\Delta p_n|$ exceeds Δp_{max}, then $\delta p_n = 0$. This may occasionally cause the control loss, however, as was numerically found, the robust control can still be achieved because when $\Delta\mathbf{x}_n$ is small, Δp_n is also small, and therefore setting $\Delta p_n = 0$ seldom happens.

The method has been demonstrated through numerical simulations in a two-dimensional map to control both fractal basin boundaries and riddled basins.

4.2.3. Reinforcement learning

The feedback control outlined in Section 4.1 and the two targeting methods discussed in Section 4.2 are restricted to relatively low noise levels. In case of larger noise, it is advisable to use the reinforcement learning method [257,261,262] to steer the trajectory to any selected metastable state. In contrast to the previously discussed techniques, this method does not require any knowledge on the system model and can be entirely based on data. This offers a much wider applicability since in many practical situations one encounters various systems for which no model equations available.

The aim of this control is again to drive the system to a particular preselected metastable state in a shortest possible time. Once more, we will use the dissipative standard map as a paradigm to design a discrete control strategy. To do so, a small state-dependent perturbation u_n is added to the forcing f_0 of the map equation (2):

$$x_{n+1} = x_n + y_n + \delta_x \bmod 2\pi, \tag{33}$$

$$y_{n+1} = (1-\nu)y_n + (f_0 + u_n)\sin(x_n + y_n) + \delta_y, \tag{34}$$

where δ_x and δ_y are the components of uniformly distributed noise with $\sqrt{\delta_x^2 + \delta_y^2} \le \delta$ (δ being the noise strength). The reinforcement learning method [257] considers the learning from interactions of a decision maker, called agent, with a controlled environment.

At each time step $n = 1, 2, \ldots$ the agent gets a representation $\mathbf{w}_n \in \mathbf{W}$ of the environment's state $\mathbf{x}_n \in \mathbf{X}$, where W is the finite set of all possible state representations, $\mathbf{x}_n = (x_n, y_n)$ is the state vector, and $\mathbf{X}$ is the state space. Upon the basis of $\mathbf{w}_n$ the agent chooses a control $u_n \in U$ from the set of all possible controls U, based on a given control strategy $\pi_n(\mathbf{w}, u)$ defined by the probability distribution of choosing $u_n = u$ with the conditions that $\mathbf{w}_n = \mathbf{w}$. At the next time step $n+1$ the agent obtains a reward r_{n+1} and a new representation $\mathbf{w}_{n+1}$ based on the chosen control u_n. The goal is to maximize the rewards. For the specific example of the dissipative standard map, the possible set of control actions is chosen as $U = (0, u_{max}, -u_{max})$, so that the forcing f_0 is either increased or diminished by u_{max} or no action is taken. The finite set $\mathbf{W}$ is taken as a finite approximation of the true state space $\mathbf{X}$ using a vector quantization technique [263].

This technique leads to a cell form, coarse-grained partitioning of the state space. Each state $\mathbf{x}$ of the true state space $\mathbf{X}$ is projected onto one vector $\mathbf{w}(\mathbf{x})$ of the reduced space $\mathbf{W}$, in such a way that $\mathbf{w}$ is the closest vector according to some (in general, the Euclidean) norm. The policy is defined by assigning an action $Q(\mathbf{w}(\mathbf{x}), u)$ to each pair of reduced state $\mathbf{w}$ and allowed control u. The algorithm is then as follows: Whenever the system trajectory is in the state $\mathbf{x}$, the corresponding vector $\mathbf{w}$ is determined and a control $u(\mathbf{x})$ is chosen in agreement with the action Q. The reward is defined by $r_{n+1} = -0.5$ if the trajectory is far away from the metastable state one wants to reach, i.e. $|\mathbf{x}_B - \mathbf{x}_n| > 1$ and $r_{n+1} = 1$ otherwise. In this case, the selected fixed point to approach is $\mathbf{x}_B$, but this scheme can be applied to reach any of possible metastable fixed points in the dissipative standard map.

4.3. Trajectory selection by a periodic feedback

The idea of employing a periodic feedback to select a certain attractor was developed by Yu Jiang [264] who considered the periodically driven Duffing oscillator [239]

$$\frac{d^2x}{dt^2} + 0.05\frac{dx}{dt} + x^3 = a + b\cos(t) + \epsilon F(x, s) \tag{35}$$

with a driving force

$$F(x, s) = s(t) - x(t), \tag{36}$$

where $s(t)$ stands for a particular trajectory, that one attempts to obtain for an arbitrary initial condition, and $\epsilon = 0.37$ represents a driving strength. The system equation (35) at $a = 15$ and $b = 0.21$ exhibits the coexistence of three stable periodic orbits (period 1, period 2, and period 3); the period 2 and period 3 overlap in the $(x, \dot{x})$ subspace.

Suppose that the target trajectory $s(t)$ is the period-2 orbit. Indeed, when the feedback signal equation (36) is applied, the trajectory $x(t)$, being initially in either the period-1 or period-3 attractor, goes to the target trajectory $s(t)$ which lies in

the period-2 attractor. This control works when the amplitude strength ϵ exceeds some threshold value, i.e. when $\epsilon > \epsilon_c$. After the system is in the target trajectory, the feedback $F(x, s)$ vanishes. Since the desired trajectory is stable, the feedback driving can be removed as soon as the system falls in the basin of attraction of the desired state. Thus, the feedback periodic driving equation (36) allows the selection of desired attractors in a multistable system.

4.4. Control of multistability in delayed feedback systems

We already mentioned in Section 2.1.4 that coexistence of attractors often appears in systems with time-delayed feedback, as was predicted by Ikeda [169,170]. In this section we will show how this kind of multistability can be controlled in order to make the system monostable. The control of multistability can also be used in combination with methods for controlling chaos. A control technique which combines the Pyragas method for chaos control [265] and attractor annihilation by harmonic modulation was outlined in Refs. [176,178]. In the Pyragas method, the feedback signal, proportional to the difference between the current variable and its previous value taken at a delay time τ, stabilizes an unstable periodic orbit embedded in the chaotic attractor; the period of this orbit is equal to τ. At the same time, the delayed feedback can stabilize other periodic orbits with periods multiple of τ, thus leading to multistability. Although chaos is replaced by a periodic motion, the system becomes multistable. To avoid undesirable attractors or to make the system monostable, the application of attractor annihilation technique is appropriate in this situation. In the following, we will demonstrate how this approach works on the example of the logistic map and in a laser.

4.4.1. Delayed feedback logistic map

The time-delayed logistic map is one of the simplest systems which displays bistability. It can be described as follows

$$x_{n+1} = ax_n(1 - x_n) - \eta x_{n-k}, \tag{37}$$

where x_{n+1} is measured as time series with $x \in [0, 1]$ and $a \in [1, 4]$, k is the delay time, and η is the feedback strength. It was found [176] that short delays ($k \leq 3$) induce a new attractor, so that the system becomes bistable for certain values of the parameters a and η; in particular, a period 3 appears.

Fig. 19 illustrates the changes induced by the delayed feedback in the bifurcation diagrams constructed using a as a control parameter for four different delays $k = 1, 2, 3, 100$ and fixed feedback strength $\eta = 0.19$. One can see that short delays induce bistability in the system, while long delays do not. For $k = 1$ (Fig. 19(a)) the period-2 branch coexists with the period-3 branch in the parameter range of $a \in [3.60, 3.65]$, instead of the chaotic attractor without feedback. Bistability is also observed for $k = 2$ (Fig. 19(b)) and $k = 3$ (Fig. 19(c)) but in the narrower parameter ranges. Instead, very large delays (e.g. $k = 100$) do not induce new attractors, and hence only the chaotic attractor remains (Fig. 19(d)).

In the following, we will consider the short delay $k = 1$ because in this case the parameter range for bistability is largest. The calculations show that when the feedback strength η is increased, the bistability range enlarges and the original cascade of period-doubling bifurcations shifts towards larger values of a, while the induced period-3 attractor is located approximately around the same values of a. The bifurcation diagram with respect to the feedback strength ν for the fixed parameter $a = 3.815$ is shown in Fig. 20. As the feedback strength is increased, the map equation (37) undergoes an inverse cascade of period-doubling bifurcations on the period-2 branch which coexists with the period-3 branch within $\nu \in [0.04, 0.25]$.

Next, to control multistability in a delayed-feedback system the method of attractor annihilation can be used. Specifically, a harmonic modulation can be applied either to a system parameter or to a system variable x. Any of these ways allows annihilation of coexisting attractors thus making the system monostable. Consider now how these modulation strategies work with the above example of the logistic map equation (37).

(i) *Parameter modulation.* The control in form of a harmonic modulation is introduced as

$$a = a_0 - a_c \sin(2\pi f_c), \tag{38}$$

where a_0 is the initial value of the parameter, and a_c and f_c are the modulation amplitude and frequency, respectively. While $\eta = 0.145$ and $a_0 = 3.815$ are fixed in the middle range of bistability, where the period-2 and period-3 attractors coexist, the control modulation equation (38) is applied with $a_c \leq 0.0225$ to be within the range of bistability.

(ii) *Modulation of the feedback strength.* In a similar way the control modulation can be applied to the feedback strength as follows

$$\eta = \eta_0 - \eta_c \sin(2\pi f_c), \tag{39}$$

where η_0 and η_c are the initial values of the feedback strength and modulation amplitude, respectively. While $a = 3.815$ and $\eta_0 = 0.145$ are fixed in the middle range of bistability, the control modulation equation (39) is applied with $\eta_c \leq 0.1985$.

(iii) *Modulation of the variable.* The delayed-feedback logistic map with modulated variable can be written in the following form

$$x_{n+1} = ax_n(1 - x_i) - \eta x_{n-k} - \delta \sin(2\pi f_c n), \tag{40}$$

where δ is the modulation amplitude. This modulation is equivalent to an external harmonic forcing. As in the above cases, $a = 3.815$ and $\eta = 0.145$ are fixed and the control modulation equation (40) with $\delta \leq 0.025$ is applied to be always within the range of bistability.

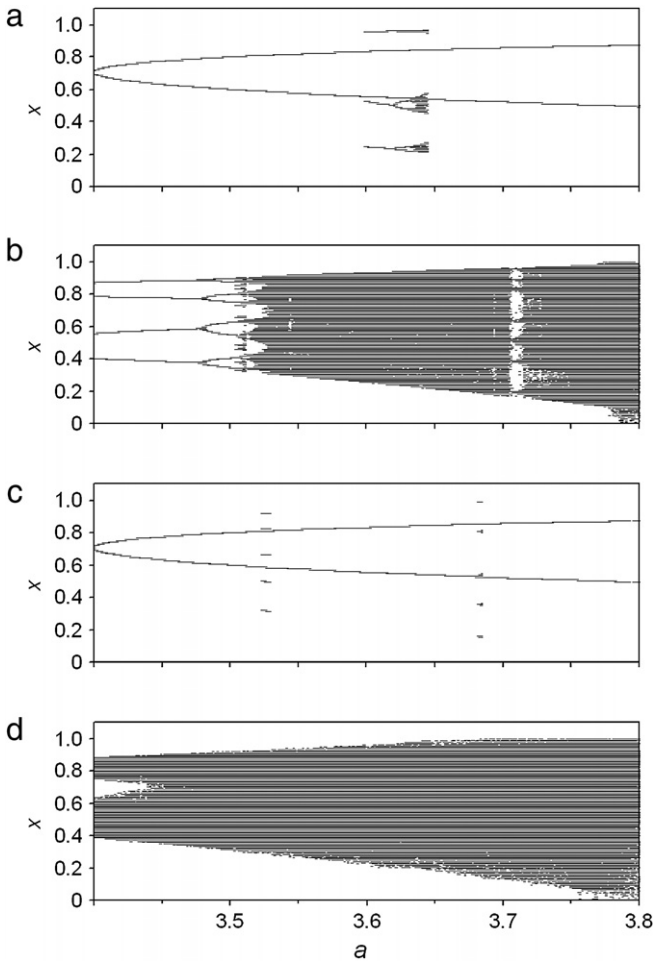

Fig. 19. Bifurcation diagrams of the delayed logistic map with respect to a at $\eta = 0.19$ and (a) $k = 1$, (b) 2, (c) 3, and (d) 100.

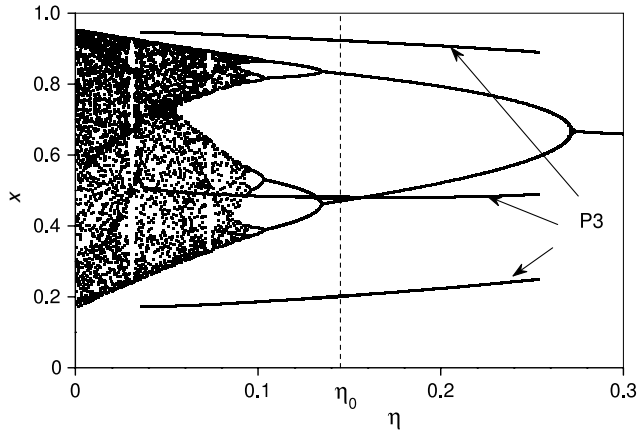

Fig. 20. Bifurcation diagram of the delayed logistic map with respect to feedback strength η for $a = 3.815$. The dashed line indicates the initial value of feedback strength $\eta_0 = 0.145$ at which the control is applied.

The effect of the control modulation in the case (ii) is illustrated in Fig. 21. Fig. 21(a) shows how the map being in the period 3 responds to the feedback modulation. When the modulation amplitudes η_c is small, the system response is lineal, i.e., there are resonances at the mapping frequency $f_c = 1/3$ and its subharmonic $f_c = 1/6$. For high η_c, additional resonances appear due to increasing nonlinearity.

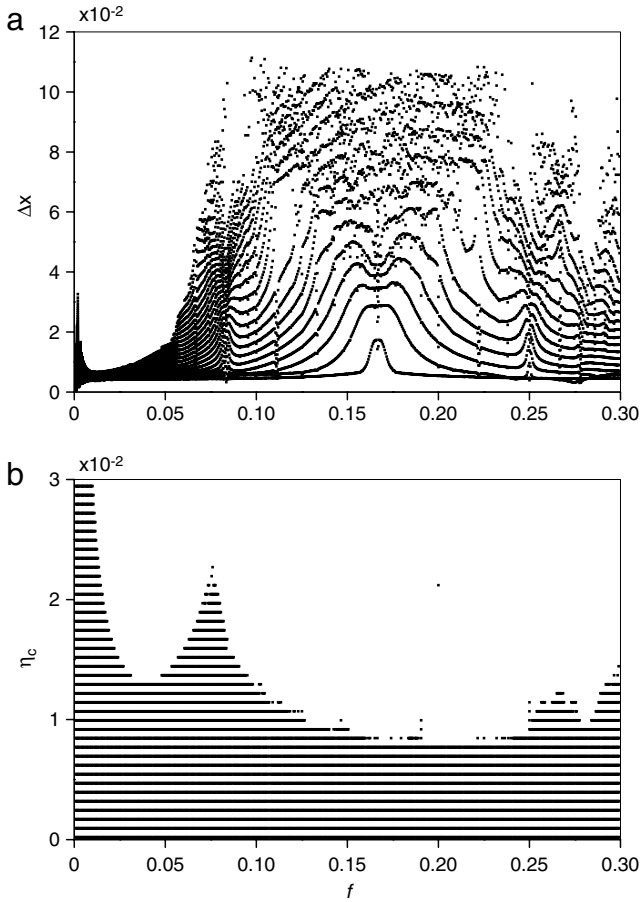

Fig. 21. Alternative amplitude Δx of system response to control modulation of feedback strength η versus modulation frequency f_c and (b) stability boundary of period-3 attractor in (f_c, η_c) space. Each curve in (a) corresponds to fixed η_c starting from $\eta_{c1} = 2 \times 10^{-4}$ (lowest curve) with interval $\Delta\eta_c = 7.5 \times 10^{-4}$.

The stability boundary of the period-3 attractor in the parameter space of the modulation frequency and amplitude is shown in Fig. 21(b). For the parameter values inside the dashed region, two attractors (period 2 and period 3) coexist, whereas in the blank region the map is monostable, i.e., only period-2 attractor exists. Indeed, the absolute minimum in the annihilation curve appears at the frequency of damped oscillations $f_0 \approx 0.22$ when the trajectory approaches the period-3 attractor. The other (local) minima occur at combined frequencies (at $f_0 - 1/3 \approx 0.05$ and $1/2 - f_0 \approx 0.28$).

The attractor annihilation by low-frequency modulation can be easily realized in practice. Slowly increasing the modulation frequency from zero, one can find the first local maximum in the system response without any preliminary knowledge of the system dynamics. The comparative analysis of efficiencies of these different types of the control allows us to conclude that the modulation of the multiplicative parameter is the most efficient way for annihilating attractors in a bistable system.

4.4.2. CO_2 *laser with electronic feedback*

Next, we will show how multistability can be controlled in a CO_2 laser with delayed feedback. The specific property of this laser is that it displays chaos of Shilnikov type [266]. This chaotic motion is characterized by an erratic behavior when a parameter is varied towards the homoclinic condition associated with a saddle focus [267]. A specific feature of Shilnikov chaos is that it exists within very narrow parameter ranges and the distance between these narrow chaotic windows changes exponentially when a control parameter is varied [268,269]. Moreover, it is extremely difficult to find this type of chaos experimentally due to unavoidable noise and small fluctuations of the system parameters. However, Shilnikov chaos has been found numerically in a CO_2 laser with delayed electronic feedback [268,269].

The model is based on a four-level scheme for the active medium [270] leading to the following six-equation dynamical model

$$\dot{x_1} = k_0 x_1 \left\{ x_2 - 1 - k_1 \sin^2 \left[\varepsilon x_6 (\theta - T_0) + (1 - \varepsilon) x_6 \right] \right\}, \tag{41}$$

$$\dot{x_2} = -\Gamma_1 x_2 - 2k_0 x_1 x_2 + \gamma x_3 + x_4 + P_0, \tag{42}$$

Table 1
Parameter values used in simulations.

Γ_1	10.0643	α	32.8767	k_0	28.5714	γ	0.05
Γ_2	1.0643	β	0.4286	k_1	4.5556	P_0	0.016

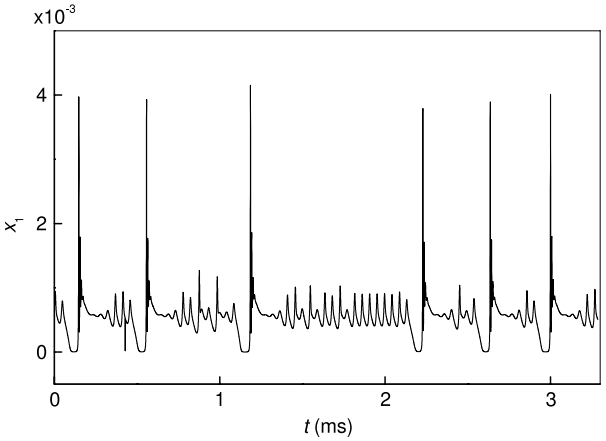

Fig. 22. Time series of chaotic oscillations in a CO_2 laser with feedback $R = 160$, $B_0 = 0.10315$.

$$\dot{x_3} = -\Gamma_1 x_3 + x_5 + \gamma x_2 + P_0, \tag{43}$$

$$\dot{x_4} = -\Gamma_2 x_4 + \gamma x_5 + z x_2 + z P_0, \tag{44}$$

$$\dot{x_5} = -\Gamma_2 x_5 + z x_3 + \gamma x_4 + z P_0, \tag{45}$$

$$\dot{x_6} = -\beta x_6 + \beta B - \beta f(x_1), \tag{46}$$

where $f(x_1) = Rx_1/(1 + \alpha x_1)$ is the feedback function, x_1 is the normalized photon number proportional to the laser intensity, x_2 is proportional to the population inversion, x_3 is proportional to the sum of the populations on the two resonant levels, x_4 and x_5 are proportional, respectively, to difference and sum of the populations of the rotational manifolds coupled to the lasing levels. It is assumed that each manifold contains $z = 10$ sublevels. The variable x_6 is proportional to the feedback voltage that affects the cavity loss parameter through the relation $k_0(1 + k_1 \sin^2 x_6)$. θ is the time rescaled to the collision relaxation rate $\gamma_r = 7 \times 10^5$ s^{-1}, i.e. $\theta = t\gamma_r$, where t is the real time. The control parameters B and R are proportional to the bias voltage and the gain of the feedback, respectively. The parameters Γ_1, Γ_2, γ, and β represent decay rates, α is a saturation factor of the feedback loop, and P_0 is the pump parameter. The fixed parameter values are collected in Table 1. They correspond to accurate measurements performed on the experimental system [271].

Eq. (46) contains the delayed variable $\varepsilon x_6(\theta - T_0)$, where ε is the strength of the delay signal and T_0 is the delay time. The laser without delay ($T_0 = 0$ and $\varepsilon = 0$) operates in a chaotic regime characterized by large and small spikes (Fig. 22) corresponding to alternative large and small loops forming respectively inward and outward spirals in the phase space in the vicinity of an unstable saddle focus. This fixed point has two real (λ_1 and λ_2) and four complex conjugate eigenvalues. The inward spiral motion is related to a nonstationary solution of the equation model characterized by a stable manifold with complex eigenvalues $(-\rho_2 \pm i\omega_2)$. For a homoclinic orbit associated with such a saddle focus Shilnikov showed that, if $|\rho_2/\lambda_2| < 1$, then a homoclinic orbit is created and the system represents a chaotic behavior of Shilnikov type [267].

Synchronization of Shilnikov chaos by delayed feedback, referred to as *delayed self-synchronization*, was demonstrated by Arecchi et al. [272]. However, at certain delay times the delayed feedback induces multiple coexisting attractors, whose period T is a linear function of the delay time T_0. For example, two coexisting periodic attractors appear at $\varepsilon = 0.25$ in the range of delay times $110 < T_0 < 160$ (in normalized units of γ_r), as shown in Fig. 23(a). At fixed $T_0 = 140$ the coexisting attractors have periods $T_1 = 147.3$ and $T_2 = 74.7$ (horizontal dashed lines) that are close to T_0 and $T_0/2$. The dependences in Fig. 23 are obtained by calculating the autocorrelation function of the laser intensity and measuring the correlation period [272]. The chaotic regime yields zero autocorrelation function and hence $T = 0$ (Fig. 23(c)). Next, we will show how harmonic modulation to the feedback variable locks one of the coexisting periodic orbits.

In the laser with harmonic modulation of the feedback variable, Eq. (46) becomes

$$\dot{x_1} = k_0 x_1 \left\{ x_2 - 1 - k_1 \sin^2[\varepsilon x_6(\theta - T_0) + (1 - \varepsilon)x_6 + \zeta \sin(2\pi f \theta)] \right\}, \tag{47}$$

where ζ is the modulation amplitude. The effect of the modulation is strongly dependent on the modulation frequency. One of the coexisting periodic orbits can be locked when either (i) the modulation frequency is proportional to the reciprocal

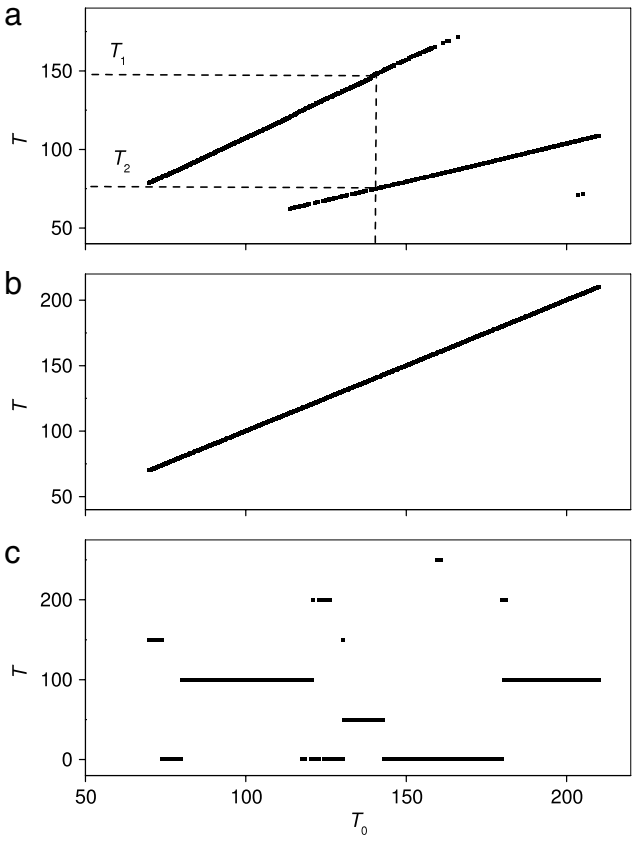

Fig. 23. (a) Coexisting stable periodic orbits in a CO_2 laser with delayed feedback. (b) Locking of the periodic orbit of period $T = T_0$ when the feedback variable is modulated with delay-dependent frequency $f = 1/T_0$ or (c) with fixed frequency $f = 1/50$. $\zeta = 0.01$ and $\varepsilon = 0.25$. The horizontal dashed lines show the periods $T_1 = 147.3$ and $T_2 = 74.7$ of the coexisting states, which appear when the modulation with $T_0 = 140$ (shown by the vertical dashed line) is applied.

delay time ($f = n/T_0$, where $n = 1, 2, \ldots$) or (ii) the modulation frequency is fixed ($f = const$). These cases are illustrated, respectively, in Fig. 23(b) and (c). Note, that T, T_0, f in the text and figures are normalized to γ_r. In both cases the modulation amplitude is relatively small ($\zeta = 0.02$) and there are ranges of T_0 where only one periodic state exists.

The analysis of these results allows us to reveal the following main features of this kind of control: (i) Time dependent modulation of the delay variable locks a state whose period is equal to T_0, i.e. $T = T_0$ (Fig. 23(b)). (ii) Fixed frequency modulation locks a periodic orbit multiple of T_0, i.e. $T = (i/j)T_0$ ($i, j = 1, 2, \ldots$) (Fig. 23(c)).

Fig. 24 demonstrates the effect of the control modulation with the time series. The delay time is fixed at $T_0 = 140$ and the control is switched on at time $\theta = 2.5 \times 10^4$. The left-hand column shows the case when the control is applied to the orbit with period $T_1 = 147.3$, while the right-hand column to the orbit with $T_2 = 74.7$. One can see that after transients both attractors are simultaneously destroyed and the trajectory goes to the periodic orbit whose period is equal to the period of the control modulation.

Fig. 25 shows the stability diagram for the attractor with period $T_2 = 74.7$ in the space of the modulation parameters ζ and f. The crosses indicate the region in the parameter space where this attractor does not exist. This region forms tongues whose minima are located at the relaxation oscillation frequency of the attractor, $f_r \approx 7.25 \times 10^{-3}$ and at the frequencies equal to approximately second and third harmonics of f_r. For the parameters inside the tongues (shown by the crosses), the attractor $T_2 = 74.7$ is destroyed and only attractor $T_1 = 147.3$ remains. Thus, the modulation of the feedback variable makes the system monostable.

5. Stochastic control of multistability

The interplay between stochasticity and nonlinearity is a current issue in the study of different dynamical systems, including radio-physical [273], climatic [274,275], populational [276,277], geophysical [278], epidemiological [279], and optical models [280], as well as in the analysis of medical data [281]. Several experimental and theoretical works have demonstrated that noise sometimes plays a positive role in multistable systems, e.g., inducing stochastic [282], coherence [283] and vibrational [284] resonances, preference of attractors [8,140,145,285,286], attractor hopping

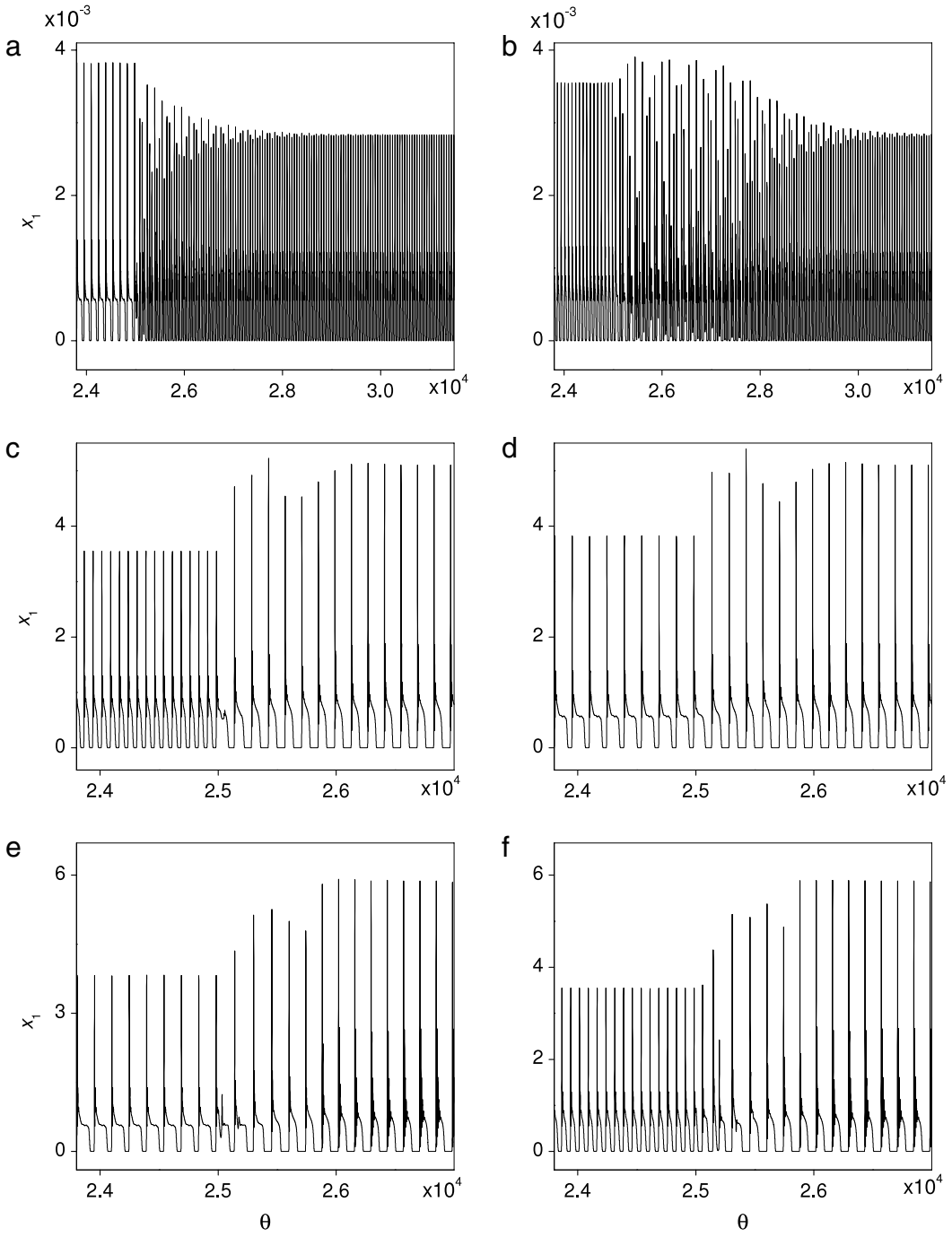

Fig. 24. Time series of CO_2 laser intensity when feedback modulation with $\zeta = 0.02$ is applied at time $\theta = 2.5 \times 10^4$ with frequencies (a, b) $f = 1/50$, (c, d) $1/T_0$ and (e, f) $f_r = 7.25 \times 10^{-3}$. The initial states periods are (a, c, e) $T_1 = 147.3$ and (b, d, f) $T_2 = 74.7$.

[287–290], and enhancing multistability [7,291]. The influence of noise on multistability was first investigated by Arecchi et al. [58,292], who observed noise-induced switches between coexisting states. Later, it was also found that noise can induce new attractors. This phenomenon has been demonstrated in a laser system [293] and in coupled oscillators [291]. The role of stochastic resonance in attractor destruction was discussed with Duffing oscillators [239]. Noise-induced preference of attractors was also observed in coupled oscillators [145], in the Hénon map [179], and in a multistable fiber laser [294,295].

In general, when discussing the effects of noise in a dynamical system, three different ranges of the noise amplitude can be distinguished: low, intermediate, and strong noise. While at low noise the phase–space trajectory stays essentially in the neighborhood of an attractor resulting in small deviations from the deterministic dynamics, an intermediate noise level

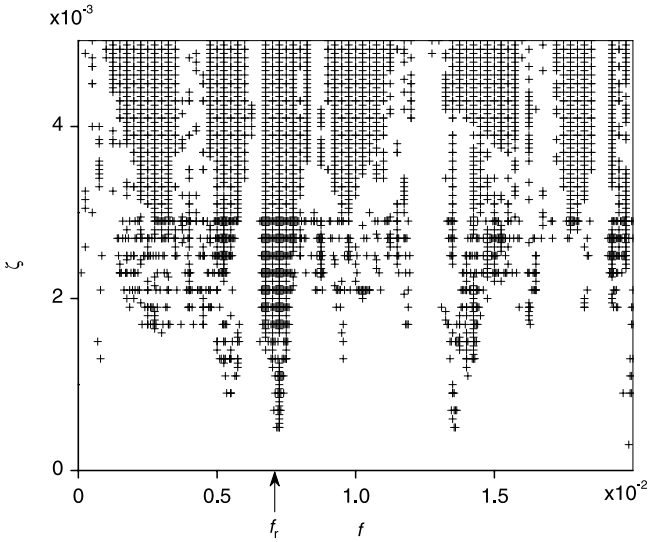

Fig. 25. Stability diagram of the period-74.7 attractor in the CO_2 laser with periodic modulation of feedback variable. The crosses indicate the region where the period 74.7 is annihilated. For other parameters the period 74.7 is stable and coexists with the period-147.3 attractor. The arrow indicates the relaxation oscillation frequency f_r of the period-74.7 orbit.

leads to the characteristic hopping dynamics between the now metastable states, the former deterministic attractors. Due to a nontrivial relationship between the coexisting states and their basins of attraction, the final state depends crucially on the initial conditions [140]. Noise a multistable system results in so complex behavior that the overall dynamics can be divided in two different phases: a rather regular motion in the neighborhood of attractors and noise-induced jumps between coexisting metastable states. The dynamics is then characterized by a large number of periodic states "embedded" in a sea of transient chaos [138]. The time the system spends close to an attracting state corresponds to its "ordered" phase, and the transient time to its "random" or "chaotic" phase. Strong noise can prevent the system from settling down into any ordered phase. For the large-amplitude noise most of the former attractors cannot be identified anymore. Instead, the dynamics corresponds to a diffusion process over the state space. These different effects of noise on the attractors' structure have been established experimentally in a fiber laser [290,295,296].

Since any noise, regardless of its amplitude, makes the system dynamics probabilistic, one needs to solve stochastic equations. For every initial condition, the system will follow a trajectory and reach one or another of the coexisting attractors with a certain probability depending on the noise amplitude. In general, the trajectory will stay only for a certain time span in the neighborhood of an attractor before it is kicked out and approaches another or again the same attractor. Taking this hopping dynamics into account, the important concept of the basin of attraction belonging to one attractor only needs to be interpreted in another way. While a basin of attraction does not exist in noisy dynamical systems in a strict mathematical sense, one can still consider the basin in a statistical sense. As a first approach, one can look for each initial condition which of the attractors will be reached first after the iteration is started regardless the fact that it will be kicked out of this attractor at a later time. As a second approach, one can always start from the same initial condition and change the noise realization to find the probability with which each of the attractors is reached. This probability again gives some measure of the size of the basin of attraction under the noise influence. Therefore, in both cases only statistic stability of the attractors can be measured.

Besides the importance for specific applications, a further motivation to study the dynamics of noisy multistable systems is their possible role in neural information processing [11], because with adequate noise, the system can rapidly access different ordered states. The control of such systems under different conditions would then offer the opportunity to utilize this multistable behavior for information processing and storage, i.e., different ordered states could be identified with different "memorized" pieces of information. External input can be thought of as triggering a certain control mechanism that stabilizes a selected ordered state that would be associated with the given input.

The high sensitivity of a multistable system to noise can be used to control multistability. In the following we will show how noise (i) induces preference for certain attractors [140], (ii) selects desired attractors [145], and (iii) annihilates attractors in stochastic resonance [179,252,295].

5.1. Noise-induced preference of attractors

Although in a deterministic case the basins of attraction of multiple coexisting attractors can have a very complicated structure, under random perturbations this structure becomes blurred and particularly close to the deterministic basin boundaries; the attractor to which a trajectory, starting for certain initial conditions, will go depends on the noise realization.

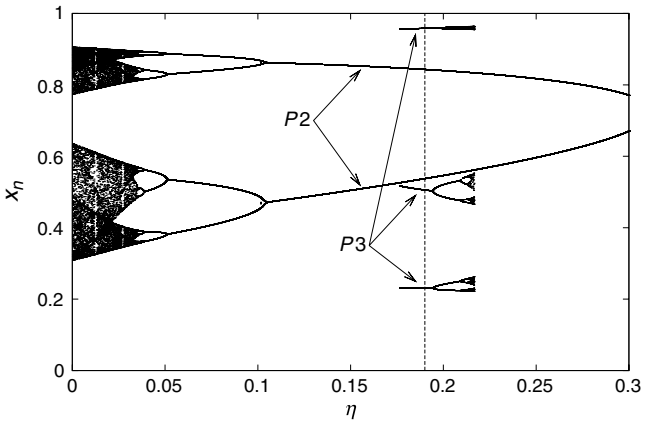

Fig. 26. Bifurcation diagram of the delayed logistic map equation (49) for $a = 3.625$ and $\tau = 1$. For $\eta = 0.19$ (vertical dashed line) there are two coexisting stable solutions, $P2$ and $P3$, found using different initial conditions.

This effect of blurring basin boundaries leads to the fact that small basins of attraction cannot be discerned anymore when the noise amplitude becomes too large. These basins become "buried" under the noise and these attractors cannot be found anymore in the phase space. As a consequence, only the attractors with large basins of attraction in the deterministic case are preferred in a noisy system, while the attractors with small basins of attraction disappear. In the following sections we will illustrate this effect called *noise-induced preference of attractors* with two examples.

5.1.1. Kicked mechanical rotor

The first example is a periodically kicked mechanical rotor without gravity equations (1) and (2) already considered in Section 2.1.1. Taking into account that the kicks are only applied at certain discrete times $t = 0, T, 2T, \ldots$ and adding noise to each variable, the rotor is modeled by the following two-dimensional map [140]:

$$\begin{aligned} x_{n+1} &= x_n + y_n + \delta_x \mod 2\pi, \\ y_{n+1} &= (1-\nu)y_n + f_0 \sin(x_n + y_n) + \delta_y, \end{aligned} \tag{48}$$

where δ_x and δ_y are the components of the uniformly and independently distributed noise with a bounded norm $\sqrt{\delta_x^2 + \delta_y^2} \leq \delta$ and f_0 is the strength of the forcing. For the parameter values $f_0 = 3.5$ and $\nu = 0.02$, Kraut et al. [140] found numerically 111 stable periodic orbits in the noiseless limit. Most of these orbits belong to the period-1 family and some of them have period 3. Only 0.01% of all found orbits have periods other than 1 and 3, so these orbits do not play an important role. With noise added, three different types of behavior are observed. For small noise level ($\delta \lessapprox 0.05$) the trajectory may be trapped in the open neighborhood of an attractor forever. For intermediate noise ($0.05 \lessapprox \delta \lessapprox 0.1$) attracting periodic orbits could be still identified because the characteristic hopping process between them takes place. However, one cannot find all the deterministic attractors in this hopping dynamics. Instead, the number of attractors is drastically reduced to only 11 attractors when the noise level is increased to $\delta = 0.01$.

There are two reasons for such a behavior. First, the basins of attraction of many stable periodic orbits shrink exponentially as the noise level is increased. This shrinking is more pronounced for attractors having small basins of attraction in the deterministic case [140]. Second, the hopping process is also determined by the structure of the chaotic saddles embedded in the basin boundaries. Only those states which are accessible by the noisy trajectory can take part in the hopping process [288]. Changing the noise level in an appropriate way, it is possible to involve more or less states in the hopping dynamics. Therefore, using noise one can control the number of attractors which can be observed.

5.1.2. Delayed feedback logistic map

The second example is the popular logistic map described in Section 4.4.1. Now we will apply the delayed feedback in the form used by Pyragas [265] as follows

$$x_{n+1} = a x_n (1 - x_n) + \eta (x_{n-\tau} - x_n), \tag{49}$$

where the strength of delayed feedback η can be either positive ($\eta > 0$) or negative ($\eta < 0$) [176]. Bistability in the logistic map equation (49) is observed in the bifurcation diagram in Fig. 26, where the coexisting period-2 (P2) and period-3 (P3) attractor branches appear within a certain range of η.

Now, we will show that in the presence of additional small noise these attractors remain stable only statistically and the probability of their emergence can be controlled by noise added at each iteration as follows

$$x_{n+1} = a x_n (1 - x_n) + \eta (x_{n-1} - x_n) + D\xi_n, \tag{50}$$

where D is the noise amplitude and ξ_n is a random variable in the interval $[-1, 1]$ with a Gaussian probability distribution.

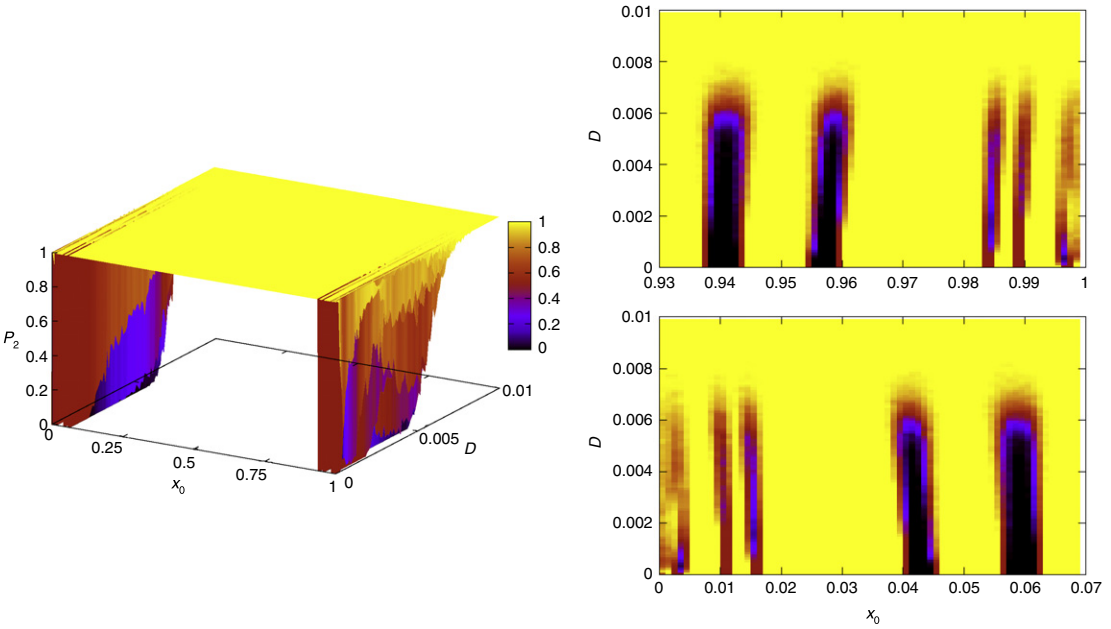

Fig. 27. (Left) Probability of period-2 attractor emergence, P_2, in the delayed noisy logistic map equation (50) for different initial conditions x_0 and noise amplitudes D. (Right) Projections on the (x_0, D) plane close to $x_0 = 1$ (top) and $x_0 = 0$ (bottom). The color scale denotes the probability with which an initial condition leads to the period 2. The period-3 attractor does not exist for $D > 0.008$. $a = 3.625$, $\eta = 0.19$, and $\tau = 1$. (For interpretation of the references to color in this figure legend, the reader is referred to the web version of this article.)

Fig. 27(a) shows the probability to obtain a stable P2 solution (P_2) in the space of initial condition x_0 and noise amplitude D. The period 3 exists only within narrow windows of the initial conditions close to $x_0 = 0$ and $x_0 = 1$ (Fig. 27(b) and (c)). The probabilities P_2 and P_3 to obtain P2 and P3 complement each other, i.e., when $P_2 = 1$ then $P_3 = 0$. In the noisy map equation (50), when D is increased, P_3 decreases and the P3 attractor disappears at $D = 0.008$ resulting in monostability.

Since the basins' volumes (the number of initial conditions leading to the corresponding stable solution) have a probabilistic character, for every fixed noise amplitude D the basins' volumes were calculated 1000 times exploring as many as 10^5 initial conditions and the probability distribution was measured [297]. Fig. 28 illustrates statistical properties of the coexisting $P2$ and $P3$ attractors under the influence of noise. The probability distributions of the sizes of the basins of attraction of the two coexisting states are shown in the upper panels of Fig. 28. The lower panel demonstrates how the most probable basins' size N_{max} (the number of initial conditions leading to the corresponding attractor with maximum probability) depends on D. While small and large noise amplitudes have no influence on N_{max}, an intermediate noise ($0.005 < D < 0.008$) changes the basins' structure increasing the basin of attraction of $P2$ and decreasing the $P3$ basin up to zero, hence giving rise to monostability at $D = 0.008$. This behavior demonstrates that bistability can be simply controlled by noise.

5.2. Attractor selection by noise

High-dimensional globally coupled dynamical systems can have a very large number of attractors. Multistability in one of such systems, globally coupled maps (GCM), was studied by Kaneko et al. [164,298–301] under the influence of noise [145,302]. They found that a change in the time span during which noise is applied, leads to different final attractors. Hence, a certain predefined attractor can be reached employing an appropriate noise realization. To explain the mechanism for this controlled selection let us consider GCM expressed as [302]

$$x^i_{n+1} = (1-\varepsilon) f(x^i_n) + \frac{\varepsilon}{N}\sum_{j=1}^{N} g(x^j_n), \tag{51}$$

where $f(x^i_n)$ is the local map and $g(x^j_n)$ is a map applied to the elements coupled to. The subscript n and superscript i indicate respectively the discrete time and the element, while N is the system size and ε is the coupling constant. It is supposed, for simplicity, that $g(x) = x$ and that the map is logistic, i.e., $f(x_n) = x_{n+1} = 1 - \alpha x_n^2$. As usually done for GCM, elements are grouped into clusters that oscillate in unison, taking nearly identical x values. In particular, by adding a suitable amount of noise for some time, one can switch attractors such that the cluster number, i.e. the number of possible coexisting attractors, is eventually reduced one by one [302]. Conversely, by adding a larger amount of noise, it is possible to desynchronize the elements and increase the cluster number. Thus, the controlled attractor selection is possible by just changing the noise amplitude and its duration.

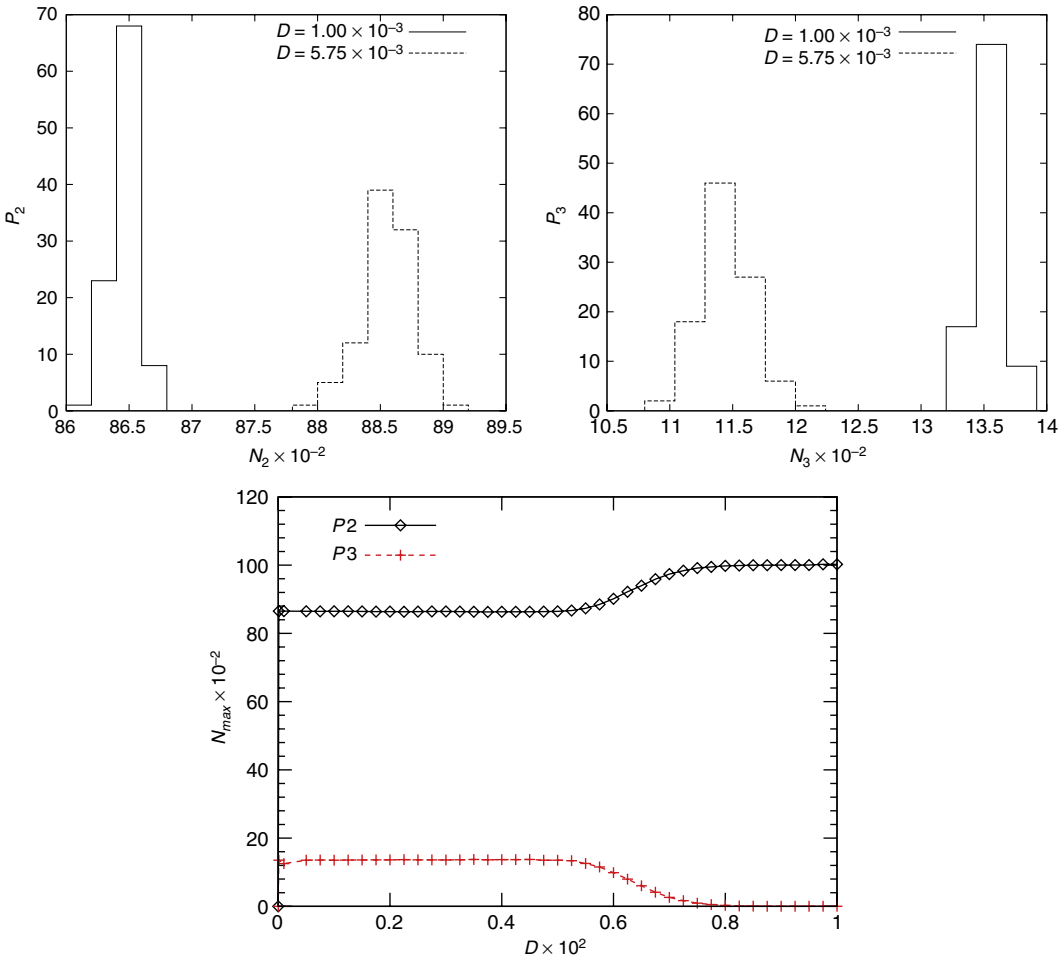

Fig. 28. Statistical characteristics of noisy delayed feedback logistic map equation (50). (Up) Probability distributions P_2 (left) and P_3 (right) of $P2$ and $P3$ basins' sizes N_2 and N_3, respectively, for two different noise amplitudes D. (Down) Most probable basins' sizes N_{max} of $P2$ and $P3$ attractors as functions of D.

Fig. 29 shows how the number of coexisting attractors is controlled by noise. Starting from random initial conditions and allowing for a transient of 10^5 time steps, a short "down-level" noise burst is applied for ten times every 10^3 time steps, and then, starting from time 13×10^3 a short "up-level" noise burst is applied six times. The line marked with the circles represents the average number of clusters just before and just after applying the noise bursts over 10^3 runs. The "down level" for the noise is 5% and the "up level" is 9%, while the "down-burst time" is 25 time steps and the "up-burst time" is 5 steps. The solid line shows a single run with the number of clusters determined at every time step. Again, noise bursts are applied as for the averaged case, except that the "burst-up" time is five time steps and the "burst-down time" is two time steps. It is important to note that noise is only required for the switching of the attractors and not for sustaining them once selected. The observed phenomenon is explained by increasing system stability when a number of elements in a synchronized cluster increases.

5.3. Robustness of the control to noise

As discussed above, some control strategies have been developed to keep the system in a preselected attractor in spite of noise. Another control approach has been designed to annihilate undesirable attractors and make the system monostable. A fundamental problem of this type of multistability control is then its robustness to noise. Is it still possible to drive the system from multistability to monostability in the presence of noise? Fortunately, recent studies with two paradigmatic models, namely, the tristable Hénon map and the bistable delayed logistic map, give the positive answer to this question.

5.3.1. Multistable noisy Hénon map

Let us consider the Hénon map subject to both random and periodic modulations as [8]: $x_{n+1} = 1 - \mu x_n^2 + y_n + \xi_n$, and $y_{n+1} = -Jx_n + \phi_n$, where ξ and ϕ are Gaussian white noise of zero mean and identical standard deviation σ. Even without noise, the dynamics of the Hénon map is very complex and reveals self-similar organization of multiple attractors, as shown in Fig. 30.

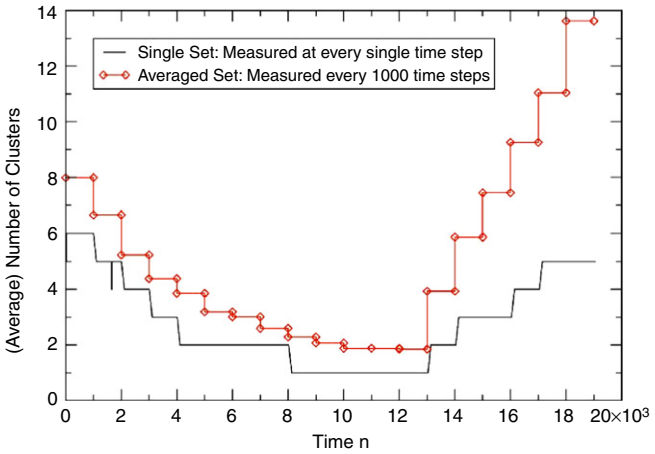

Fig. 29. Noise-induced attractor switching for $\alpha = 1.77$, $\varepsilon = 0.14$, and $N = 60$. The attractors are controlled by applying short noise bursts of 5% for reducing the cluster number and of 9% for increasing the cluster number.
Source: From Ref. [302].

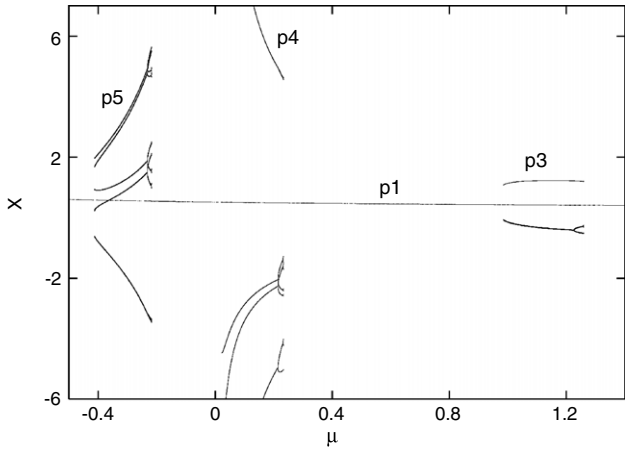

Fig. 30. Bifurcation diagram of the Hénon map demonstrating successive appearance of a series of first-order secondary cascades of period 5, 4, and 3 around the period-1 branch. $J = 0.98$.

Although noise of an adequate strength induces an intermittent transition among basins of attraction of coexisting states, the system dissipativity always attempts to pull and retain a phase–space trajectory back to the same basin, and as a consequence, no such a transition may occur. The creation and evolution of the basins of attraction of multiple coexisting states in the Hénon map are very similar to those in the Toda oscillator [155]. In particular, the basins of higher-order secondary cascades appear and always remain within the basins of the immediate lower-order secondary cascades. Higher the order of the cascades, progressively smaller their basins. Consequently, the noise effect is more pronounced for higher-order secondary cascades, for example, strong enough noise can induce a transition from higher-order to lower-order secondary cascades.

The bifurcation diagram in Fig. 31(a) demonstrates the effect of moderate noise ($\sigma = 0.001$) on the period-16 (p_{16}) branch around the period-4 (p_4) branch. For the parameter values just past the crisis point, the period-16 attractor no longer exists. Since, the p_4 basin is much larger then the p_{16} basin, the p_4 attractor can withstand stronger noise. Fig. 31(b) shows the bifurcation diagram at stronger noise ($\sigma = 0.005$), where it is seen that beyond boundary crisis p_4 settles in p_1.

The combined effect of noise and periodic modulation applied to μ, $\mu = \mu_0(1+\eta \sin(2\pi ft))$, is demonstrated in Fig. 31(c) and (d). By increasing the modulation amplitude η, the destruction of p_{16} and consequent transition to p_4 are observed [shown by the arrows in Fig. 31(c)]. Similar destruction is also observed in the case of noisy p_{12} and p_{20}. Each destruction is followed by a transition to noisy p_4, which can be also destroyed by increasing η and keeping μ_0 fixed. Fig. 31(d) shows a typical destruction of noisy p_4 in the presence of relatively strong noise ($\sigma = 0.005$). After destruction of p_4, the system jumps (shown by the arrow) to the remaining p_1.

The time series in Fig. 32 demonstrate the robustness of attractor annihilation to relatively strong noise which induces a spontaneous transition between coexisting states. In particular, Fig. 32(a) shows that noise of $\sigma = 0.01$ in the system being

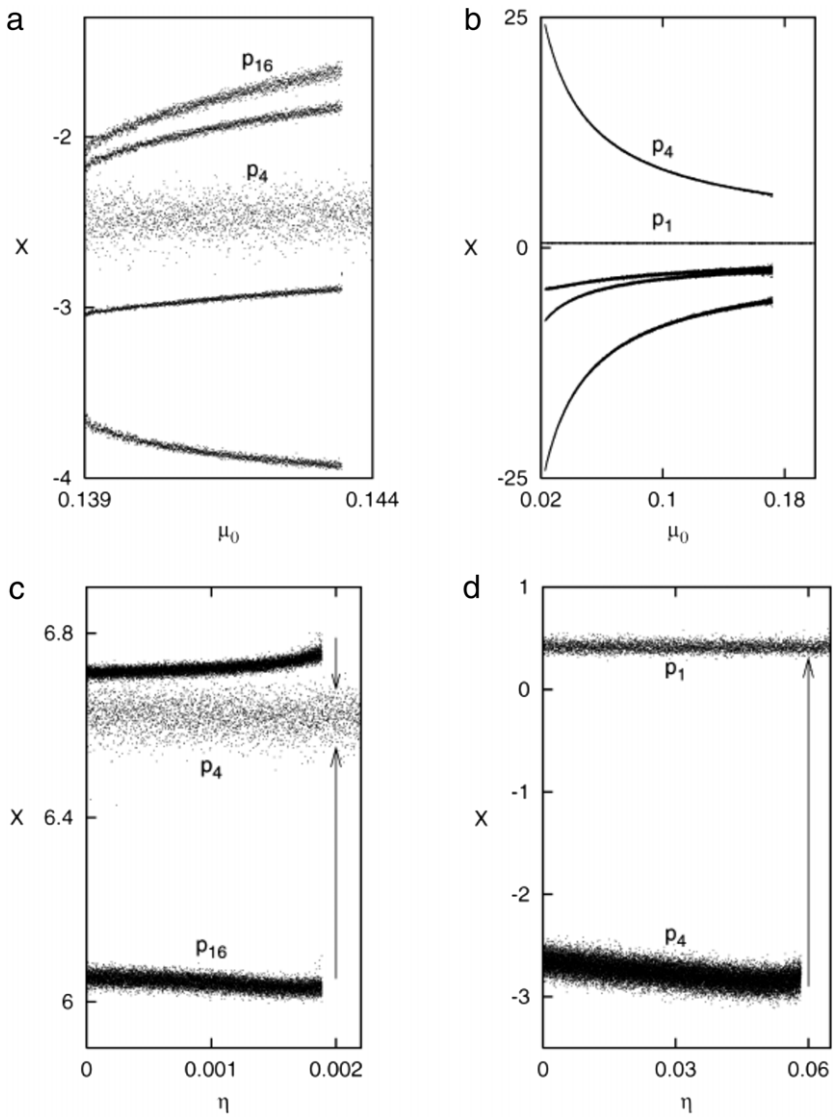

Fig. 31. Bifurcation diagrams demonstrating combined effect of noise and periodic parameter modulation. (a) Destruction of period-16 branch (p_{16}) around period 4 (p_4) by noise with $\sigma = 0.001$. Sampling period is four. (b) Destruction of period-4 branch (p_4) around period 1 (p_1) by noise with $\sigma = 0.005$. (c) Destruction of noisy p_{16} by parameter modulation with $f = 0.005$; the system jumps (shown by the arrows) to p_4; $\sigma = 0.001$ and $\mu_0 = 0.142$. (d) Destruction of noisy p_4 by modulation with $f = 0.005$; the system jumps (shown by the arrow) to period 1; $\sigma = 0.005$ and $\mu_0 = 0.12$.

initially in p_{16} induces a transition to $p4$. Since the period-4 basin of attraction is large enough to deter further transition to any other basin, the periodic control is added to destroy the lower-order cascades. One can see that the control modulation with $\eta = 0.04$ and $f = 0.005$ applied at $n = 1000$ (shown by the arrow) destroys $p4$ and the system goes to $p1$ after transients. Similar behavior occurs when the initial attractor is chosen to be a period 25 ($p25$). As illustrated in Fig. 32(b), $p25$ is destroyed by noise so that the system goes to $p5$ which is annihilated by periodic modulation.

Thus, if noise is capable of inducing a transition from basins of higher-order secondary cascades to basins of lower-order secondary cascades, then the control modulation is required only to destroy these lower-order secondary cascades and bring the system to the remaining period-1 attractor.

5.3.2. Bistable noisy logistic map

Now we will demonstrate how noise can enhance multistability control by attractor annihilation. Let us consider again the delayed logistic map equation (50) described in Section 5.1.2. We apply combined control in form of both periodic and stochastic modulations [297]:

$$x_{n+1} = ax_n(1 - x_n) + \eta(x_{n-1} - x_n) - \delta \sin(2\pi nf) + D\xi_n, \tag{52}$$

where δ and f are, respectively, the modulation amplitude and frequency. Here, we suppose that the modulation amplitude δ is so small that no qualitative changes occur in a stationary case, i.e. when $f \to 0$.

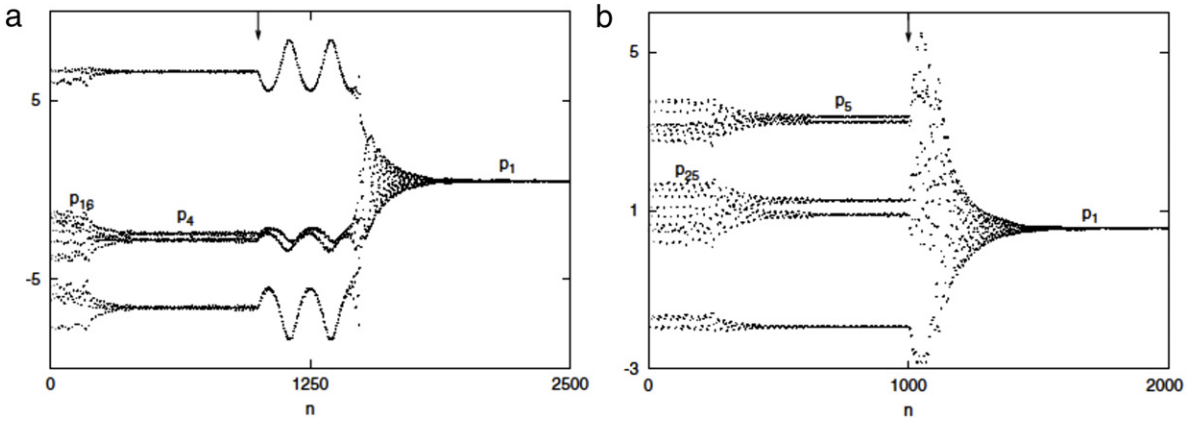

Fig. 32. Time series demonstrating combined effect of noise and parameter modulation in the multistable Hénon map. Noise with $\sigma = 0.01$ induces the transition from period 16 ($p16$) to period 4 ($p4$) and the periodic modulation with $\eta = 0.04$ and $f = 0.005$ applied at $n = 1000$ (shown by the arrow) destroys p_4 so that only period 1 remains. $\mu_0 = 0.142$.

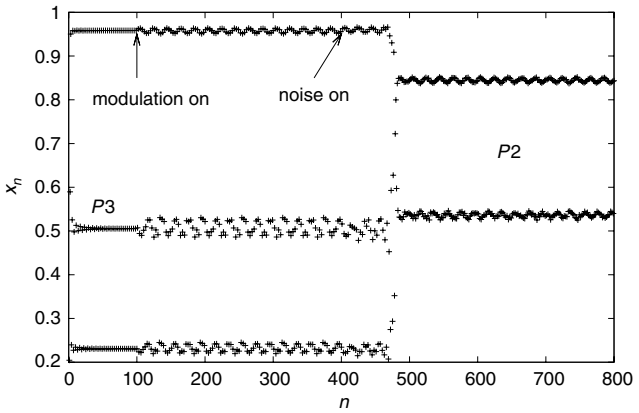

Fig. 33. Time series demonstrating the combined effect of noise and harmonic modulation in the bistable delayed logistic map equation (52). Starting from the initial condition for $P3$, harmonic modulation with $\delta = 0.006$ and $f = 0.06$ applied after 100 iterations is not capable to destroy the attractor, but noise with $D = 0.006$ added after 400 iterations does this. $x_0 = 0.94$, $a = 3.625$, $\eta = 0.19$.

The effect of this combined control is illustrated in Fig. 33. First, the bistable logistic map with coexisting $P2$ and $P3$ attractors, in the absence of periodic modulation ($\delta = 0$) and without noise ($D = 0$), is iterated from the initial condition x_0 for the $P3$ attractor, and after 100 iterations a small periodic modulation is applied; then, after 400 iterations noise is added. Although neither small-amplitude periodic modulation, nor weak noise applied separately is not capable to annihilate $P3$, their combination does it.

Fig. 34 shows the state diagrams in the (f, δ) parameter space for three noise amplitudes: $D = 0$ (Fig. 34(a)), $D = 0.002$ (Fig. 34(b)), and $D = 0.006$ (Fig. 34(c)). For each value of the control parameters (f, δ) the probability P_2 of the system equation (52) to be attracted to $P2$ when starting from an initial condition for $P3$ is calculated. $P_2 = 1$ (yellow region) means that every trajectory is only attracted to $P2$, i.e., the system is monostable. One can see that while without noise ($D = 0$) (Fig. 34(a)) the border between the bistable (black) and monostable (yellow) regions is well defined, noise degrades the border and shifts it towards lower values of δ. Thus, weak noise facilitates attractor annihilation by slow harmonic modulation.

5.3.3. Multistable fiber laser

In the next example, we will demonstrate how attractor selection by noise is obtained in a multistable erbium-doped fiber laser described by the following equations [252,294,295]

$$\frac{dP}{dt} = \frac{2L}{T_r} P \{r_w \alpha_0 [N(\xi_1 - \xi_2) - 1] - \alpha_{th}\} + P_{sp}, \tag{53}$$

$$\frac{dN}{dt} = -\frac{\sigma_{12} r_w P}{\pi r_0^2}(N\xi_1 - 1) - \frac{N}{\tau} + P_{pump}, \tag{54}$$

where P is the intracavity laser power, $N = (1/n_0 L)\int_0^L N_2(z)dz$ is the averaged (over the active fiber length L) population of the upper lasing level, N_2 is the upper level population at the z coordinate, n_0 is the refractive index of a "cold" erbium-

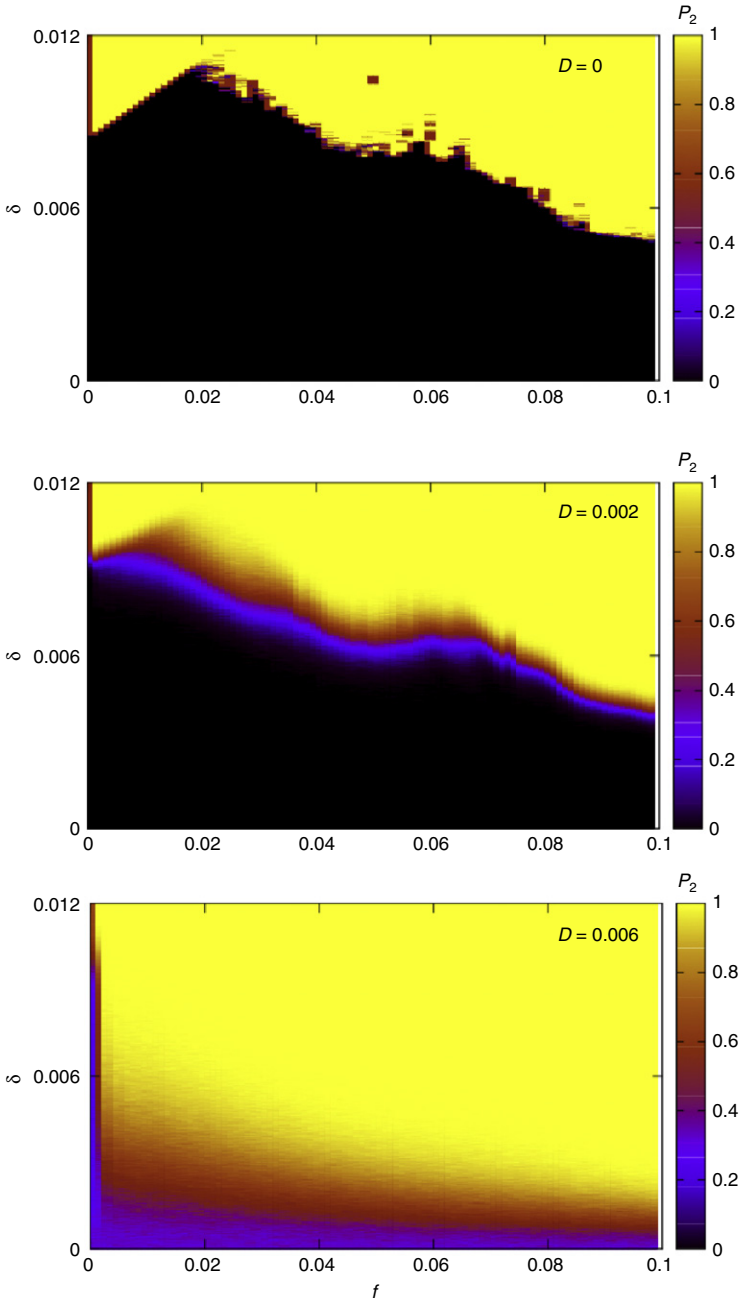

Fig. 34. State diagrams of noisy delayed logistic map under harmonic modulation equation (52) in (f, δ) space for $x_0 = 0.94$, $a = 3.625$, and $\eta = 0.19$. The color shows the average probability over all initial conditions leading to $P2$ for three different noise amplitudes: (a) $D = 0$, (b) $D = 0.002$, and (c) $D = 0.006$. Noise facilitates annihilation of the $P3$ attractor by harmonic modulation. (For interpretation of the references to color in this figure legend, the reader is referred to the web version of this article.)

doped fiber core, ξ_1 and ξ_2 are parameters defined by the relationship between cross sections of ground state absorption (σ_{12}), return stimulated transition (σ_{12}), and excited state absorption (σ_{23}). T_r is the photon intracavity round-trip time, α_0 is the small-signal absorption of the erbium fiber at the laser wavelength, α_{th} accounts for the intracavity losses on the threshold, τ is the lifetime of erbium ions in the excited state, r_0 is the fiber core radius, w_0 is the radius of the fundamental fiber mode, and r_w is the factor addressing a match between the laser fundamental mode and erbium-doped core volumes inside the active fiber. The spontaneous emission into the fundamental laser mode is derived as

$$P_{sp} = N\frac{10^{-3}}{\tau T_r}\left(\frac{\lambda_g}{w_0}\right)^2 \frac{r_0^2\alpha_0 L}{4\pi^2\sigma_{12}}, \tag{55}$$

where λ_g is the laser wavelength. The pump power is expressed as

$$P_{pump} = P_p \frac{1 - \exp\left[-\alpha_0 \beta L\,(1 - N)\right]}{N_0 \pi r_0^2 L}, \tag{56}$$

where P_p is the pump power at the fiber entrance and β is a dimensionless coefficient. The parameters are chosen to correspond to real experimental conditions: $L = 0.88$ m, $T_r = 8.7$ ns, $r_w = 0.308$, $\alpha_0 = 40\ \mathrm{m}^{-1}$, $\xi_1 = 2$, $\xi_2 = 0.4$, $\alpha_{th} = 3.92 \times 10^{-2}$, $\sigma_{12} = 2.3 \times 10^{-17}\ \mathrm{m}^2$, $r_0 = 2.7 \times 10^{-6}$ m, $\tau = 10^{-2}$ s, $\lambda_g = 1.65 \times 10^{-6}$ m, $w_0 = 3.5 \times 10^{-6}$ m, $\beta = 0.5$, and $N_0 = 5.4 \times 10^{25}\ \mathrm{m}^{-3}$.

When harmonic modulation and noise are added to the pump parameter as follows

$$P_p = p\left[1 - m_d \sin\left(2\pi f_d t\right) + \eta\zeta\right], \tag{57}$$

where $\zeta \in [-1, 1]$ is a random number and η is the noise amplitude, the system equations (53)–(54) become stochastic with probabilistic solutions. For small noise ($\eta < 0.1$), the laser's asymptotic state remains in the vicinity of one of the coexisting periodic orbits, because small noise does not introduce intermittent switches between the attractors; however it does change statistical properties of the system giving more preference to some attractors over others. The probability for each point in phase space to belong to a particular basin of attraction depends on the noise amplitude, i.e., the number of attracted points for each coexisting attractor (basin's volume) has a probabilistic character.

In the 3D plots in Fig. 35, the Renka–Cline gridding method was used to illustrate how the probability to find certain values for the volumes of the basins of attraction of the three coexisting states depends on the noise amplitude. These diagrams were constructed as follows. For each noise amplitude, the basins of attraction in the phase space region were computed 100 times, then the number of initial conditions leading to every coexisting attractor was calculated, and finally the probability distribution of these basins' volumes was evaluated. For example, for the fixed noise amplitude $\eta = 0.1$ and fixed all other parameters, about 1.3×10^3 initial conditions were found to be belong to the basin of attraction of P1 with a 30% probability and about 1.9×10^3 points belong to the same basin but with a 10% probability. In general, the most probable number of the basins' points is an almost linear function of noise; as the noise amplitude is increased, the P1 and P3 basins' volumes increase while the P4 basin decreases. On the other hand, the probability distribution of the basins' volumes is not such a simple function of noise; for certain noise values some maxima and minima are found. The existence of these extremes may be related to a stochastic resonance phenomenon which may occur in basins of attraction of the coexisting states.

Thus, the stochastic control has a noise-dependent probabilistic character displaying a resonance-like behavior in the basins' volumes.

5.4. Attractor annihilation in stochastic resonance

The collective effect of noise and periodic modulation gives rise to attractor annihilation through a mechanism similar to stochastic resonance [239,254]. To demonstrate this effect, let us consider two coupled randomly driven oscillators governed by the following general equation [254]:

$$\ddot{\mathbf{x}} + \gamma\,\dot{\mathbf{x}} - q\xi x = -\nabla V(\mathbf{x}), \tag{58}$$

where $\mathbf{x} \equiv (x, y)$ is the system variables, γ is a damping factor, ξ is uniformly distributed noise of level q in the unit interval [0,1], and $V(x)$ is a two-dimensional anharmonic potential function of coupled oscillators that for symmetric Duffing oscillators can be expressed as follows [303]:

$$V(x, y) = (1 - x^2)^2 + (y^2 - a^2)^2 (x - d) + b(y^2 - a^2)^4, \tag{59}$$

where a, d, and $b > 0$ are parameters. It is assumed that one of the coupled subsystems (in the x direction) is noisy. Then, the system equations (58) and (59) can be written as four first-order differential equations in terms of the dynamical variables $x_1 = x$, $x_2 = \dot{x}$, $x_3 = y$, and $x_4 = \dot{y}$:

$$\dot{x_1} = x_2, \tag{60}$$

$$\dot{x_2} = -\gamma x_2 + 4x_1(1 - x_1^2) - (x_3^2 - a^2)^2 + q\xi x_1, \tag{61}$$

$$\dot{x_3} = x_4, \tag{62}$$

$$\dot{x_4} = -\gamma x_4 - 4x_3(x_3^2 - a^2)(x_1 - d) - 8bx_3(x_3^2 - a^2)^3. \tag{63}$$

The system equations (60)–(63) exhibit different dynamical regimes, from regular states to on–off intermittency, in a wide range of parameter values [304]. While for $\gamma = 0.04$, $a = 0.73$, $b = 0.008$, and $d = -1.8$ two-state on–off intermittency is observed, at relatively low noise levels ($q < 3$) one-state and two-state on–off intermittency appear in transients only. The two-state on–off intermittent attractor is created at relatively strong noise ($q \geq 3$) and coexists with two stable steady states associated with two potential wells.

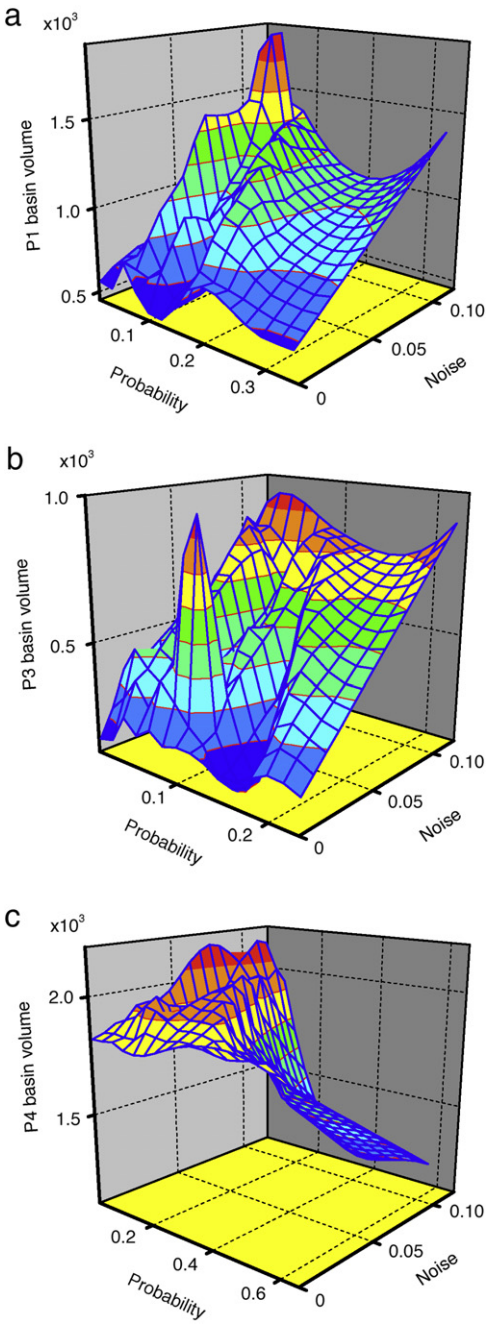

Fig. 35. Probability distribution of basins' volumes of coexisting (a) period-1, (b) period-3, and (c) period-4 attractors in the erbium-doped fiber laser in the presence of noise applied to diode pump current at $m_d = 0.8$ and $f_d = 70.2$ kHz.

For the purpose of eliminating intermittent chaotic attractors, so that a trajectory initiated from a random initial condition will remain forever in the vicinity of one of the potential wells, the control modulation is applied to the parameter a as

$$a = a_0[1 - m\sin(2\pi ft)], \tag{64}$$

where m and f are the modulation depth and frequency and a_0 is the initial value of the parameter ($a_0 = 0.73$).

The time series in Fig. 36 illustrate annihilation of the chaotic attractor. The system, prior to the control, is in the chaotic (intermittency) state. The control modulation applied at $t = 5000$ destroys the chaotic attractor, so that the trajectory remains in the vicinity of one of the steady states. Since the harmonic modulation creates a limit cycle around each fixed point, the final state is a stable periodic orbit. When the modulation amplitude is not large enough to eliminate the chaotic attractor, the system exhibits the coexistence of five attractors: intermittent switches between two fixed points (two-state

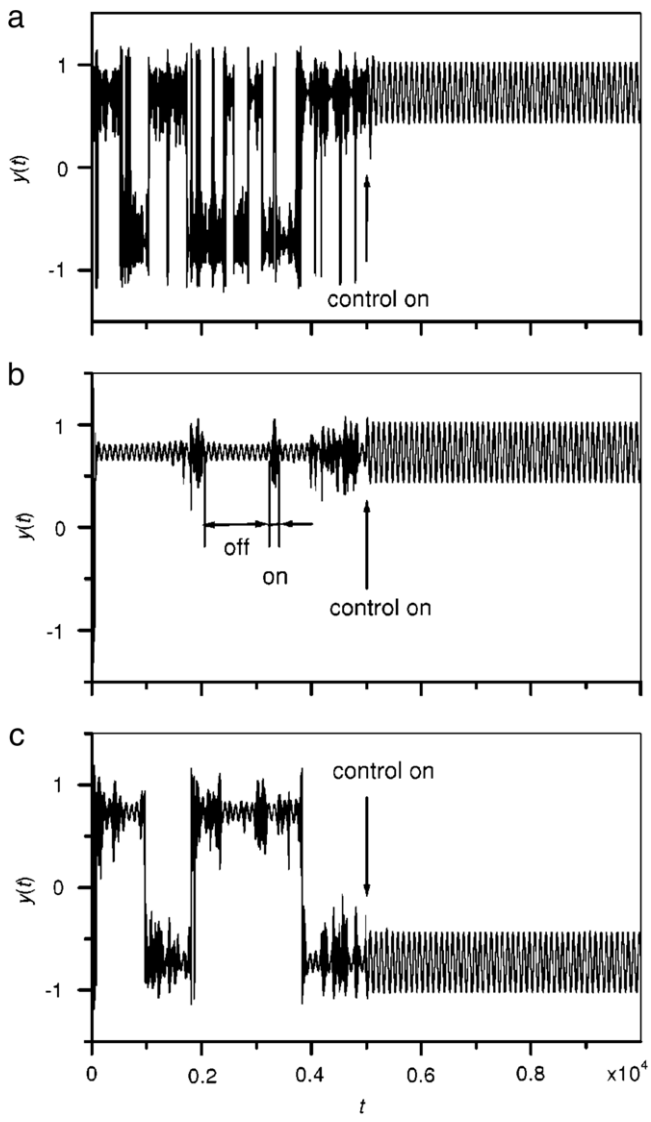

Fig. 36. Slow parametric modulation in noisy Duffing oscillators leads to annihilation of chaotic (intermittency) attractors. The initial states are (a) two-state on–off intermittency without modulation ($m = 0$), and (b) one-state and (c) two-state on–off intermittency with small-amplitude parameter modulation ($m = 0.1$). The arrows indicate the instants of time when the control modulation with $m = 0.4$ and $f = 0.01$ is applied. The trajectory is attracted to the created limit cycle in the vicinity of one of the potential wells. This demonstrates the flexibility of the control to select a desirable periodic orbit.

intermittency) (2I), intermittent jumps out of each fixed point and returns to the same fixed point (two regimes of on–off intermittency) (1I), and a periodic orbit (PO) in the vicinity of each fixed point. The realization of each of these coexisting attractor depends on the initial conditions. Fig. 36(b) and (c) show that an increase in the modulation amplitude leads to annihilation of the intermittent states resulting in the coexistence of two periodic orbits only.

The modulation amplitude required for attractor annihilation depends on both the noise level and the modulation frequency as shown in Fig. 37. In the presence of the parametric modulation equation (64), the intermittent attractors appear only at a certain noise level ($q > 1.9$ for $f = 0.01$) (Fig. 37(a)). To eliminate these attractors, the control amplitude should be larger than a critical value m_c, i.e. lie above the bifurcation lines m_c shown by the arrows. As seen from Fig. 37(a), for relatively low noise ($1.9 < q < 3$), there are two critical values for the modulation amplitude, which correspond to the onset and offset of on–off intermittency. As seen from Fig. 37(b), the chaotic attractors can be destroyed by slow modulation only ($f < 0.05$) and only when $m > m_c$ (inside the striped region). The period of the modulation should be of the same order of magnitude as the characteristic time a trajectory spends in the vicinity of one invariant subspace before being repelled. Of course, the duration of the laminar phase depends on the noise level. This suggests that the reason for the control effect is a resonant interaction of the modulation frequency with the frequency at which the trajectory was repelled from one of the invariant subspaces.

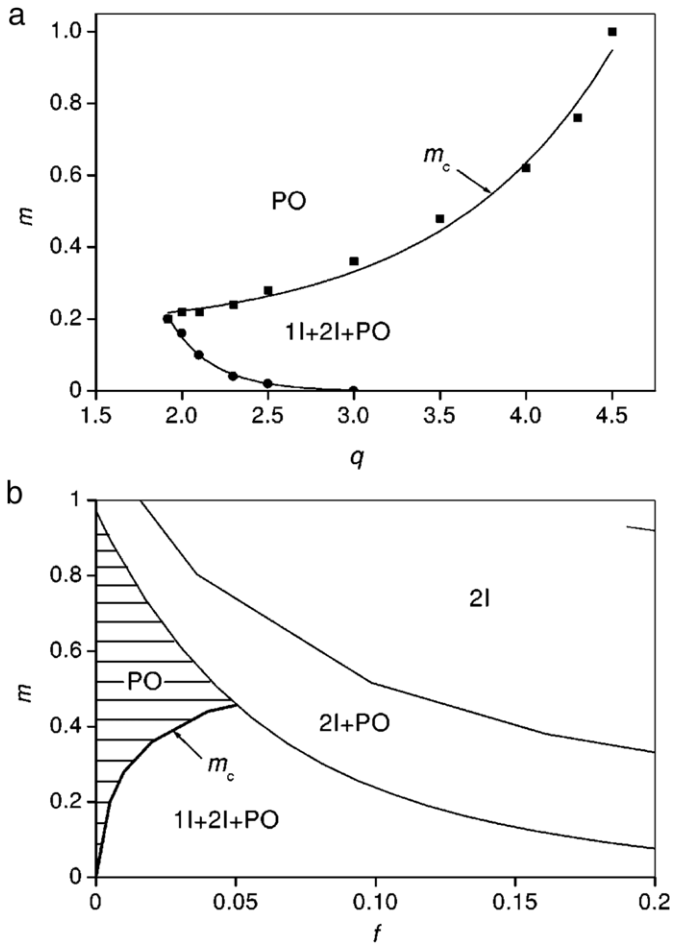

Fig. 37. Stability boundary of chaotic attractors in spaces of (a) noise and modulation amplitudes for $f = 0.01$ and (b) modulation parameters for $q = 3.$ 1I, 2I and PO are respectively one-state and two-state intermittency and the periodic orbit induced by control modulation. The arrows indicate the bifurcation lines for the intermittency onset at critical modulation depth m_c.

The mechanism for the attractor annihilation can be better understood from Fig. 38 which shows the signal-to-noise ratio (SNR) versus the noise amplitude for different modulation depths m_c. By comparing Fig. 37(a) with Fig. 38, one can see that the annihilation curve, i.e. the minimum modulation amplitude m_c needed for the chaotic attractor destruction (shown by the arrow in Fig. 37(a)), is linked with the maxima (SR) of the SNR curves for the corresponding values of m and q. These results confirm that the mechanism for the attractor annihilation is related to the stochastic resonance phenomenon.

6. New challenges and perspectives

During the last decade a lot of progress has been made to control multistable systems. As outlined above, various control strategies have been developed theoretically and implemented experimentally. However, there are still many open problems in the field of multistability which need to be understood in future. Here we mention only some of them.

Green problem. One crucial issue is connected with the important "green" problem in nonlinear optics, where irregular intensity fluctuations appear in second harmonic generation (SHG) when a SHG crystal is located inside the laser cavity. These fluctuations are amplified from the beginning by the quality factor Q of the laser cavity and by the presence of the laser amplifier media. Strong fluctuations arise then in the laser intensity. This is clearly a undesirable situation for practical applications. To give an example of what discussed above, the green light generated in a diode-pumped intracavity doubled Nd:YAG laser (1.06 μm) [60] is normally accompanied with strong intensity fluctuations. This irregular behavior was largely investigated and attributed to the destabilization of relaxation oscillations, always present in this kind of lasers due to nonlinear coupling of longitudinal modes. Another reason of such a behavior is the coexistence of multiple attractors which often appear in a system with many degrees of freedom. The irregularity in the laser intensity results from involuntary switches between the coexisting states induced by noise or any external interference. A possible approach to controlling this kind of irregular laser behavior would be annihilation of undesirable coexisting attractors.

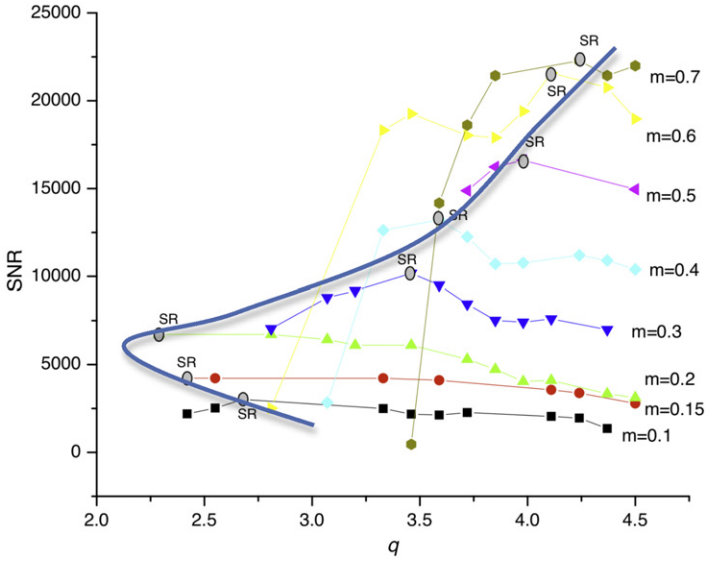

Fig. 38. Signal-to-noise ratio versus noise amplitude for different modulation amplitudes m at $f = 0.01$. The maxima for every m marked by the gray dots (SR) are connected by the blue curve which has a similar shape as the annihilation curve in Fig. 37(a).

Synchronization. A second challenge for future research is synchronization of multistable systems. We believe that further investigation in this direction will help to gain significant insight to many natural phenomena, because this topic is of great interest in diverse areas of science and can have various applications. In this context, the question would be interesting to study, how multistable systems synchronize and how to control them. Which of the attractors would be chosen when multistable systems are coupled and can one design control algorithms to choose particular attractors on demand? A first attempt to tackle this problem has been already done by studying synchronization of two bistable uni-directionally coupled Rössler-like oscillators with coexistence of two different chaotic attractors [305]. Many interesting nonlinear regimes have been found, including anticipated intermittent phase synchronization, period-doubling synchronization, and intermittent switches between coexisting states exhibiting type-I and on–off intermittency [306,307].

Communication. Some types of lasers, e.g. semiconductor lasers with external cavity, exhibit complex dynamics which allows multistability, i.e. coexistence of steady-state, periodic, and chaotic attractors. Synchronization of coupled multistable semiconductor lasers with external cavities [206] might be of interest for optical communication if information could be encrypted in switches between different coexisting states. We believe that special efforts will be made to find out general relationships in control methods described in this Report and their applications in secure communications.

Complex networks. Special attention should be given to studying and controlling multistability in complex networks [308]. Recently, not only nearest neighbor interactions, like diffusion or globally coupled systems, have been studied, but general networks possessing identical or almost identical nodes on which some nonlinear phenomena take place. These nodes are interconnected to form a network with some given topology or even with adjusting topology [309,310]. Of particular interest is thereby the relation between dynamics on the nodes and the network topology. If the dynamics on the nodes is assumed to be multistable, then a complicated network dynamics should emerge.

Fractional systems. In recent years, many scientists have become aware of a potential use of fractional-order calculus and their application to various fields, including physics, engineering, and biology. The dynamics of fractional-order systems have attracted increasing attention because generalization of differential equations using fractional derivatives proved to be more accurate from various interdisciplinary areas. It has been shown that these systems can behave chaotically [311]. Coexistence of multiple attractors have also been found in fractional-order systems [312–314]. One of the main advantages of fractional-order systems over classical integer-order models is that the former systems are characterized by infinite memory that provides a good tool for description of hereditary properties of neural networks [314]. On the other hand, the dynamical behavior of multistable fractional systems is still needing pay more attention. In particular, control of multistability in such systems has not yet been applied.

Genetic oscillators. The existence of multiple operating regimes is essential for biological systems, because they provide functional flexibility in responding to external stimuli [34]. This subject has been largely investigated in relation to genetic oscillators [40,42,44], with strong emphasis on biological mechanisms and topological structures leading to multistability [41,43]. It was found that synthetic gene networks are able to generate various dynamical regimes in relation to the topology of their interactions. Furthermore, the coexistence of multiple final frustration states has been recently found in collective dynamics of oscillator networks with phase-repulsive coupling [315]. The role of multiple dynamical regimes was also

examined in neuronal interactions [111]. The proper control of multistability in these networks could lead to a new insight in the interplay between topology and functioning of genetic and neuronal networks.

Climate. The coexistence of different stable states is a topic of a growing interest in environmental sciences and climate research, since many processes in the ocean, atmosphere, and ecosystems reveal multiple states. For example, one of possible mechanisms for the emergence of rogue waves in the ocean is the interaction of deterministic and random processes in a multistable environment [294,295]. We believe that a deep study of this interaction will bring up new challenging questions for future theoretical and experimental work on controlling multistability in these very complex systems.

Extreme multistability. Lastly, the exciting phenomenon of extreme multistability recently discovered in coupled systems with a specially designed coupling [184] is still not completely understood. An infinite number of attractors would have diverse applications if a proper control of this kind of multistability could be realized. However, an experimental verification of this type of multistability has not been realized so far due to its high sensitivity to noise. This is another challenge for designing control strategies to make the coexistence of a very large number of attractors possible.

Acknowledgments

The authors acknowledge all scientists with whom we collaborate and had many fruitful discussions on this topic. Without their help it would be hardly possible to write the review on this rapidly growing field of research. In this spirit, the authors would like to thank V. Aboites, V. Afraimovich, J. Almendral, F.T. Arecchi, Yu.O. Barmenkov, I. Belykh, E. Ben-Jacob, B. Bezruchko, S. Bielawski, S. Boccaletti, J. Buldú, L. Bunimovich, H. Cerdeira, V.N. Chizhevsky, R. Corbalán, S.K. Dana, D. Dignowity, M.I. Dykman, W. Ebeling, A.R. Fermat-Flores, I. Fischer, J.A.C. Gallas, J. García-Ojalvo, A. Gavrielides, P. Glorieux, B.K. Goswami, C. Grebogi, P. Hänggi, B. Hunt, R. Jaimes-Reátegui, N. Janson, K. Kaneko, T. Kapitaniak, V. B. Kazantsev, A.V. Kirýanov, A.A. Koronovskii, B.F. Kuntsevich, J. Kurths, A.S. Landsman, I. Leyva, J.M. Liu, D.G. Luchinsky, F. Maestú, Yu.L. Maistrenko, V. Makarov, B. Martínez-Zérega, C. Masoller, P.V.E. McClintock, R. Meucci, C. Mirasso, G. Orriols, E. Ott, C. Panda, A. Pikovsky, V. Pinto, F. del Pozo-Guerrero, A. Politi, K. Pyragas, R. Ramaswami, J. Rios-Leite, M.G. Rosenblum, R. Roy, N. Rulkov, M. Sausedo-Solorio, L. Schimansky-Geier, E. Schöll, I. Sendina, J.R. Sevilla-Escoboza, A. Shilnikov, S. Sinha, K. Showalter, R. Stoop, E. Surovyatkina, M. Taki, T. Tél, V. Tereshko, L.S. Tsimring, R. Vilaseca, E. Volkov, C. Weiss, S. Wieczorek, J.A. Yorke, M. Zanin, and G.M. Zaslavsky.

This work was supported by CONACYT (project 100429), Deutsche Forschungsgemeinschaft (DFG, project FE 259/1) and German Academic Exchange Service (DAAD-PPP-NSF).

References

[1] F. Atteneave, Multistability in perception, Sci. Am. 225 (1971) 63–71.
[2] J. Maurer, A. Libchaber, Effect of the Prandtl number on the onset of turbulence in liquid-He-4, J. Phys. Lett. (Paris) 41 (1980) L515–L518.
[3] M. Giglio, S. Musazzi, U. Perini, Transition to chaotic behavior via a reproducible of sequence of period-doubling bifurcations, Phys. Rev. Lett. 47 (1981) 243–246.
[4] F.T. Arecchi, F. Lisi, Hopping mechanism generating 1/f noise in nonlinear systems, Phys. Rev. Lett. 49 (1982) 94–97.
[5] M.R. Beasley, D. D'Humieres, B.A. Huberman, Comment on "hopping mechanism generating 1/f noise in nonlinear systems", Phys. Rev. Lett. 50 (1983) 1328–1331.
[6] F.T. Arecchi, R. Meucci, G. Puccioni, J. Tredicce, Experimental evidence of subharmonic bifurcations, multistability, and turbulence in a *q*-switched gas laser, Phys. Rev. Lett. 49 (1982) 1217–1220.
[7] U. Feudel, Complex dynamics in multistable systems, Int. J. Bifurcation Chaos 18 (2008) 1607–1626.
[8] B.K. Goswami, A.N. Pisarchik, Controlling multistability by small periodic perturbation, Int. J. Bifurcation Chaos 18 (2008) 1645–1673.
[9] E. Brun, B. Derighetti, D. Meier, R. Holzner, M. Ravani, Observation of order and chaos in a nuclear spin-flip laser, J. Opt. Soc. Amer. B Opt. Phys. 2 (1985) 156–167.
[10] J.M.T. Thompson, H.B. Stewart, Nonlinear Dynamics and Chaos, Wiley, Chichester, 1986.
[11] J. Foss, A. Longtin, B. Mensour, J. Milton, Multistability and delayed recurrent loops, Phys. Rev. Lett. 76 (1996) 708–711.
[12] E. Eschenazi, H.G. Solari, R. Gilmore, Basins of attraction in driven dynamical systems, Phys. Rev. A 39 (1989) 2609–2627.
[13] J.-L. Schwartz, N. Grimault, J.-M. Hupé, C.J.B.C.J. Moore, D. Pressnitzer, Multistability in perception: sensory modalities, an overview, Philos. Trans. R. Soc. B 367 (2012) 896–905.
[14] P. Kruse, M. Stadler, Ambiguity in Mind and Nature: Multistable Cognitive Phenomena, Springer, Berlin, 1995.
[15] D.O. Hebb, The Organization of Behavior, Wiley, New York, 1949.
[16] W. Köhler, H. Wallach, Figural after-effects, an investigation of visual processes, Proc. Am. Phil. Soc. 88 (1944) 269–357.
[17] D. Alais, R. Blake (Eds.), Binocular Rivalry, MIT Press, 2005.
[18] L. Parkkonen, J. Andersson, M. Hämäläinen, R. Hari, Early visua brain areas reflect the percept of an ambiguous scene, Proc. Natl. Acad. Sci. USA 105 (2008) 20500–20504.
[19] R. Moreno-Bote, J. Rinzel, N. Rubin, Noise-induced alternations in an attractor network model of perceptual bistability, J. Neurophysiol. 98 (2007) 1125–1139.
[20] G. Gigante, M. Mattia, J. Braun, P. Del Giudice, Bistable perception modeled as competing stochastic integrations at two levels, PLoS Comput. Biol. 5 (2009) e1000430.
[21] S.P. Meyn, R.L. Tweedie (Eds.), Markov Chains and Stochastic Stability, Cambridge University Press, Cambridge, 2008.
[22] D.A. Leopold, M. Wilke, A. Maier, N.K. Logothetis, Stable perception of visually ambiguous patterns, Nature Neuroscience 5 (2002) 605–609.
[23] P. Mamassian, R. Goutcher, Temporal dynamics in bistable perception, J. Vision 5 (2005) 361–375.
[24] R.M. Warren, Illusory changes of distinct speech upon repetition—the verbal transformation effect, Br. J. Psychol. 52 (1961) 249–258.
[25] R.M. Warren (Ed.), Auditory Perception: A New Analysis and Synthesis, Cambridge University Press, Cambridge, 1999.
[26] D. Deutsch, The tritone paradox: effects of spectral variables, Percept. Psychophys. 41 (1987) 563–575.
[27] B.H. Repp, Spectral envelope and context effects in the tritone paradox, Perception 26 (1997) 645–665.
[28] M. Roberts, Q. Summerfield, Audiovisual presentation demonstrates that selective adaptation in speech perception is purely auditory, Perception and Psychophysics 30 (1981) 309–314.

[29] B.H. Repp, Hearing a melody in different ways: multistability of metrical interpretation, reflected in rate limits of sensorimotor synchronization, Cognition 102 (2007) 434–454.
[30] B.H. Repp, J.R. Iversen, A.D. Patel, Tracking an imposed beat, Music Percept. 26 (2008) 1–18.
[31] R. van Ee, L.C. van Dam, G.J. Brouwer, Voluntary control and the dynamics of percetual bi-stability, Vision Res. 45 (2005) 41–55.
[32] A. Kohler, L. Haddad, W. Singer, L. Muckli, Deciding what to see: the role of intention and attention in the perception of apparent motion, Vision Res. 48 (2008) 1096–1106.
[33] W. Knorre, F. Bergter, Z. Simon, Multistability in metabolic systems, Stud. Biophys. 49 (1975) 81–89.
[34] D. Angeli, J.E. Ferrell Jr., E.D. Sontag, Detection of multistability, bifurcations, and hysteresis in a large class of biological positive-feedback systems, Proc. Natl. Acad. Sci. USA 101 (2004) 1822–1827.
[35] M. Laurent, N. Kellershohn, Multistability: a major means of differentiation and evolution in biological systems, Trends Biochem. Sci. 24 (1999) 418–422.
[36] K. Kaneko, T. Yomo, Isologous diversification: a theory of cell differentiation, Bull. Math. Biol. 59 (1997) 139–196.
[37] K. Kaneko, T. Yomo, Sympatric speciation: compliance with phenotype diversification from a single genotype, Bull. Math. Biol. 267 (2000) 2367–2373.
[38] S. Huang, G. Eichler, Y. Bar-Yam, D.E. Ingber, Cell fates as highdimensional attractor states of a complex gene regulatory network, Phys. Rev. Lett. 94 (2005) 128701.
[39] K. Kaneko, Life: An Introduction to Complex Systems Biology, vol. 371, Springer-Verlag, Berlin, 2006.
[40] E. Ullner, A. Zaikin, E.I. Volkov, J. Garcia-Ojalvo, Multistability and clustering in a population of synthetic genetic oscillators via phase-repulsive cell-to-cell communication, Phys. Rev. Lett. 99 (2007) 148103.
[41] A. Koseska, E. Volkov, A. Zaikin, J. Kurths, Inherent multistability in arrays of autoinducer coupled genetic oscillators, Phys. Rev. E 75 (2007) 031916.
[42] Z. Yuan, J. Zhang, T. Zhou, Coherence, collective rhythm, and phase difference distribution in populations of stochastic genetic oscillators with cellular communication, Phys. Rev. E 78 (2008) 031901.
[43] E. Ullner, A. Koseska, J. Kurths, E. Volkov, H. Kantz, J. Garcia-Ojalvo, Multistability of synthetic genetic networks with repressive cell-to-cell communication, Phys. Rev. E 78 (2008) 031904.
[44] A. Koseska, J. Kurths, Topological structures enhance the presence of dynamical regimes in synthetic networks, Chaos 20 (2010) 045111.
[45] I. Potapov, B. Zhurov, E. Volkov, Quorum sensing generated multistability and chaos in a synthetic genetic oscillator, Chaos 22 (2012) 023117.
[46] J.E. Ferrell, E.M. Machleder, The biochemical basis of an all-or-none cell fate switch in Xenopus oocytes, Science 280 (1998) 895–898.
[47] C.P. Bagowski, J.E. Ferrell, Bistability in the JNK cascade, Curr. Biol. 11 (2001) 1176–1182.
[48] U.S. Bhalla, P.T. Ram, R. Iyengar, Map kinase phosphatase as a locus of flexibility in a mitogen-activated protein kinase signaling network, Science 297 (2002) 1018–1023.
[49] F.R. Cross, V. Archambault, M. Miller, M. Klovstad, Testing a mathematical model of the yeast cell cycle, Mol. Biol. Cell. 13 (2003) 5270.
[50] J.R. Pomerening, E.D. Sontag, J.E. Ferrell, Testing a mathematical model of the yeast cell cycle, Nat. Cell Biol. 5 (2003) 346–351.
[51] C. Bagowski, J. Besser, C.R. Frey, J.E. Ferrell, The JNK cascade as a biochemical switch in mammalian cells: ultrasensitive and all-or-none responses, Curr. Biol. 13 (2003) 315–320.
[52] W. Sha, J. Moore, K. Chen, A.D. Lassaletta, C.S. Yi, J.J. Tyson, J.C. Sible, Hysteresis drives cell-cycle transitions in Xenopus laevis egg extracts, Proc. Natl. Acad. Sci. USA 100 (2003) 975–980.
[53] B.M. Slepchenko, M. Terasaki, Bio-switches: what makes them robust? Curr. Opin. Genet. Dev. 14 (2003) 428–434.
[54] J.D. Chung, G. Stephanopoulos, On physiological multiplicity and population heterogeneity of biological systems, Chem. Eng. Sci. 51 (1996) 1509–1521.
[55] J.E. Ferrell, Self-perpetuating states in signal transduction: positive feedback, double-negative feedback, and bistability, Curr. Opin. Chem. Biol. 6 (2002) 140–148.
[56] Y.-H. Shiau, Y.-F. Peng, R.R. Hwang, C.-K. Hu, Multistability and symmetry breaking in the two-dimensional flow around a square cylinder, Phys. Rev. E 60 (1999) 6188–6191.
[57] F. Ravelet, L. Marié, A. Chiffaudel, F. Daviaud, Multistability and memory effect in a highly turbulent flow: experimental evidence for a global bifurcation, Phys. Rev. Lett. 93 (2004) 164501.
[58] F.T. Arecchi, R. Badii, A. Politi, Generalized multistability and noise-induced jumps in a nonlinear dynamical system, Phys. Rev. A 32 (1985) 402–408.
[59] H.M. Gibbs, S.L. McCall, T.N.C. Venkatesan, Differential gain and bistability using a sodium-filled Fabry–Perot interferometry, Phys. Rev. Lett. 19 (1976) 1135–1138.
[60] T. Baer, Large-amplitude fluctuations due to longitudinal mode coupling in diode-laser pumped intracavity-doubled Nd:YAG lasers, J. Opt. Soc. Amer. B Opt. Phys. 3 (1986) 1175–1180.
[61] P.C. de Jagher, W.A. van der Graaf, D. Lenstra, Relaxation-oscillation phenomena in an injection-locked semiconductor laser, Quant. Semiclass. Opt. 8 (1996) 805–822.
[62] A. Gavrielides, V. Kovanis, P.M. Varangis, T. Erneux, G. Lythez, Coexisting periodic attractors in injection-locked diode lasers, Quant. Semiclass. Opt. 9 (1997) 785–796.
[63] A.N. Pisarchik, Yu.O. Barmenkov, A.V. Kir'yanov, Experimental characterization of bifurcation structure in an erbium-doped fiber laser with pump modulation, IEEE J. Quantum. Electron. 39 (2003) 1567–1571.
[64] J.M. Saucedo-Solorio, A.N. Pisarchik, A.V. Kir'yanov, V. Aboites, Generalized multistability in a fiber laser with modulated losses, J. Opt. Soc. Am. B. 20 (2003) 490–496.
[65] M. Brambilla, L.A. Lugiato, V. Penna, F. Prati, C. Tamm, C. Weiss, Transverse laser patters. II. Variational principle for pattern selection, spatial multistability and laser hydrodynamics, Phys. Rev. A 43 (1991) 5114–5120.
[66] E. Pampaloni, S. Residori, S. Soria, F.T. Arecchi, Phase-locking in nonlinear optical patterns, Phys. Rev. Lett. 78 (1997) 1042–1045.
[67] M. Brambilla, L.A. Lugiato, M. Pinna, F. Prati, P. Pagani, V. Vanotti, M. Li, C. Weiss, The laser as nonlinear element for an optical associative memory, Opt. Commun. 92 (1992) 145–164.
[68] J. Kastrup, H. Grahn, K. Ploog, F. Prengel, A. Wacker, E. Schöll, Multistability of the current–voltage characteristics in doped GaAs-AlAs superlattices, Appl. Phys. Lett. 65 (1994) 1808–1810.
[69] F. Prengel, A. Wacker, E. Schöll, Simple model for multistability and domain formation in semiconductor superlattices, Phys. Rev. B 50 (1994) 1705–1712.
[70] L.L. Bonilla, R. Escobedo, G. Dell'Acqua, Voltage switching and domain relocation in semiconductor superlattices, Phys. Rev. B 73 (2006) 115341–115353.
[71] R. Aguado, G. Platero, Photo-induced multistable phenomena in the tunneling current through doped superlattices, Phys. Rev. Lett. 81 (1998) 4971–4974.
[72] J. Hirschinger, W. Eberle, W. Prettl, F.-J. Niedernostheide, H. Kostial, Self-organized current-density patterns and bifurcations in n-GaAs with a circular symmetry of contacts, Phys. Lett. A 236 (1997) 249–255.
[73] G. Schwarz, C. Lehmann, E. Schöll, Self-organized symmetry-breaking current filamentation and multistability in Corbino disks, Phys. Rev. B 61 (2000) 10194–10200.
[74] W.G. Teich, G. Mahler, Optically controlled multistability in nanostructures semiconductors, Phys. Scr. 40 (1989) 688–693.
[75] I. Hudson, J. Mankin, Chaos in the Belousov–Zhabotinskii reaction, J. Chem. Phys. 74 (1981) 6171–6177.
[76] R. Simonyi, A. Wolf, H. Swinney, One-dimensional dynamics in a multi-component chemical reaction, Phys. Rev. Lett. 49 (1982) 245–248.
[77] J. Wang, P. Sorensen, F. Hymne, Transient period doublings, torus oscillations, and chaos in a closed chemical system, J. Chem. Phys. 98 (1994) 725–727.
[78] N. Ganapathisubramanian, K. Showalter, Bistability, mushrooms, and isolas, J. Chem. Phys. 80 (1984) 4177–4184.

[79] P. Marmillot, M. Kaufman, J.-F. Hervagault, Multiple steady states and dissipative structures in a circular and linear array of three cells: numerical and experimental approaches, J. Chem. Phys. 95 (1991) 1206–1214.
[80] J.P. Laplante, T. Erneux, Propagation failure and multiple steady-states in an array of diffusion coupled flow reactors, Physica A 188 (1992) 89–98.
[81] M. Orban, I. Epstein, Systematic design of chemical oscillators. Part 13. Complex periodic and aperiodic oscillation in the chlorite thiosulfate reaction, J. Phys. Chem. 86 (1982) 3907–3910.
[82] I. Nagypal, I. Epstein, Systematic design of chemical oscillators. 37. Fluctuations and stirring rate effects in the chlorite thiosulfate reaction, J. Phys. Chem. 90 (1986) 6285–6292.
[83] H. Sun, S. Scott, K. Showalter, Uncertain destination dynamics, Phys. Rev. E 60 (1999) 3876–3880.
[84] A.M. Turing, The chemical basis of morfogenesis, Philos. Trans. R. Soc. Lond. B Biol. Sci. 237 (1952) 37–72.
[85] L. Yang, M. Dolnik, A.M. Zhabotinsky, I.R. Epstein, Turing patters beyond hexagons and stripes, Chaos 16 (2006) 037114.
[86] R. May, Thresholds and breakpoints in ecosystems with a multiplicity of stable states, Nature 269 (1977) 471–477.
[87] P.M. Groffman, J.S. Baron, T. Blett, A.J. Gold, I. Goodman, L.H. Gunderson, et al., Ecological thresholds: the key to successful environmental management or an important concept with no practical application? Ecosystems 269 (2006) 1–13.
[88] N. Knowlton, Thresholds and multiple stable states in coral-reef community dynamics, Amer. Zool. 32 (1992) 674–682.
[89] O. Hoegh-Guldberg, P.J. Mumby, R.S. Steneck, P. Greenfield, E. Gomez, et al., Coral reefs under rapid climate change and ocean acidification, Science 318 (2007) 1737–1742.
[90] V. Brovkin, M. Claussen, V. Petoukhov, A. Ganopolski, On the stability of the atmosphere-vegetation system in the Sahara/Sahel region, J. Geophys. Res. 103 (1998) 31613–31624.
[91] M. Scheffer, S. Carpenter, J. Foley, C. Folke, B. Walker, Catastrophic shifts in ecosystems, Nature 413 (2001) 31613–31624.
[92] M. Rietkerk, S.F. Dekker, P.C. de Ruiter, J. van de Koppel, Self-organized patchiness and catastrophic shifts in ecosystems, Science 305 (2004) 1926–1929.
[93] E.H. van Nes, M. Scheffer, Slow recovery from perturbations as a generic indicator of a nearby catastrophic shift, Amer. Nat. 169 (2007) 738–747.
[94] J. Huisman, F. Weissing, Fundamental unpredictability in multispecies competition, Amer. Nat. 157 (2001) 171–187.
[95] M. Baurmann, U. Feudel, Turing patterns in a simple model of a nutrient-microorganism system in the sediment, Ecol. Complex. 1 (2004) 77–94.
[96] E. Meron, E. Gilad, J. von Hardenberg, M. Shachak, Y. Zarmi, Vegetation patterns along a rainfall gradient, Chaos, Solitons Fractals 19 (2004) 367–376.
[97] S. Kéfi, M.B. Eppinga, P.C. de Ruiter, M. Rietkerk, Bistability and regular spatial patterns in arid ecosystems, Theor. Ecol. 3 (2010) 257–269.
[98] J. Hertz, A. Krogh, R. Palmer, Introduction to the Theory of Neural Computation, Addison-Wesley, New York, 1991.
[99] C. Canavier, D. Baxter, J. Clark, J. Byrne, Nonlinear dynamics in a model neuron provide a novel mechanism for transient synaptic inputs to produce long-term alterations of postsynaptic activity, J. Neurophysiol. 69 (1993) 2252–2257.
[100] C.C. Canavier, D.A. Baxter, J.W. Clark, J.H. Byrne, Multiple modes of activity in a model neuron suggest a novel mechanism for the effects of neuromodulators, J. Neurophysiol. 72 (1994) 872–882.
[101] S. Kim, S.H. Park, C.S. Ryu, Multistability in coupled oscillator systems with time delay, Phys. Rev. Lett. 79 (1997) 2911–2914.
[102] S.H. Park, S. Kim, H.-B. Pyo, S. Lee, Multistability analysis of phase locking patterns in an excitatory coupled neural system, Phys. Rev. E 60 (1999) 2177–2181.
[103] J. Foss, J. Milton, Multistability in recurrent neural loops arising from delay, J. Neurophysiol. 84 (2000) 975–985.
[104] J. Braun, M. Mattia, Attractors and noise: twin drivers of decisions and multistability, NeuroImage 52 (2010) 740–751.
[105] J. Foss, F. Moss, J. Milton, Noise, multistability, and delayed recurrent loops, Phys. Rev. E 55 (1997) 4536–4543.
[106] A. Roxin, N. Brunel, D. Hansel, Role of delays in shaping spatiotemporal dynamics of neuronal activity in large networks, Phys. Rev. Lett. 94 (2005) 238103.
[107] Z. Yi, K.K. Tan, T.H. Lee, Multistability analysis for recurrent neural networks with unsaturating piecewise linear transfer functions, Neural Comput. 15 (2003) 639–662.
[108] L.A. Safonov, Y. Yamamoto, Noise-driven switching between limit cycles and adaptability in a small-dimensional excitable network with balanced coupling, Neural Comput. 73 (2006) 031914.
[109] L. Gammaitoni, P. Hänggi, P. Jung, F. Marchesoni, Stochastic resonance, Rev. Modern Phys. 78 (2006) 775–778.
[110] A.S. Pikovsky, J. Kurths, Coherence resonance in a noise-driven excitable system, Phys. Rev. Lett. 78 (1997) 775–778.
[111] J.P. Newman, R.J. Butera, Mechanism, dyanamics and biological existence of multistability in a large class of bursting neurons, Chaos 20 (2010) 023118.
[112] F. Wolf, Symmetry, multistability, and long-range interactions in brain development, Phys. Rev. Lett. 95 (2003) 208701.
[113] D. Paillard, The timing of pleistocene glaciations from a simple multiple-state climate model, Nature 391 (1998) 208701.
[114] T.N. Palmer, A nonlinear dynamical perspective on climate prediction, J. Clim. 12 (1998) 575–591.
[115] R. Calov, A. Ganopolski, Multistability and hysteresis in the climate-cryosphere system under orbital forcing, Res. Lett. 12 (2005) L21717.
[116] S. Bathiany, M. Claussen, K. Fraedrich, Implications of climate variability for the detection of multiple equilibria and for rapid transitions in the atmosphere-vegetation system, Clim. Dynam. 38 (2012) 1775–1790.
[117] J. Sr, R.P. Rial, M. Beniston, M. Claussen, J. Canadell, P. Cox, H. Held, N. de Noblet Ducoudré, R. Prinn, J. Reynolds, J. Salas, Nonlinearities, feedbacks and critical thresholds within the Earth's climate system, Clim. Dynam. 65 (2004) 11–38.
[118] T.M. Lenton, H. Held, E. Kriegler, J.W. Hall, W. Lucht, S. Rahmstorf, H.J. Schellnhuber, Tipping elements in the Earth's climate system, PNAS (USA) 105 (2008) 1786–1793.
[119] G. Lenderink, R. Haarsma, Variability and multiple equilibria of the thermohaline circulation associated with deep-water formation, J. Phys. Oceanogr. 24 (1994) 1480–1493.
[120] S. Rahmstorf, Multiple convection patterns and thermohaline flow in an idealized OGCM, J. Clim. 8 (1995) 3028–3039.
[121] T. Kuhlbrodt, S. Titz, U. Feudel, S. Rahmstorf, A simple model of seasonal open ocean convection. Part II: Labrador sea stability and stochastic forcing, Ocean Dyn. 52 (2001) 36–49.
[122] M.V. Kurgansky, K. Dethloff, I.A. Pisnichenko, H. Gernandt, F.-M. Chmilevsky, W. Jansen, Long-term climate variability in a simple, nonlinear atmospheric model, J. Geophys. Res. (Atmosphere) 101 (1996) 4299–4314.
[123] T.J. Crowley, S.K. Baum, Is the Greenland ice sheet bistable? Paleoceanography 10 (1995) 357–363.
[124] A. Robinson, R. Calov, A. Ganopolski, Multistability and critical thresholds of the Greenland ice sheet, Nature Clim. Change 2 (2012) 429–432.
[125] J. Marotzke, P. Welander, J. Willebrand, Instability and multiple steady states in a meridional-plane model of the thermohaline circulation, Tellus 40A (1988) 162–172.
[126] J. Marotzke, J. Willebrand, Multiple equilibria of the global thermohaline circulation, J. Phys. Oceanogr. 21 (1991) 1372–1385.
[127] Y. Ashkenazy, E. Tziperman, A wind-induced thermohaline circulation hysteresis and millennial variability regimes, J. Phys. Oceanogr. 37 (2007) 2446–2457.
[128] E. Hawkins, R.S. Smith, L.C. Allison, J.M. Gregory, T.J. Woollings, H. Pohlmann, B. de Cuevas, Bistability of the atlantic overturning circulation in a global climate model and links to ocean freshwater transport, Geophys. Res. Lett. 38 (2011) L10605.
[129] S.B. Power, R. Kleeman, Multiple equilibria in a global ocean general circulation model, J. Phys. Oceanography 23 (1994) 1670–1681.
[130] J. Xie, S. Sreenivasan, G. Korniss, W. Zhang, C. Lim, B.K. Szymanski, Social consensus through the influence of committed minorities, Phys. Rev. E 71 (2011) 011130.
[131] X. Castello, A. Baronchelli, V. Loreto, Consensus and ordering in language dynamics, Eur. Phys. J. B 71 (2009) 557–564.
[132] G.C.M.A. Ehrhardt, M. Marsili, F. Vega-Redondo, Phenomenological models of socioeconomic network dynamics, Phys. Rev. E 74 (2006) 036106.
[133] K. Sneppen, N. Mitarai, Multistability with a metastable mixed state, Phys. Rev. Lett. 109 (2012) 100602.
[134] M.A. Lieberman, K.Y. Tsang, Transient chaos in dissipatively perturbed, near-integrable Hamiltonian systems, Phys. Rev. Lett. 55 (1985) 908–911.
[135] U. Feudel, C. Grebogi, B.R. Hunt, J.A. Yorke, Map with more than 100 coexisting low-period periodic attractors, Phys. Rev. E. 54 (1996) 71–81.

[136] U. Feudel, C. Grebogi, Why are chaotic attractors rare in multistable systems? Phys. Rev. Lett. 91 (2003) 134102.
[137] P. Rech, M. Beims, J. Gallas, Basin size evolution between dissipative and conservative limits, Phys. Rev. E 71 (2006) 017202.
[138] L. Poon, C. Grebogi, Controlling complexity, Phys. Rev. Lett. 75 (1995) 4023–4026.
[139] U. Feudel, C. Grebogi, Multistability and the control of complexity, Chaos 7 (1997) 597–603.
[140] S. Kraut, U. Feudel, C. Grebogi, Preference of attractors in noisy multistable systems, Phys. Rev. E 59 (1999) 5253–5260.
[141] S. Kraut, U. Feudel, Enhancement of noise-induced escape through the existence of a chaotic saddle, Phys. Rev. E 67 (2003) 015204(R).
[142] B. Blazejczyk-Okolewska, T. Kapitaniak, Co-existing attractors of impact oscillator, Chaos Solitons Fractals 9 (1998) 1439–1443.
[143] S.T. Mário de Freitas, R.L. Viana, C. Grebogi, Basins of attraction of periodic oscillations in suspension bridges, Nonlinear Dynam. 37 (2004) 207–226.
[144] R. Weigel, E. Atlee Jackson, Multistability and the control of complexity, Int. J. Bifurcation Chaos 8 (1998) 173–178.
[145] K. Kaneko, Dominance of milnor attractors and noise-induced selection in a multiattractor system, Phys. Rev. Lett. 78 (1997) 2736–2739.
[146] N.K. Gavrilov, L.P. Silnikov, On three dimensional dynamical systems close to systems with structurally unstable homoclinic curve. I, Math. USSR Sbornik 17 (1972) 467–485.
[147] S. Newhouse, Non density of axiom A(a) on S2, Proc. A. M. S. Symp. Pure Mat. 14 (1970) 191–202.
[148] S. Newhouse, Diffeomorphisms with infinitely many sinks, Topology 13 (1974) 9–18.
[149] S. Newhouse, The abundance of wild hyperbolic sets and nonsmooth stable sets for diffeomorphisms, Publ. Math. Inst. Hautes Études Sci. 50 (1979) 101–151.
[150] J. Palis, M. Viana, High dimension diffeomorphisms displaying infinitely many periodic attractors, Ann. of Math. 140 (1994) 207–250.
[151] J.M. Gambaudo, C. Tresser, Simple models for bifurcations creating horseshoes, J. Stat. Phys. 32 (1983) 455–476.
[152] X.-J. Wang, The Newhouse set has a positive Hausdorff dimension, Comm. Math. Phys. 131 (1990) 317–332.
[153] E. Colli, Coexistence of infinitely many strange attractors. Technical Report IMPA report F-086/96, Ann. de l' Institut Henri Poincare, 1996.
[154] B. Goswami, Multiple attractors in the self-similar bifurcation-structure, Riv. Nuovo Cimento 23 (2005) 1–115.
[155] B. Goswami, Newhouse sinks in the self-similar bifurcation structure, Phys. Rev. E 62 (2000) 2068–2077.
[156] B. Goswami, S. Basu, Self-similar organization of Gavrilov-Shilnikov-Newhouse sinks, Phys. Rev. E 62 (2002) 036210.
[157] R. Carvalho, B. Fernandez, R.V. Mendes, From synchronization to multistability in two coupled quadratic mapss, Phys. Lett. A 285 (2001) 327–338.
[158] V. Astakhov, A. Shabunin, W. Uhm, S. Kim, Multistability formation and synchronization loss in coupled Hénon maps: Two sides of the single bifurcational mechanism, Phys. Rev. E 63 (2001) 056212.
[159] J.M. Sausedo-Solorio, A.N. Pisarchik, Dynamics of unidirectionally coupled Hénon maps, Phys. Lett. A 375 (2011) 3677–3681.
[160] A. Campos-Mejia, A.N. Pisarchik, D.A. Arroyo-Almanza, Noise-induced on-off intermittency in mutually coupled semiconductor lasers, Chaos, Solitons Fractals 54 (2013) 96–100.
[161] A. Pikovsky, O. Popovych, Y. Maistrenko, Resolving clusters in chaotic ensembles of globally coupled identical oscillators, Phys. Rev. Lett. 87 (2001) 044102.
[162] S. Osipov, M. Sushchik, Synchronized clusters and multistability in arrays of oscillators with different natural frequencies, Phys. Rev. Lett. 58 (1998) 7198–7207.
[163] K. Wiesenfeld, P. Hadley, Attractor crowding in oscillator array, Phys. Rev. Lett. 62 (1989) 1335–1338.
[164] K. Kaneko, Clustering, coding, switching, hierarchical ordering, and control in network of chaotic elements, Physica D 41 (1990) 137–172.
[165] V.V. Astakhov, B.P. Bezruchko, E.N. Erastova, E.P. Seleznev, Oscillation types and their evolution in dissipatively coupled Feigenbaum systems, Sov. Phys. Tech. Phys. 35 (1990) 1122–1129; Zh. Tekh. Fiz. 60 (1990) 19–26.
[166] A. Shabunin, U. Feudel, V. Astakhov, Phase multistability and phase synchronization in an array of locally coupled period-doubling oscillators, Phys. Rev. E 80 (2009) 026211.
[167] T.E. Vadivasova, O.V. Sosnovtseva, A.G. Balanov, V. Astakhov, Phase multistability of synchronous chaotic oscillations, Discrete Dyn. Nat. Soc. 4 (2000) 231–243.
[168] J. Rasmussen, E. Mosekilde, C. Reick, Bifurcations in two coupled Rössler systems, Math. Comput. Simul. 40 (1996) 247–270.
[169] K. Ikeda, Multiple-valued stationary state and its instability of the transmitted light by a ring cavity system, Opt. Commun. 39 (1979) 257–261.
[170] K. Ikeda, High-dimensional chaotic behavior in systems with time-delayed feedback, Physica D 29 (1987) 223–235.
[171] H.M. Gibbs, F.A. Hopf, D.L. Kaplan, R.L. Shoemaker, Observation of chaos in optical bistability, Phys. Rev. Lett. 46 (1981) 474–477.
[172] T. Aida, P. Davis, Synchronization of chaotic mode hopping in dbr lasers with delayed opto-electric feedback, IEEE J. Quantum Electron. 28 (1992) 686–699.
[173] K. Ikeda, K. Kondo, Successive higher-harmonic bifurcations in systems with delayed feedback, Phys. Rev. Lett. 49 (1982) 1467–1470.
[174] A. Balanov, N. Janson, E. Schöll, Delayed feedback control of chaos: bifurcation analysis, Phys. Rev. E 71 (2005) 016222.
[175] J. Losson, M.C. Mackey, A. Longtin, Solution multistability in first-order nonlinear differential delay equations, Chaos 3 (1993) 167–176.
[176] B.E. Martínez-Zérega, A.N. Pisarchik, L. Tsimring, Using periodic modulation to control coexisting attractors induced by delayed feedback, Phys. Lett. A 318 (2003) 102–111.
[177] G.-Q. Xia, S.-C. Chan, J.-M. Liu, Multistability in a semiconductor laser with optoelectronic feedback, Optics Express 15 (2007) 572–576.
[178] B.E. Martínez-Zérega, A.N. Pisarchik, Efficiency of the control of coexisting attractors by harmonic modulation applied in different ways, Phys. Lett. A 340 (2005) 212–219.
[179] B.E. Martínez-Zérega, A.N. Pisarchik, Stochastic control of attractor preference in multistable systems, Commun. Nonlinear Sci. Numer. Simul. 17 (2012) 4023–4028.
[180] D.H. Zanette, Propagating structures in globally coupled systems with time delays, Phys. Rev. E 62 (2000) 3167–3172.
[181] Y.-C. Lai, C. Grebogi, Complexity in Hamiltonian-driven dissipative chaotic dynamical systems, Phys. Rev. E 54 (1996) 4667–4675.
[182] C.N. Ngonghala, U. Feudel, K. Showalter, Extreme multistability in a chemical model system, Phys. Rev. E 83 (2011) 056206.
[183] J. Wang, H. Sun, S.K. Scott, K. Showalter, Uncertain dynamics in nonlinear chemical reactions, Phys. Chem. Chem. Phys. 5 (2003) 5444–5447.
[184] C.R. Hens, R. Banerjee, U. Feudel, S.K. Dana, How to obtain extreme multistability in coupled dynamical systems, Phys. Rev. E 85 (2012) 035202(R).
[185] Sanju, V.S. Varma, Quadratic map modulated by additive periodic forcing, Phys. Rev. E 48 (1993) 1670–1675.
[186] H.G. Davies, K. Rangavajhula, A period-doubling bifurcation with slow parametric variation and additive noise, Proc. R. Soc. Lond. Ser. A 457 (2001) 2965–2982.
[187] A.N. Pisarchik, Dynamical tracking of unstable periodic orbits, Phys. Lett. A 242 (1998) 152–162.
[188] A.N. Pisarchik, B.F. Kuntsevich, R. Corbalán, Stabilizing unstable orbits by slow modulation of a control parameter in a dissipative dynamic system, Phys. Rev. E 57 (1998) 4046–4053.
[189] A.N. Pisarchik, R. Corbalán, V.N. Chizhevsky, R. Vilaseca, B.F. Kuntsevich, Dynamic stabilization of unstable perodic orbits in a CO_2 laser by slow modulation of cavity detuning, J. Bifurcation. Chaos 8 (1998) 1783–1789.
[190] V.N. Chizhevsky, R. Corbalán, A.N. Pisarchik, Attractor splitting induced by resonant perturbations, Phys. Rev. E 56 (1997) 1580–1584.
[191] V.N. Chizhevsky, R. Vilaseca, R. Corbalán, Experimental switchings in bistability domains induced by resonant perturbations, Int. J. Bifurcation Chaos 8 (1998) 1777–1782.
[192] T.C. Newell, A. Gavrielides, V. Kovanis, D. Sukow, T. Erneux, S.A. Glasgow, Unfolding of the period-two bifurcation in a fiber laser pumped with two modulation tones, Phys. Rev. E 56 (1997) 7223–7231.
[193] V.N. Chizhevsky, Multistability in dynamical systems induced by weak periodic perturbations, Phys. Rev. E 64 (2001) 036223.
[194] G.L. Oppo, A. Politi, Toda potential in laser equations, Z. Phys. B: Condens. Matter 59 (1985) 111–115.
[195] J. Buceta, K. Lindenberg, Comprehensive study of phase transitions in relaxational systems with field-dependent coefficients, Phys. Rev. E 69 (2004) 011102.
[196] K. Wood, J. Buceta, K. Lindenberg, Comprehensive study of pattern formation in relaxational systems, Phys. Rev. E 73 (2006) 022101.
[197] Y.V. Pershin, M. Di Ventra, Memory effects in complex materials and nanoscale systems, Adv. Phys. 60 (2011) 145–227.

[198] A. Stotland, M. Di Ventra, Stochastic memory: memory enhancement due to noise, Phys. Rev. E 85 (2012) 011116.
[199] C. Grebogi, E. Ott, J.A. Yorke, Basin boundary metamorphoses: changes in accessible boundary orbits, Physica D 24 (1987) 243–262.
[200] T. Kapitaniak, Yu. Maistrenko, Multiple choice bifurcations as a source of unpredictability in dynamical systems, Phys. Rev. E 58 (1998) 5161–5163.
[201] K. Pyragas, F. Lange, T. Letz, J. Parisi, A. Kittel, Stabilization of an unstable steady state in intracavity frequency-doubled lasers, Phys. Rev. E 61 (2000) 3721–3731.
[202] R.J. Reategui, A.V. Kir'yanov, A.N. Pisarchik, Y.O. Barmenkov, N.N. Il'ichev, Experimental study and modeling of coexisting attractors and bifurcations in an erbium-doped fiber laser with diode-pump modulation, Laser Phys. 14 (2004) 1277–1281.
[203] W. Lauterborn, R. Steinhoff, Bifurcation structure of a laser with pump modulation, J. Opt. Soc. Amer. B Opt. Phys. 5 (1988) 1097–1104.
[204] A. Hohl, H.J.C. Van der Linden, R. Roy, Scalling laws for dynamical hysteresis in a multidimensional laser system, Phys. Rev. Lett. 74 (1996) 2220–2223.
[205] S. Wieczorek, B. Krauskopf, D. Lenstra, Mechanisms for multistability in a semiconductor laser with optical injection, Opt. Commun. 183 (2000) 215–226.
[206] F.R. Ruiz-Oliveras, A.N. Pisarchik, Synchronization of semiconductor lasers with coexisting attractors, Phys. Rev. E 79 (2009) 016202.
[207] M.R. Guevara, L. Glass, A. Shrier, Phase locking, period-doubling bifurcations, and irregular dynamics in periodically stimulated cardiac cells, Science 214 (1981) 1350–1353.
[208] A.R. Yehia, D. Jeandupeux, F. Alonso, M.R. Guevara, Hysteresis and bistability in the direct transition from 1:1 to 2:1 rhythm in periodically driven single ventricular cells, Chaos 9 (1999) 916–931.
[209] E. Ott, C. Grebogi, J.A. Yorke, Controlling chaos, Phys. Rev. Lett. 64 (1990) 1196–1199.
[210] T. Carroll, I. Triandaf, I. Schwartz, L. Pecora, Tracking unstable orbits in an experiment, Phys. Rev. A 46 (1992) 6189–6192.
[211] D.J. Christini, J.J. Collins, Using chaos control and tracking to suppress a pathological nonchaotic rhythm in a cardiac model, Phys. Rev. E 53 (1996) R49–R52.
[212] R.P. Kline, B.M. Baker, A dynamical systems approach to membrane phenomena underlying cardiac arrhythmias, Int. J. Bifurcation Chaos 5 (1995) 75–88.
[213] B.F. Kuntsevich, A.N. Pisarchik, V.N. Chizhevsky, V.V. Churakov, Amplitude modulation of the radiation of a CO_2 laser by optically controlled absorption in semiconductors, J. Appl. Spectr. 38 (1983) 107–112; Translated from Zhurnal Prikladnoi Spektroskopii 38 (1983) 126–133.
[214] V.N. Chizhevsky, S.I. Turovets, Small signal amplification and classical squeezing near period-doubling bifurcations in a modulated CO_2-laser, Opt. Commun. 102 (1993) 175–182.
[215] E. Li, Chromatin modification and epigenetic reprogramming in mammalian development, Nat. Rev. Genet. 3 (2002) 662–673.
[216] T.S. Gardner, C.R. Cantor, J.J. Collins, Construction of a genetic toggle switch in Escherichia coli, Nature 403 (2000) 324–339.
[217] E.M. Ozbudak, M. Thattai, H.N. Lim, B.I. Shraiman, A. van Oudenaarden, Multistability in the lactose utilization network of *Escherichia coli*, Nature 427 (2004) 737–740.
[218] R.D. Thomas, Biological Feedback, CRC Press, Boca Raton, FL, 1990.
[219] J.L. Cherry, F.R. Adler, How to make a biological switch, J. Theoret. Biol. 203 (2000) 117–133.
[220] A. Becskei, B. Seraphin, L. Serrano, Positive feedback in eukaryotic gene networks: cell differentiation by graded to binary response conversion, Embo J. 20 (2001) 2528–2535.
[221] M. Acar, A. Becskei, A. van Oudenaarden, Enhancement of cellular memory by reducing stochastic transitions, Nature 435 (2005) 228–232.
[222] A. Kashiwagi, I. Urabe, K. Kaneko, T. Yomo, Adaptive response of a gene network to environmental changes by fitness-induced attractor selection, PLoS ONE 1 (2006) e49. http://dx.doi.org/10.1371/journal.pone.0000049.
[223] J. Huisman, F. Weissing, Biodiversity of plankton by species oscillations and chaos, Nature 402 (1999) 407–410.
[224] K. Kaneko, Chaotic but regular posi-nega switch among coded attractors by cluster size variation, Phys. Rev. Lett. 63 (1989) 219–223.
[225] A.M. Samson, S.I. Turovets, V.N. Chizhevskii, V.V. Churakov, Nonlinear dynamics of a loss-switched CO_2 laser, Sov. Phys.—JETP 74 (1992) 628–639. Zh. Eksp. Teor. Fiz. 101 (1992) 1177–1188.
[226] V.N. Chizhevsky, S.I. Turovets, Periodically loss-modulated CO_2 laser as an optical amplitude and phase multitrigger, Phys. Rev. A 50 (1994) 1840–1843.
[227] V.N. Chizhevsky, E.V. Grigorieva, S.A. Kashchenko, Optimal timing for targeting periodic orbits in a loss-driven CO_2 laser, Opt. Commun. 133 (1997) 189–195.
[228] V.N. Chizhevsky, Coexisting attractors in a CO_2 laser with modulated losses, J. Opt. B: Quantum Semiclass. Opt 2 (2000) 711–717.
[229] V.N. Chizhevsky, P. Glorieux, Targeting unstable periodic orbits, Phys. Rev. E 51 (1995) R2701–R2704.
[230] A.A. Andronov, S.E. Chaikin, Theory of Oscillations, Princeton University Press, Princeton, NJ, 1949.
[231] C. Hayashi, Theory of Oscillations, Princeton University Press, Princeton, NJ, 1964.
[232] J. Guckenheimer, P. Holmes, Nonlinear Oscillations, Dynamical Systems, and Bifurcations of Vector Fields, Springer-Verlag, New York, 1983.
[233] L.M. Pecora, T.L. Carroll, Pseudoperiodic driving: eliminating multiple domain of attraction using chaos, Phys. Rev. Lett. 67 (1991) 945–948.
[234] T.L. Carroll, L.M. Pecora, Using chaos to keep period-multiplied systems in phase, Phys. Rev. E 48 (1993) 2426–2436.
[235] F.T. Arecchi, R. Badii, A. Politi, Scaling of first passage times for noise induced crises, Phys. Lett. A 103 (1990) 3–7.
[236] T. Kapitaniak, Chaos in Systems with Noise, World Scientific, Singapore, 1990.
[237] J.C. Sommerer, W.L. Ditto, C. Grebogi, E. Ott, M.L. Spano, Experimental confirmation of the scaling theory for noise-induced crises, Phys. Rev. Lett. 66 (1991) 1947–1950.
[238] O. Kornadt, S.J. Linz, M. Lücke, Ricker model: influence of periodic and stochastic parametric modulation, Phys. Rev. A 44 (1991) 940–955.
[239] W. Yang, M. Ding, H. Gang, Trajectory (phase) selection in multistable systems: stochastic resonance, signal bias, and the effect of signal phase, Phys. Rev. Lett. 74 (1995) 3955–3958.
[240] A.N. Pisarchik, B.K. Goswami, Annihilation of one of the coexisting attractors in a bistable system, Phys. Rev. Lett. 84 (2000) 1423–1426.
[241] A.N. Pisarchik, Controlling the multistability of nonlinear systems with coexisting attractors, Phys. Rev. E 64 (2001) 046203.
[242] B.K. Goswami, S. Euzzor, K. Al Naimee, A. Geltrude, R. Meucci, F.T. Arecchi, Control of stochastic multistable systems: experimental demonstration, Phys. Rev. E 80 (2009) 016211.
[243] A.N. Pisarchik, Y.O. Barmenkov, A.V. Kir'yanov, Experimental demonstration of attractor annihilation in a multistable fiber laser, Phys. Rev. E 68 (2003) 066211.
[244] B.K. Goswami, Controlled destruction of chaos in the multistable regime, Phys. Rev. E 76 (2007) 016219.
[245] J.M. Saucedo Solorio, A.N. Pisarchik, V. Aboites, Shift of saddle–node bifurcation points in modulated Hénon map, Rev. Mexicana Fís. 48 (2002) 290–294.
[246] A.N. Pisarchik, R. Corbalán, Shift of attractor boundaries in a system with a slow harmonic parameter perturbation, Physica D 150 (2001) 14–24.
[247] M. Hénon, 2-dimensional mapping with a strange attractor, Comm. Math. Phys. 50 (1976) 69–77.
[248] C. Scheffczyk, U. Parlitz, T. Kurz, W. Knop, W. Lauterborn, Comparison of bifurcation structures of driven dissipative nonlinear oscillators, Phys. Rev. A 43 (1991) 6495–6502.
[249] C. Grebogi, E. Ott, J.A. Yorke, Crises, sudden changes in chaotic attractors, and transient chaos, Physica D 7 (1983) 181–200.
[250] E.N. Egorov, A.A. Koronovskii, Dynamical control in multistable systems, Tech. Phys. Lett. 30 (2004) 186–189.
[251] A.N. Pisarchik, B.K. Kuntsevich, Control of multistability in a directly modulated diode laser, IEEE J. Quantum Electron. 38 (2002) 1594–1598.
[252] A.N. Pisarchik, R. Jaimes-Reátegui, Control of basins of attractors in a multistable fiber laser, Phys. Lett. A 374 (2009) 228–234.
[253] A.N. Pisarchik, Oscillation death in coupled nonautonomous systems with parametrical modulation, Phys. Lett. A 318 (2003) 65–70.
[254] R. Jaimes-Reategui, A.N. Pisarchik, Control of on–off intermittency by slow parametric modulation, Phys. Rev. E 69 (2004) 067203.
[255] Y.-C. Lai, Driving trajectories to a desirable attractor by using small, Phys. Lett. A 221 (1996) 375–383.
[256] E.E.N. Macau, C. Grebogi, Driving trajectories in complex systems, Phys. Rev. E 59 (1999) 4062–4070.
[257] S. Gadaleta, G. Dangelmayr, Learning to control a complex multistable system, Phys. Rev. E 63 (2001) 036217.

[258] T. Shinbrot, E. Ott, C. Greboggi, J.A. Yorke, Using chaos to direct trajectories to targets, Phys. Rev. Lett. 65 (1990) 3215–3218.
[259] D.P. Bertsekas, J.N. Tsitsiklis, Neuro-Dynamic Programming, Athena Scientific, 1996.
[260] K.J. Åström, B. Wittenmark, Computer-Control Systems: Theory and Design, third ed., Prentice Hall, Englewood Cliffs, NJ, 1997.
[261] R. Der, M. Herrmann, Q-learning chaos controller, in: Proceedings of the 1994 IEEE International Conference on Neural Networks, vol. 4, IEEE, New York, 1994, pp. 2472–2475.
[262] S. Gadaleta, G. Dangelmayr, Optimal chaos control through reinforcement learning, Chaos 9 (1999) 775–788.
[263] T.M. Martinetz, S.G. Berkovich, K.J. Schulten, Neural-gas network for vector quantization and its application to time-series prediction, IEEE Trans. Neural Netw. 4 (1993) 558–569.
[264] Yu Jiang, Trajectory selection in multistable systems using periodic drivings, Phys. Lett. A 4 (1999) 22–29.
[265] K. Pyragas, Continuous control of chaos by self-controlling feedback, Phys. Lett. A 170 (1992) 421–428.
[266] F.T. Arecchi, R. Meucci, W. Gadomski, Laser dynamics with competing instabilities, Phys. Rev. Lett. 58 (1987) 2205–2208.
[267] L.P. Shilnikov, A case of the existence of a denumerable set of periodic motions, Sov. Math. Dokl. 6 (1965) 163–166.
[268] A.N. Pisarchik, R. Meucci, F.T. Arecchi, Discrete homoclinic orbits in a laser with feedback, Phys. Rev. E 62 (2000) 8823–8825.
[269] A.N. Pisarchik, R. Meucci, F.T. Arecchi, Theoretical and experimental study of discrete behavior of Shilnikov chaos in a CO_2 laser, Eur. Phys. J. D 13 (2001) 385–391.
[270] R. Meucci, A. Labate, M. Ciofini, Controlling chaos by negative feedback of subharmonic components, Phys. Rev. E 56 (1997) 2829–2834.
[271] M. Ciofini, A. Labate, R. Meucci, M. Galanti, Stabilization of unstable fixed points in the dynamics of a laser with feedback, Phys. Rev. E 60 (1999) 398–402.
[272] F.T. Arecchi, R. Meucci, E. Allaria, A. Di Garbo, L.S. Tsimring, Delayed self-synchronization in homoclinic chaos, Phys. Rev. E 65 (2002) 046237.
[273] S.A. Akhmanov, Y.E. D'yakov, A.S. Chirkin, Introduction to Radiophysics and Optics, Nauka, Moscow, 1981.
[274] A.V. Fedorov, S.L. Harper, B. Winter, A. Wittenberg, How predictable is El Niño? Bull. Am. Meteorol. Soc. 84 (2003) 911–919.
[275] D. Chen, M.A. Cane, A. Kaplan, S.E. Zabiak, D. Huang, Predictability of El Niño in the past 148 years, Nature 428 (2004) 733–736.
[276] J.V. Greenman, T.G. Benton, The amplification of environmental noise in population models: causes and consequences, Amer. Nat. 161 (2003) 225–239.
[277] K. Erguler, M.P.H. Strumpf, Statistical interpretation of the interplay between noise and chaos, Math. Biosci. 216 (2008) 90–99.
[278] E. Surovyatkina, Prebifurcation noise amplification and noise-dependent hysteresis as indicators of bifurcations in nonlinear geophysical systems, Nonlinear Process. Geophys. 12 (2005) 25–29.
[279] D. Alonso, A.J. McKane, M. Pascual, Stochastic amplification in epidemics, J. R. Soc. Interface 4 (2007) 575–582.
[280] J. García-Ojalvo, R. Roy, Noise amplification in a stochastic Ikeda model, Phys. Lett. A 224 (1996) 51–56.
[281] A.N. Pisarchik, O.N. Pochepen, L.A. Pisarchyk, Increasing blood glucose variability is a precursor of sepsis and mortality in burned patients, PLoS One 7 (2012) e46582.
[282] G. Giacomelli, F. Marin, I. Rabbiosi, Stochastic and bona fide resonance: an experimental investigation, Phys. Rev. Lett. 82 (1999) 675–678.
[283] G. Giacomelli, M. Giudici, S. Balle, J.R. Tredicce, Experimental evidence of coherence resonance in an optical system, Phys. Rev. Lett. 84 (2000) 3298–3301.
[284] V.N. Chizhevsky, E. Smeu, G. Giacomelli, Experimental evidence of "vibrational resonance" in an optical system, Phys. Rev. Lett. 91 (2003) 220602.
[285] K. Kaneko, On the strength of attractors in a high-dimensional system, Physica (Amsterdam) 124D (1998) 322–344.
[286] A.N. Pisarchik, Control of multistability in systems with coexisting attractors, in: Some Topics of Modern Optics, Rinton Press, Paramus, 2008, pp. 326–391.
[287] U. Feudel, C. Grebogi, L. Poon, J.A. Yorke, Dynamical properties of a simple mechanical system with a large number of coexisting periodic attractors, Chaos Solitons Fractals 9 (1998) 171–180.
[288] S. Kraut, U. Feudel, Multistability, noise, and attractor hopping: the crucial role of chaotic saddles, Phys. Rev. E 66 (2002) 015207.
[289] C. Masoller, Noise-induced resonance in delayed feedback systems, Phys. Rev. Lett. 88 (2002) 034102.
[290] G. Huerta-Cuellar, A.N. Pisarchik, Yu.O. Barmenkov, Experimental characterization of hopping dynamics in a multistable fiber laser, Phys. Rev. E 78 (2008) 035202(R).
[291] S. Kim, S.H. Park, C.S. Ryu, Noise-enchanced multistability in coupled oscillator systems, Phys. Rev. Lett. 78 (1997) 1616–1619.
[292] F.T. Arecchi, A. Califano, Generalized multistability and noise-induced jumps in a nonlinear dynamical system, Europhys. Lett. 3 (1987) 5–10.
[293] A.E. Barbéroshie, I.I. Gontsya, Y.N. Nika, A.K. Rotaru, Noise-induced optical multistability, J. Exper. Theor. Phys. 104 (1993) 2655–2667.
[294] A.N. Pisarchik, R. Jaimes-Reátegui, R. Sevilla-Escoboza, G. Huerta-Cuillar, M. Taki, Rogue waves in a multistable fiber laser, Phys. Rev. Lett. 107 (2011) 274101.
[295] A.N. Pisarchik, R. Jaimes-Reátegui, R. Sevilla-Escoboza, G. Huerta-Cuellar, Multistate intermittency and extreme pulses in a fiber laser, Phys. Rev. E 86 (2012) 056219.
[296] G. Huerta-Cuellar, A.N. Pisarchik, A.V. Kir'yanov, Yu.O. Barmenkov, J. del Valle Hernández, Prebifurcation noise amplification in a fiber laser, Phys. Rev. E 79 (2009) 036204.
[297] A.N. Pisarchik, B.E. Martínez-Zérega, Noise-induced attractor annihilation in the delayed feedback logistic map, Phys. Lett. A 377 (2013) 3016–3020.
[298] J. Crutchfield, B. Huberman, Partition complexity in network of chaotic elements, J. Phys. A Math. Gen. 24 (1991) 2107–2119.
[299] A. Crisanti, M. Falcioni, A. Vulpiani, Broken ergodicity and glassy behavior in a deterministic chaotic map, Phys. Rev. Lett. 76 (1996) 2107–2119.
[300] O. Popovych, A. Pikovsky, Yu. Maistrenko, Cluster splitting bifurcation in a system of coupled maps, Physica D (2000) 168–169. 106–125.
[301] S.C. Manruiba, A. Mikhailov, Globally coupled logistic maps as dynamical glasses, Europhys. Lett. 53 (2001) 451–457.
[302] F.H. Willeboordse, K. Kaneko, Externally controlled attractor selection in a high-dimensional system investigated and shown to be controllable by external inputs, Phys. Rev. E 72 (2005) 026207.
[303] Y. Nagai, X.-D. Hua, Y.-C. Lai, Controlling on–off intermittent dynamics, Phys. Rev. E 54 (1996) 1190–1199.
[304] Y.-C. Lai, C. Grebogi, Intermingled basins and two-state on–off intermittency, Phys. Rev. E 52 (1995) R3313–R3316.
[305] A.N. Pisarchik, R. Jaimes-Reátegui, J.R. Villalobos-Salazar, J.H. Garcia-Lopez, S. Boccaletti, Synchronization of chaotic systems with coexisting attractors, Phys. Rev. Lett. 96 (2006) 244102.
[306] A.N. Pisarchik, R. Jaimes-Reátegui, J.H. García-Lopez, Synchronization of coupled bistable chaotic systems: experimental study, Phil. Trans. Roy. Soc., Ser. A 366 (2008) 459–473.
[307] A.N. Pisarchik, R. Jaimes-Reátegui, J.H. García-Lopez, Synchronization of multistable systems, Int. J. Bifurcation Chaos 18 (2008) 1801–1819.
[308] H. Riecke, A. Roxin, S. Madruga, S. Solla, Multiple attractors, long chaotic transients, and failure in small-world inetworks of excitable neurons, Chaos 17 (2007) 026110.
[309] R. Albert, A.-L. Barabási, Statistical mechanics of complex networks, Rev. Modern Phys. 74 (2002) 47–97.
[310] T. Gross, C.D. D'Lima, B. Blasius, Epidemic dynamics on an adaptive network, Phys. Rev. Lett. 96 (2006) 208701.
[311] T.T. Hartley, C.F. Lorenzo, H.K. Qammer, Chaos in fractional order Chua's systems, IEEE Trans. Circuits Syst.-I 42 (1995) 485–490.
[312] K. Sun, X. Wang, J.C. Sprott, Bifurcations and chaos in fractional-order simplified Lorenz system, Int. J. Bifurcation Chaos 20 (2010) 1209–1219.
[313] N. Hamri, T. Houmor, Chaotic dynamics of the fractional order nonlinear Bloch systems, Electron. J. Theor. Phys. 25 (2011) 233–244.
[314] E. Kaslik, S. Sivasundaram, Nonlinear dynamics and chaos in fractional-order neural networks, Neural Netw. 32 (2012) 245–256.
[315] Z. Levnajić, Emergent multistability and frustration in phase-repulsive networks of oscillators, Phys. Rev. E 84 (2011) 016231.